



**AN EMBEDDED SYSTEM FOR
MEASURING DUST DENSITY USING
TRIBLOW EFFECT**

Master of Science Thesis

Özcan KAMIŞLI

Eskişehir 2019

**AN EMBEDDED SYSTEM FOR MEASURING DUST DENSITY USING
TRIBLOW EFFECT**

Özcan KAMIŞLI

MASTER OF SCIENCE THESIS

Department of Electrical and Electronics Engineering

Program in Control Systems

Supervisor: Assoc. Prof. Dr. Hakan ŞENEL

Eskişehir

Eskişehir Technical University

Institute of Graduate Programs

July 2019

FINAL APPROVAL FOR THESIS

This thesis titled “AN EMBEDDED SYSTEM FOR MEASURING DUST DENSITY USING TRIBLOW EFFECT” has been prepared and submitted by Özcan KAMIŞLI in partial fulfillment of the requirements in “Eskişehir Technical University Directive on Graduate Education and Examination” for the Degree of Master of Science in Electrical and Electronics Engineering Department has been examined and approved on June 24th, 2019.

Committee Members

Title, Name and Surname

Signature

Member (Supervisor)

: Assoc. Prof. Dr. Hakan ŞENEL.



Member

: Prof. Dr. Atakan DOĞAN



Member

: Asst. Prof. Dr. Gökhan DINDİŞ



.....
(Title, Name and SURNAME)

Director of Graduate School of Eskişehir Technical University

ÖZET

TRİBOFLOW ETKİSİYLE TOZ ÖLÇÜMÜ GERÇEKLEŞTİREN GÖMÜLÜ SİSTEM

Özcan KAMIŞLI

Elektrik-Elektronik Mühendisliği Bölümü
Kontrol ve Kumanda Sistemleri (İngilizce)

Eskişehir Teknik Üniversitesi, Lisansüstü Eğitim Enstitüsü Temmuz 2019

Danışman: Doç Dr. Hakan ŞENEL

Hava akımı içerisinde bulunan katı parçacıkların akışı endüstriyel sistemde katı parçacıkları taşımak için kullanılır. Bu yöntem çok sayıda değişken ve karmaşık olaylar içerir ve bu doğası gereği çözümlenmesi zordur. Karmaşık akış rejimlerinden dolayı, çevrim-içi akış parametrelerinin ölçümü, partikül büyüklüğü, ortalama akış hızı, nem, boru hattı tipi, malzeme tipi, karışık malzeme özellikleri ve geometri ile ilişkili zorluklar gibi bazı zorlayıcı faktörlerden etkilenmektedir. Bu tezin amacı hava akımı içerisindeki katı akışının teorik bir çalışmasını gerçekleştirmek ve akış parametrelerinin ölçümü için elektrostatik temelli bir test donanımı tasarlamaktır.

Bu tezde, test donanımında kullanılan halka biçimli sensör tipi basitliği nedeniyle seçilmiştir. Sensör içersinden geçen yüklü parçacıklar nedeniyle oluşan gerilimi ölçmek için düşük gürültülü ve yüksek kazançlı yükselticiler tasarlanmıştır. Deneylerde kullanılmış yük kuvvetlendirici devre havada uçan parçacıkları, iyonları ve hatta elektronları hem şimdiki çalışmamızda hem de gelecek çalışmalarda ölçme yeteneğine sahiptir. Deneyler, genişlikleri çapa göre değişen on farklı sensör kullanılarak gerçekleştirilmiştir. Bu çalışmada, eğri önceki çalışmalara göre Gauss uygunlaştırılmış eğri modeli doğrulanmakta ve yerçekimi ile düşen sensörün içinden parçacıkların hızları ölçülmektedir.

Anahtar Kelimeler: Elektrostatik yük ölçümü, Parçacık akış ölçümü, Triboşarj, Elektrodinamik akış sensörü, Çevrim-içi akış ölçümü

ABSTRACT

AN EMBEDDED SYSTEM FOR MEASURING DUST DENSITY USING TRIBLOW EFFECT

Özcan KAMIŞLI

Department of Electrical and Electronics Engineering
Program in Control Systems

Eskişehir Technical University, Institute of Graduate Programs, July 2019

Supervisor: Assoc. Prof. Dr. Hakan ŞENEL

The flow of solid particles in air streams is used in industrial systems to transport solid particles. This method involves many variables and complex phenomena and it is inherently difficult to analyze. The measurements of on-line flow parameters due to complex flow regimes are affected by challenging factors: such as particle size, average flow velocity, humidity, pipeline type, material type, mixed material properties and geometry-related difficulties. The aim of this thesis is to perform a theoretical study of the solid flows in air streams and to design a test rig based on electrostatics for the measurement of flow parameters.

In this thesis, the ring type sensor has been chosen for the test rig due to its simplicity. Low noise and high gain amplifiers are designed to measure the voltages induced by the charged particles passing through sensors. The charge amplifier circuit used in experiments is capable of measuring the airborne particles, ions and even electrons for use in both current and future studies. Experiments have been carried out using ten different sensors with varying width to diameter. In the study, Gaussian fitted curve model according to the previous studies have been validated and velocities of particles falling with gravity through the sensors are measured.

Keywords: Electrostatic charge measurement, Particle flow measurement, Tribocharging, Electrodynamic flow sensor, On-line flow measurement

ACKNOWLEDGEMENT

The authors would like to express grateful thanks to the following for that.

Thank you to my advisor, Assoc. Professor Dr. Hakan ŞENEL, inspiring guidance, selfless service, patience and encouragement, this work could not be possible.

All my family members during my graduate program, I want to thank my wife and my sons, understanding and encouragement. Without such support, I could not have concentrated on the M.Sc research that initiated this thesis and let me conduct it.

Yours sincerely, to all those I have not said above, including those who directly or indirectly assisted in the completion of my project.

I also express my appreciation for the assistance given this thesis is dedicated to my wife for encouragement she provided throughout this project.

06/24/2019

STATEMENT OF COMPLIANCE WITH ETHICAL PRINCIPLES AND RULES

I hereby truthfully declare that this thesis is an original work prepared by me; that I have behaved in accordance with the scientific ethical principles and rules throughout the stages of preparation, data collection, analysis and presentation of my work; that I have cited the sources of all the data and information that could be obtained within the scope of this study, and included these sources in the references section; and that this study has been scanned for plagiarism with “scientific plagiarism detection program” used by Eskişehir Technical University, and that “it does not have any plagiarism” whatsoever. I also declare that, if a case contrary to my declaration is detected in my work at any time, I hereby express my consent to all the ethical and legal consequences that are involved.



Özcan KAMIŞLI

TABLE OF CONTENTS

	<u>Page</u>
TITLE PAGE	i
FINAL APPROVAL FOR THESIS.....	ii
ÖZET	iii
ABSTRACT	iv
ACKNOWLEDGEMENTS	v
STATEMENT OF COMPLIANCE WITH ETHICAL PRINCIPLES AND RULES	vi
TABLE OF CONTENTS	vii
LIST OF TABLES	xi
LIST OF FIGURES	xii
LIST OF SYMBOLS AND ABBREVIATIONS.....	xv
1. INTRODUCTION	1
1.1. Problem Statement.....	1
1.2. Research Objectives.....	1
1.3. Scope and Limitations	1
1.4. Research Contributions.....	2
2. BASIC CONCEPT, CHARGING AND DISCHARGING	3
2.1. Electrostatics.....	3
2.2. Electrostatic Theory.....	7
2.2.1. Unit of electric charge.....	7
2.2.2. Fundamental electromagnetic field equations.....	7
2.2.3. Gradient of a scalar field	8
2.2.4. Divergence theorem	8
2.2.5. Curl of a vector field	8
2.2.6. Stokes theorem	8
2.2.7. Electrostatics in free space	9
2.2.8. Electric potential	9
2.2.9. Boundary conditions	9
2.2.10. Coulomb's law	10
2.2.11. Gauss' law	11

	<u>Page</u>
2.2.12. Electric dipole.....	11
2.2.13. Electric field equation.....	12
2.2.14. Poisson's and Laplace's equations.....	12
2.2.15. Method of images.....	13
2.3. The Measurement of Charge.....	15
2.4. Conductors in Electrostatic Equilibrium.....	15
2.5. Charging of Materials.....	16
2.5.1. Tribocharging and contact charging.....	16
2.5.1.1. Metal-metal contacts.....	16
<i>Energy bands</i>	18
2.5.1.2. Metal-insulator contacts.....	18
2.5.1.3. Insulator-insulator contacts.....	19
<i>Electron transfer</i>	20
<i>Ion transfer</i>	21
<i>Material transfer</i>	22
<i>Effect of the separation state on charging</i>	22
<i>Friction charging</i>	22
<i>Charge decay</i>	23
<i>Current Flow</i>	23
2.5.2. Induction charging.....	24
2.5.3. Corona discharging.....	25
2.5.4. Particle charging by repeated impacts on a metal wall.....	27
2.5.4.1. <i>Charge transfer</i>	27
2.5.4.2. <i>Effect of elasticity</i>	27
2.5.5. Charging in gas-solids pipe flow.....	28
3. PNEUMATIC TRANSPORT.....	29
3.1. Characteristics of Pneumatically Conveyed Gas-Solids Flow.....	29
3.2. Some Challenging Features of Solids Flow in Pneumatic Pipelines.....	34
3.2.1. Nonuniform flowing solids distributions.....	34
3.2.2. Fluctuating velocity in the pipe.....	34
3.2.3. Irregular particle size in the pipe.....	34

	<u>Page</u>
3.2.4. Moisture content of particulate materials	35
3.2.5. Other flow parameters	35
4. THE METHODS AND APPLICATIONS.....	36
4.1. Background.....	36
4.2. Mass Flow Rate Measurements	36
4.2.1. Direct measurements	39
4.2.1.1. <i>Coriolis and gyroscopic mass flowmeters.....</i>	<i>39</i>
4.2.1.2. <i>Thermal methods.....</i>	<i>39</i>
4.2.1.3. <i>Electrical methods</i>	<i>39</i>
<i>Active charging-sensing methods.....</i>	<i>40</i>
<i>Passive sensing methods.....</i>	<i>40</i>
4.2.2. Indirect measurements	40
4.2.2.1. <i>Electrical sensors for measuring concentration of solid</i>	<i>40</i>
<i>Capacitance sensors.....</i>	<i>41</i>
<i>Electrodynamic sensors</i>	<i>41</i>
4.2.2.2. <i>Attenuation and scattering methods</i>	<i>42</i>
<i>Radiometric sensors.....</i>	<i>43</i>
<i>Microwave sensors.....</i>	<i>43</i>
<i>Optical sensors</i>	<i>44</i>
<i>Acoustic and ultrasonic sensors</i>	<i>44</i>
4.2.2.3. <i>Resonance sensors for measuring conc. of solids.....</i>	<i>45</i>
<i>Magnetic resonance sensors.....</i>	<i>45</i>
<i>Microwave resonance sensors</i>	<i>45</i>
<i>Acoustic resonance sensor</i>	<i>45</i>
4.2.2.4. <i>Tomography methods for measuring concentration</i>	<i>46</i>
<i>Electrostatic Tomography.....</i>	<i>46</i>
<i>Electrical Capacitance Tomography.....</i>	<i>47</i>
<i>Optical Tomography</i>	<i>47</i>
<i>Radiometric Tomography.....</i>	<i>47</i>
4.2.2.5. <i>Digital image method</i>	<i>48</i>
4.3. Measurements of Solids' Velocity	49
4.3.1. Cross correlation.....	49

	<u>Page</u>
4.3.1.1. <i>Optical sensor</i>	50
4.3.1.2. <i>Radiometric sensors</i>	50
4.3.1.3. <i>Acoustic sensors</i>	51
4.3.1.4. <i>Electrostatic sensor</i>	51
4.3.1.5. <i>Capacitive sensor</i>	51
4.3.2. Spatial filtering methods	51
4.3.2.1. <i>Capacitive and electrodynamic sensors</i>	52
4.3.2.2. <i>Microwave sensors</i>	52
4.3.2.3. <i>Optical sensors</i>	53
4.3.3. Doppler velocimetry	53
4.3.3.1. <i>Laser Doppler velocimetry</i>	53
4.3.3.2. <i>Microwave Doppler sensors</i>	54
4.3.4. Soft computing and new signal processing methods	54
4.4. Particle mean-size measurement	56
4.5. Relative measurement	56
5. HISTORICAL LITERATURE REVIEW	57
5.1. Before 1980	57
5.1.1. 1980-2000	60
5.1.2. Since 2000	70
6. ELECTROSTATIC SENSING TECHNIQUE	81
6.1. Electrostatic Method	81
6.2. Signal Generation by the Electrostatic Sensor	82
6.3. Electrostatic Sensor	84
6.3.1. Mathematical model for charge induction	84
6.3.2. Electrostatic flow probe: the physical model	84
6.3.3. Amplifier	87
7. THE STUDY ON SENSOR	89
7.1. Test Rig, Particles and Measurement	90
7.2. Results	99
8. DISCUSSION, CONCLUSIONS AND FUTURE WORK	100
REFERENCES	103
CURRICULUM VITAE	

LIST OF TABLES

	<u>Page</u>
Table 2.1. List of triboflow series for some commonly materials	6
Table 3.1 Operational flow conditions and properties of fuel particles	31
Table 3.2 Charge build up on powder	32
Table 4.1 Measurement methods of two phase solid flow parameters	38
Table 7.1 The list of test materials used in test rig.....	94
Table 7.2 The calculated velocities and elapsed times for all electrodes.....	94
Table 7.3 The peak to peak voltages	95

LIST OF FIGURES

	<u>Page</u>
Figure 2.1. Representation of fundamental electric dipole	11
Figure 2.2. Equipotential and electric field curves of an electric dipole.	12
Figure 2.3. Point charge and grounded plane conductor	13
Figure 2.4. Point charge and perpendicular conducting planes.	14
Figure 2.5. A Faraday cage to measure the induction charge	15
Figure 2.6. The methods of the measuring	15
Figure 2.7. Electron potential energy at a metal–metal contact.....	17
Figure 2.8. Charge on a chromium sphere, 4 mm in diameter, in contact with another–metal sphere, 13 mm in diameter, as a function of the CPD of chromium against each metal	18
Figure 2.9. The Fermi energy level of metal and insulator.....	18
Figure 2.10. Charge density of nylon no: 66 by contacting with various metals. The horizontal axis is the CPD of each metal against a gold reference $V_{M=Au}$ where the CPD is defined as $V_{Au/M}$	19
Figure 2.11. Contact charging between coal and metal surface.	19
Figure 2.12. Energy level diagram for insulator-insulator contact.	20
Figure 2.13. Representation of induction charging of neutral metal sphere.....	24
Figure 2.14. Induction charging of a conducting liquid.....	24
Figure 2.15. A type of an electrostatic-precipator	25
Figure 2.16. Variation in the charge of the sphere by repeated impacts (rubber sphere, drop height: 0.4 m, relative humidity: 41–43%)	27
Figure 3.1. Solids Concentration Profile in a Vertical Pipe.....	30
Figure 3.2. Solids Velocity Profile in a Vertical Pipe.....	30
Figure 3.3. Concentration profiles	34
Figure 3.4. Dimensional characteristic distribution and velocity changes for solid-air mixture in pipe cross-sectional area	35
Figure 4.1. 11×11 rectangular array with the cross-section of the pipe m onto it showing sensor positions	47
Figure 4.2. General imaging sensor arrangement	48
Figure 4.3. Sequence of operations	49

	<u>Page</u>
Figure 4.4. Cross correlation solids velocimeter using electrodynamic sensors.	50
Figure 4.5. Output signal of electrostatic sensor and processing results	55
Figure 5.1. The ring type-electrode and vacuum-tube-preamplifier	57
Figure 5.2. Representation the voltage and charge induced on the ring electrode	58
Figure 5.3. The basic representation of the test rig to measure the charge	59
Figure 5.4. The illustration of ring shaped probe and its wires and measurement connection	60
Figure 5.5. The schematic representation of ring sensor	61
Figure 5.6. Basic schematic of ring-probe	62
Figure 5.7. Estimated illustration of the impulse response	63
Figure 5.8. Estimated frequency response of the ring sensor	63
Figure 5.9. Model for the charged-particle, ring probe, wire and device for measurement	64
Figure 5.10. Model of ring-probe and measuring instrument for a point-charge	66
Figure 5.11. Basic ac signal representation the probe interaction with single point	67
Figure 5.12. Sensing levels of narrow probes	68
Figure 5.13. Sensing levels of narrow probes ($W/R=1$)	68
Figure 5.14. Probe geometry affecting on spatial-sensitivity	69
Figure 5.15. The resultant signal.....	69
Figure 5.16. Representation of charge variation with different widths	73
Figure 5.17. Relative error owing to particle size	74
Figure 5.18. For values $R=150$ mm, $V=15$ m/s, $W/R=0.5$, spatial sensitivity in frequency domain	76
Figure 5.19. The charge Amplifier	76
Figure 5.20. The transfer function of ring probe	76
Figure 5.21. For values $R=150$ mm, $V=25$ m/s, $W=40$ mm frequency characteristic of the probe.	77
Figure 5.22. For values $R=150$ mm, $V=25$ m/s, $W=40$ mm frequency characteristic of the probe sensor	77
Figure 6.1. Three electrode system: the net electric charge of solid particle in the sensing zone (1), the metal ring probe (2), and grounded electromagnetic screen.....	84
Figure 6.2. Full circuit diagram of the modeled source of a useful signal, of the real	

	<u>Page</u>
electrostatic flow probe and measuring preamplifier(a) and simplified model	85
Figure 6.3. Common electrodes used in electrostatic flow sensor.....	85
Figure 6.4. Fully ring sensor installed flush with pipe	86
Figure 6.5. Measuring head cross-section of rod electrostatic sensor	86
Figure 6.6. Measuring head cross-section of ring-shape electrostatic sensor.....	86
Figure 6.7. Sensing System: equivalent circuit and charge amplifier.....	87
Figure 6.8. Equivalent circuit diagram of the active four terminal network made up of the alternating current generator ,probe and preamplifier	88
Figure 6.9. Simulated frequency characteristic of the whole four terminal network (1),probe(2), and preamplifier (3) for $\tau=750\mu\text{s}$ and $ku = 1$	88
Figure 7.1. General diagram of the test rig	90
Figure 7.2. The view of test rig.....	91
Figure 7.3. The cross-section of test rig and test materials.....	92
Figure 7.4. The measuring head of test rig with comprehensive model.	93
Figure 7.5. The measuring head of test rig with simplified model	93
Figure 7.6. The views of test materials used in test rig.....	94
Figure 7.7. The peak to peak voltages of selected electrodes according to test material-1.....	96
Figure 7.8. The peak to peak voltages of selected electrodes according to test material-2.....	96
Figure 7.9. The peak to peak voltages of selected electrodes according to test material-8.....	97
Figure 7.10. The peak to peak voltages of selected electrodes according to test material-8.....	97

LIST OF SYMBOLS and ABBREVIATIONS

- A Cross sectional area of a circular pipe
- $A(r,W)$ Systematic factor of the circular electrode. It is dependent on electrode width and radius coordinate r and mainly determine the amplitude of charges on the electrode
- $h(t)$ Unit impulse response of the circular electrode
- $H(\bar{\omega})$ Transfer function of the circular electrode
- Con Static expression of concentration (solids mass to air volume ratio)
- $con(t)$ The fluctuation in the concentration, it is usually regarded as a bandwidth limited white noise
- Con(t) Concentration stochastic process
- $\overline{Con(t)}$ Mean concentration, emphasize it is a function of time
- $Con(\bar{\omega})$ Fourier transform function of Con(t)
- con_{rms} Root mean square (rms) value of the fluctuation in concentration
- $conm_{rms}$ rms value of mass concentration fluctuation
- Con(u,v) Concentration at location (u,v) on a given cross sectional area
- Con(x,t) Concentration wave-form along the pipeline
- \overline{ConA} Average concentration over the pipe cross-sectional area.
- Con_m Solids mass to air mass ratio mass concentration
- $\overline{Con_m}$ Average mass concentration (solids mass to air mass ratio)
- $con(\bar{\omega})$ Average mass concentration (solids mass to air mass ratio)
- conrm) Fourier transform function of the fluctuation $con(t)$ in concentration
- $con_T(t)$ sample of $con(t)$, sampling length is T
- $con(\bar{\omega}, T)$ Fourier transform function of $con_T(t)$
- D(t) Particle size diameter, emphasizing its stochastic characteristics vary with time
- $f\{D\}$ The size probability density function of particles
- $f\{D,t\}$ Size probability density function of the particles at time t
- $q(t)$ Fluctuation in charges carried by solids in the entire sensing volume
- $q_{rms}(t)$ rms value of $q(t)$
- Q(t) Charge carried by particles in the entire sensing volume
- $\overline{Q(t)}$ Mean charge carried by particles in the entire sensing volume
- $R_{qq}(\tau)$ Auto correlation function of stochastic process $q(t)$

$R_{cc}(\tau)$ Auto correlation function of bandwidth limited white noise $con(t)$
 $R_{c1c2}(\tau)$ Cross correlation function of fluctuation in concentration
 $R_{UU}(\tau)$ Sensor's output auto correlation function
 $R_{U1U2}(\tau)$ Cross correlation function of signals from two identical sensors mounted upstream and downstream in the flow respectively
 $s(r,W,x)_I$ Charge induced on the electrode of width W due to the single unit charged particle at location (r,x)
 $s(r,W,x)$ Charge induced on the electrode of width W due to the single charged particle located at (r,x)
 S_r Charges induced on the electrode due to a concentration streamline over the entire sensing volume
 S Total induced charge on the circular electrode
 Δ Definitive error
 β Surface charge density
 δ Relative error
 ϕ Electrode diameter factor
 Γ function
 λ Wavelength
 ρ_m Density of the particle material
 ρ_{air} Air density
 σ_D Standard deviation of particle size diameter
 $\sigma_q(t)$ Root mean square of $q(t)$

1. INTRODUCTION

1.1 Problem Statement

Transporting solid particles in air streams are widely used in many industrial applications, including power plants, plastics industries, paint operations, etc. Conveying solid particles in a controlled environment is a difficult task requiring an effective control of different variables that exist in the system. Online continuous measurement of the flow parameters of pneumatically conveyed particles is often required to carry out an optimum process and particularly non-intrusive ones are preferred. Some challenging properties of pneumatic processes are caused by nonuniform flowing of solids, fluctuating velocity in the pipe, irregular particle size in the pipe and moisture content of particulate materials.

Electrodynamic measurement technology requires multi-disciplinary work, such as electrical engineering, physics, chemistry and fluid dynamics. Unification of the theoretical studies in diverse fields can be quite challenging.

Recently electrostatic monitoring technologies have been applied to some fields such as prognostics and health management, aero-engine, condition-based maintenance, wear debris detection in lubrication oil. New application areas require highly sensitive and sustainable readout circuits and mechanical layouts. Conventional readout circuits often yield very low current levels with high levels of noise. Recent developments in electronics facilitate the measurement of very low currents in the measurement of flow parameters in multiphase flow regimes and new readout systems must be designed.

1.2 Research Objectives

The main objective of this thesis is to identify possible academic and engineering applications of the measurement of the flow regime parameters, determining different application areas, building an adaptable test rig for different application areas, designing a new measuring front-end for measurements.

1.3 Scope and Limitations

There are many fields, such as magnetic resonance, contact friction, electrostatics, etc, that are used for the measurement of mass flow rates. Each field may require distinct setups and equipment for measurements, the scope of this thesis is limited to electrostatic measurements. In order to simplify the test rig construction, a vertical setup based on gravity is developed and experimental studies were limited with gravitational velocity. Different particles made of various materials are used in the experiments. Each particle

is charged and allowed to fall through the sensor setup. The aim of this study is limited to test rig setup, charge amplifier setup and measurement of velocity of the particles passing in the sensor.

1.4 Research Contributions

There has been an extensive literature on the subject that has been developed by various researches over decades. A summary of the theoretical foundation of flow regimes based on electrostatics is given in this study since most of the articles are focused on the research contributions and ignored the fundamental theories. In this study, it is intended to give a literature review starting from basic theories to recent developments in online flow parameter measurements based on electrostatics. Literature review about electrostatic measurement of mass flow rates, including recent works, has been presented. A test rig has been designed in order to carry out different measurement experiments using new and improved integrated circuits and charge amplifiers. A highly sensitive front end was designed in order to gauge charges, even, ions and electrons. A compact test rig is constructed to conduct experiments.

2. BASIC CONCEPT, CHARGING AND DISCHARGING

2.1 Electrostatics

Electrostatics is a branch of physics that studies electric charges at rest. It has been known that some materials collect charge inside such as amber attracts lightweight particles after rubbing. This phenomenon arises from the forces that electric charges exert on each other. The development of electrostatic theory in elementary physics started with the experimental Coulomb's law, which is formulated in 1785, for the investigation of the force between two point-charges. Static electricity is one of the first phenomena to be known in physics as, an imbalance of electric charges within or on the surface of a material. The theory is developed in order to understand the creation and transfer of electric charges at rest. All the materials are made of atoms, which are normally electrically neutral and containing equal numbers of positive charges in their nuclei, whereas negative charges, i.e., electrons in shells surrounding the nucleus. The phenomenon of static electricity requires a separation of positive and negative charges.

In the context of electricity, the “electrical” term is first named by William Gilbert in the 16th century after well-known friction experiment that is done by rubbing amber against resin-based material. Although atmospheric static electricity was previously defined by Benjamin Franklin, the fundamental studies on electrostatic was carried out by scientists like Coulomb, Faraday, Maxwell, and Gauss. The basic research leads to the foundation of electrostatics field in the 19th century.

Electrostatic-processes are differentiated from electromagnetic-processes in terms of storage medium and travelling charges since electrostatics is an intermittent and very slow, even stationary process. Because of this fact, magnetic fields created by moving charges are often neglected in order to evaluate the effects of electrostatics alone.

When two or more dissimilar materials are brought into contact and then separated, an electrical charge is transferred from one to the other. After separation, the materials like solids remain with an equal net charge of opposite sign. This phenomenon is known as contact charging or contact electrification. Two different materials are either rubbed or approached, it is called frictional electrification, tribo-charging, triboeffect or tribo electrification. When these particles are in short contact, it can be called impact charging. In order to name the frictional electrification, Ancient Greeks used the term tribo, which means rubbing. The word electricity originates from the Greek word used for amber to explain the charging produced after rubbing amber with fur. Consequently, the fur is

charged positively whereas the amber is negatively charged. As a similar example, triboelectric charging can be obtained when rubbing a balloon against a human's head or arm. In this case the balloon is charging negatively and the hair on the head or arm of the person is positively charged. The amount of accumulated charge on the balloon can be in the order of tens of kilovolts. When the balloon is placed near a grounded surface, a discharge or spark can be observed due to flow of charge to the ground. Different materials may attract different polarities of electricity depending on the materials involved in the experiment.

The lists as given in Table 2.1 are called the triboelectric series. Shaw [1] is the first to develop the triboelectric series in 1917 in order to explain charge transfer between materials. He rubbed a variety of materials together and used an electroscope to measure the charge on their surfaces. He showed that some materials are more probably to charge negatively than positively, and vice versa as given in Table 2.1. Based on these results, Shaw proposed that for a specific pair of materials that are rubbed against each other, one material that charged negatively would be the one more probably to acquire electrons. The other, which is charged positively would give up electrons. Over the past century, this model, based on electron transfer between materials has been discussed against alternative mechanisms involving other charged materials. The fundamental work done by Shaw has been utilized to explain the contact charging phenomenon.

In triboelectric charging, it is uncertain why a large quantity of charges transfer occurs between the surfaces and what causes the polarity of each surface. Typically, when two surfaces contact each other, there is lateral motion or rubbing. On the other hand, if there is no lateral motion, this is known as contact electrification. The amount of charges accumulated and the polarity of the surface charge are accepted as the results of different material properties, such as electronic properties, hydrophilicity, surface roughness, surface stress or strain, impurities and other properties, has been described empirically by the triboelectric series which is not fully understood. Charged particles, also, cause various secondary phenomena in some applications yielding unwanted results. Repeatability is another problem since most of the experiments have been carried out under undefined conditions. In the last decade, a continuous progress has been made towards the understanding of the contact electrification of solids, mainly because of the rapid developments in theory and experimental solutions developed in solid state and surface physics. However, the exact physical phenomenon is not solved with some unexplained

points [2].

The contact charging has different properties that make the process beneficiary and at the same time hazardous. Charged particles are widely used in many industrial applications, such as in charging of fine particles, precharging of fabric filter, electrostatically enhanced cyclone separators, dry powder coating, fly ash collection, filtration with fabrics, environmental dust separation, gas cleaning, oil mist filtration electrophotography, electrostatic precipitator, separation of powder, and impurities from minerals electromechanical particulate operation, powder flow measurement, tomography aerosol particle collection pneumatic conveying, fluidized beds, pharmaceuticals and biomedical.

Tribocharging is not always useful. The hazardous side of tribocharging is the effect of shocks experienced by human when touching a grounded metal surface after walking on an insulating carpet in dry air. This aspect causes severe problems in industrial processes for example, sparks caused by the contact of charged surfaces may lead to fire hazards in manufacturing plants. Static charging of textiles and clothing can cause fires and explosions and dust explosions can occur in powder technology. Striking evidence for the harmful effect of triboelectrification is experienced in the explosion of supertankers in the 1970's, rockets during unloading and cars during refueling. Besides a wide range of operational problems, triboelectrification is thought to take place in dust explosions and natural phenomena such as sand storms, dust devils, lightning and volcanic plumes.

Table 2.1. List of triboflow series for some commonly materials [3].

Positive -->>	Polyformaldehyde 1.3-1.4	Polyisobutylene	Negative -->>
	Etylcellulose	Polyuretane flexible sponge	
	Polyamide 11	Polyethylene Terephthalate	
	Polyamide 6-6	Polyvinyl butyral	
	Melanime formol	Polychlorobutadiene	
	Wool, knitted	Natural rubber	
	Silk, woven	Polyacrilonitrile	
	Aluminum	Acrylonitrile-vinyl chloride	
	paper	Polybisphenol carbonate	
	Cotton, woven	Polychloroether	
	Steel	Polyvinylidene chloride (Saran)	
	Wood	Polystyrene	
	Hard rubber	Polyethylene	
	Nickel, copper	Polypropylene	
	Sulfur	Polyimide (Kapton)	
	Brass, silver	Polyvinyl Chloride (PVC)	
	Acetate, Rayon	Polydimethylsiloxane (PDMS)	
	Polymethyl methacrylate (Lucite)	Polytetrafluoroethylene (Teflon)	
	Polyvinyl alcohol	Polyvinyl alcohol	
	Aniline-formol resin	Polyester (Dacron) (PET)	
	Polyformaldehyde 1.3-1.4	Polyisobutylene	
	Etylcellulose	Polyuretane flexible sponge	
	Polyamide 11	Polyethylene terephthalate	
	Polyamide 6-6	Polyvinyl butyral	
	Melanime formol	Formo-phenolique, hardened	
	Wool, knitted	Polychlorobutadiene	
	Silk, woven	Butadiene-acrylonitrile copolymer	
	Polyethylene glycol succinate	Nature rubber	
	Cellulose	Polyacrilonitrile	
	Cellulose acetate	Acrylonitrile-vinyl chloride	
	Polyethylene glycol adipate	Polybisphenol carbonate	
	Polydiallyl phthalate	Polychloroether	
	Cellulose (regenerated) sponge	Polyvinylidene chloride (Saran)	
Cotton, woven	Poly(2,6-dimethyl polyphenyleneoxide)		
Polyurethane elastomer	Polystyrene		
Styrene-acrylonitrile copolymer	Polyethylene		
Styrene-butadiene copolymer	Polypropylene		
Wood	Polydiphenyl propane carbonate		
Hard rubber	Polyimide (Kapton)		
Acetate, Rayon	Polyethylene terephthalate		
Polymethyl methacrylate (Lucite)	Polyvinyl Chloride (PVC)		
Polyvinyl alcohol	Polytrifluorochloroethylene		
Polyester (Dacron)	Polytetrafluoroethylene (Teflon)		

Triboelectrification can occur not only in industrial processes but also in natural environments. The effect can be one of the factors associated with dust devils and sand storms which are observed in nature. When the wind blows, sand particles are picked up from the ground and the force of the wind causes particles to collide and collect charge. Lightning and volcanic lightning are also caused by triboelectrification of ice particles and volcanic ash, respectively, producing large potentials to cause atmospheric breakdown. While triboelectrification often causes troubles, in some applications, such as ink-jet printing, and xerography and powder coating processes benefit from this phenomenon. The toner in xerography, which is composed of toner particles with sizes ranging from 5 to 10 microns in diameter, is sprayed on a component made from a clear thermoplastic with colorant and charge control agents. The laser printer determines the polarity and amount of charging when mixed with the carrier beads. Carrier beads usually triboelectrically charge the toner particles, and this mixture is known as the component known as developer. In order to copy an image on a sheet of the paper, a charged particle is deposited on the paper using a corona discharge reflecting the image. When charged toner electrostatically adheres to the image charge on the paper, the sheet of paper is warmed and thermoplastic is molded on the paper surface, producing the desired copy of image [4].

2.2 Electrostatic Theory

Electrostatics is a branch of physics that aims to explain concepts relating charges at rest. such as charges, contact charging, induction charging and electric fields.

2.2.1 Unit of electric charge

The charge value of an electron is $e = -1.602 \times 10^{-19}$ coulombs (C) The electron charge is the fundamental unit charge in electrostatics. All calculations are carried out using this constant value.

2.2.2 Fundamental electromagnetic field equations

Electromagnetism is related but not directly involved with electrostatics however a brief introduction to electromagnetics is given in this section for the sake of conciseness since most equations with electrostatics is shared when electrostatic charges move slowly in a material. Some fundamental equations are given below

$$D = \epsilon E \frac{C}{m^2} \quad (2.1)$$

$$D = \epsilon E, \epsilon = \epsilon_r \epsilon_0, \epsilon = (1 + \chi) \epsilon_r \quad (2.2)$$

$$B = \mu H T \quad (2.3)$$

$$c = \frac{1}{\sqrt{\mu_0 \epsilon_0}} \quad (2.4)$$

where $\mu = \mu_r \mu_0, C \cong 3 \times 10^8$, $\mu_0 = 4\pi \times 10^{-7} \text{ H/m}$, $\epsilon_0 = \frac{1}{36\pi} \times 10^{-9} = 8.854 \times 10^{-12} \text{ Fm}$,

E : electric field intensity V/m D : electric flux density (electric displacement) C/m^2 ,

B : magnetic flux density T , H : magnetic field intensity A/m .

2.2.3 Gradient of a scalar field

The gradient of any scalar field is defined as the summation of the rate change of the field along each spatial axis, thus the gradient is a vectorial quantity. It is defined as vector that represents both the magnitude and the direction of the maximum space rate of increase of a scalar as the gradient of that scalar as follows [5].

$$\text{grad } V = \nabla V \triangleq a_n \frac{dV}{dn} = \left[a_x \frac{\partial}{\partial x} + a_y \frac{\partial}{\partial y} + a_z \frac{\partial}{\partial z} \right] V \quad (2.5)$$

2.2.4 Divergence theorem

It is defined that the volume integral of the divergence of a vector field equals the total outward flux of the vector through the surface that bounds the volume;

$$\int_V \nabla \cdot A \, dv = \oint_S A \cdot dS \quad (2.6)$$

The Divergence theorem is utilized to transform a triple-integral operation to a dual-integral operation

Divergence of a vector field is calculated as follows

$$\text{div } A = \nabla \cdot A = \frac{\partial A_x}{\partial x} + a_y \frac{\partial A_y}{\partial y} + a_z \frac{\partial A_x}{\partial z} \quad (2.7)$$

2.2.5 Curl of a vector field

The curl of a vector field A , denoted by $\text{curl } A$ or $\nabla \times A$, is a vector whose magnitude is the maximum net circulation of A per unit area as the area is inclined to zero. Its direction is the normal direction of the area when the area is oriented to make the net circulation maximum [5].

$$\text{curl } A = \text{rot } A \equiv \nabla \times A = \begin{vmatrix} a_x & a_y & a_z \\ \frac{\partial}{\partial x} & \frac{\partial}{\partial y} & \frac{\partial}{\partial z} \\ A_x & A_y & A_z \end{vmatrix} \quad (2.8)$$

2.2.6 Stokes theorem

The theorem states that the surface integral of the curl of a vector field over an open surface is equal to the closed line integral of the vector along the contour bounding the surface and it gives the relationship between a surface integral of the curl of the vector

field and a line integral of the vector field around the edge of the surface.

$$\int_s (\nabla \times A) \cdot dS = \oint_c A \, dl \quad (2.9)$$

$$E = -\text{grad } V = -\nabla V \quad (2.10)$$

$$\nabla \times (\nabla V) \equiv 0 \quad (2.11)$$

$$\nabla \cdot (\nabla \times V) \equiv 0 \quad (2.12)$$

2.2.7 Electrostatics in free space

Two fundamental postulates of electrostatics in free space specify the divergence and curl of E , the electric field [5]. It is stated that static electric fields are irrotational. Postulates of electrostatics in free space both differential and integral form are given below:

Differential Form

$$\nabla \cdot E = \frac{\rho}{\epsilon_0} \quad (2.13)$$

$$\nabla \times E = 0 \quad (2.14)$$

Integral Form

$$\oint_s E \cdot ds = \frac{Q}{\epsilon_0} \quad (2.15)$$

$$\oint_c E \cdot dl = 0 \quad (2.16)$$

2.2.8 Electric potential

Similar to the concept of potential energy in mechanics, Eq. (2.21) represents the difference in electric potential energy of a unit charge between point P_2 and point P_1 . Expressing the electric potential energy per unit charge by V , the electric potential is given as follows

$$\frac{W}{q} = V_2 - V_1 = -\int_{P_1}^{P_2} E \cdot \bar{dl} \quad (2.17)$$

2.2.9 Boundary conditions

Boundary conditions are essential to solve electrostatic problems for medium changes. Electromagnetic problems usually include media having different physical properties and require the knowledge of the relations of the field quantities at an interface between two media. Basically, it is needed to determine how the E (electrical field density) and D (electrical flux density) vectors change in crossing an interface [5]. It is stated that the tangential component of an E field is continuous across an interface and the normal component of D field is discontinuous across an interface where a surface

charge exists. The amount of discontinuity is equal to the surface charge density.

Tangential components are given below:

$$E_{1t} = E_{2t} \quad \left(\frac{V}{m}\right) \quad (2.18)$$

Normal components are given below

$$D_{1n} = D_{2n} \quad \left(\frac{C}{m^2}\right) \quad (2.19)$$

$$D_1 = \epsilon_1 E_1, \quad D_2 = \epsilon_2 E_2 \quad (2.20)$$

where D_1, D_2 are electric flux densities and E_1, E_2 are electric field intensities.

The equations for the boundary conditions is given as follows

$$\begin{aligned} \Phi(r, \theta, z)|_{(r, \theta, z) \in \Gamma_p} &= 0 \\ \Phi(r, \theta, z)|_{(r, \theta, z) \in \Gamma_s} &= 0 \\ \Phi(r, \theta, z)|_{(r, \theta, z) \in \Gamma_e} &= c \end{aligned} \quad (2.21)$$

where $\Gamma_p, \Gamma_s, \Gamma_e$ are the boundaries of the pipe, the insulator and the electrode, respectively and c is any constant.

2.2.10 Coulomb's law

Coulomb's law defines the amount of force between two electrically charged but stationary particles. The electric field intensity of a positive point charge is in the outward radial direction and has a magnitude proportional to the charge and inversely proportional to the square of the distance from the charge [5].

The law can be represented as electrostatic force

$$\mathbf{F} = \frac{q_1 q_2}{4\pi\epsilon_0 R^2} \mathbf{a}_R \quad (2.22)$$

or as an electric field below

$$\mathbf{E} = -\nabla V = \frac{q}{4\pi\epsilon_0 R^2} \mathbf{a}_R \quad (2.23)$$

or an electrostatic potential as follows

$$V = \frac{p}{4\pi\epsilon_0 R^2} a_R \quad (2.24)$$

2.2.11 Gauss' law

Gauss's law states that the total outward flux of the E -field over any closed surface in free space is equal to the total charge enclosed in the surface divided by ϵ_0 .

$$\oint_s E \cdot ds = \frac{Q}{\epsilon_0} \quad (2.25)$$

2.2.12 Electric dipole

Electrical dipole defines the relationship of two equal charges and it is frequently used in electrostatic related studies. Electric dipole is defined as the product of the charge q and the vector d (going from $-q$ to $+q$) as the electric dipole moment, p [5]. As shown below, electric dipole consists of a pair of equal and opposite charges $+q$ and $-q$, separated by a small distance, d ,

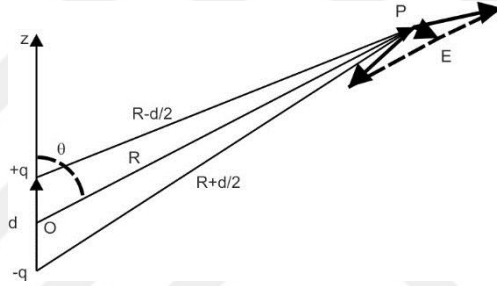


Figure 2.1 Representation of fundamental electric dipole [5].

$$E = \frac{q}{4\pi\epsilon_0} \left[\frac{R - \frac{d}{2}}{|R - \frac{d}{2}|^3} - \frac{R + \frac{d}{2}}{|R + \frac{d}{2}|^3} \right] \quad (2.26)$$

$$E \cong \frac{q}{4\pi\epsilon_0 R^3} \left[3 \frac{Rd}{R^2} R - d \right] \quad (2.27)$$

$$E \cong \frac{p}{4\pi\epsilon_0 R^3} \left[3 \frac{Rp}{R^2} - p \right] \quad (2.28)$$

$$E = \frac{p}{4\pi\epsilon_0 R^3} [a_R^2 \text{Cos}\theta + a_\theta \text{Cos}\theta] \text{ (V/m)} \quad (2.29)$$

$$P = qd \text{ and } R \cdot p = Rp \text{Cos}\theta \quad (2.30)$$

Equipotential and electric field lines of an electric dipole are represented in Figure 2.2;

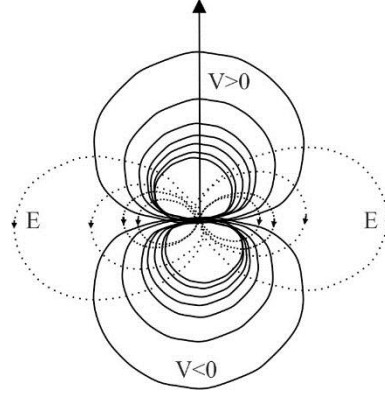


Figure 2.2 Equipotential and electric field curves of an electric dipole [5].

$$V = \frac{q}{4\pi\epsilon_0} \left(\frac{1}{R_+} - \frac{1}{R_-} \right) \quad (2.31)$$

$$V = \frac{qd\cos\theta}{4\pi\epsilon_0 R^2} = \frac{pa_R}{4\pi\epsilon_0 R^2} \quad (V) \quad (2.32)$$

2.2.13 Electric field equation

$$E = -\nabla V = -a_R \frac{\partial V}{\partial R} - a_\theta \frac{\partial V}{R\partial\theta} = \frac{p}{4\pi\epsilon_0 R^3} [a_R^2 \cos\theta + a_\theta \cos\theta] \quad (V/m) \quad (2.33)$$

$$V = \frac{1}{4\pi\epsilon_0} \int_v \frac{\rho_v}{R} dv \quad (2.34)$$

$$V = \frac{1}{4\pi\epsilon_0 R^3} \int_s \frac{\rho_s}{R} dS \quad (2.35)$$

$$V = \frac{1}{4\pi\epsilon_0 R^3} \int_l \frac{\rho_l}{R} dl \quad (2.36)$$

2.2.14 Poisson's and Laplace's equations

Poisson's equation is calculated:

$$\begin{aligned} \nabla^2 V &= -\frac{\rho}{\epsilon} \quad (2.37) \\ \nabla^2 V &= \nabla \cdot \nabla V = \left(a_x \frac{\partial}{\partial X} + a_y \frac{\partial}{\partial Y} + a_z \frac{\partial}{\partial Z} \right) \cdot \left(a_x \frac{\partial V}{\partial X} + a_y \frac{\partial V}{\partial Y} + a_z \frac{\partial V}{\partial Z} \right) \\ &= \left(a_x \frac{\partial^2 V}{\partial X^2} + a_y \frac{\partial^2 V}{\partial Y^2} + a_z \frac{\partial^2 V}{\partial Z^2} \right) = -\frac{\rho}{\epsilon} \quad (V/m^2) \quad (2.38) \end{aligned}$$

For cylindrical coordinates:

$$\nabla^2 V = \frac{1}{r} \frac{\partial V}{\partial r} \left(r \frac{\partial V}{\partial r} \right) + \frac{1}{r^2} \left(\frac{\partial^2 V}{\partial \phi^2} \right) + \frac{\partial^2 V}{\partial z^2} \quad (2.39)$$

For spherical coordinates:

$$\nabla^2 V = \frac{1}{R^2} \frac{\partial V}{\partial R} \left(R^2 \frac{\partial V}{\partial R} \right) + \frac{1}{R^2 \sin\theta} \frac{\partial}{\partial \theta} \left(\sin\theta \frac{\partial V}{\partial \theta} \right) + \frac{1}{R^2 \sin^2\theta} \left(\frac{\partial^2 V}{\partial \phi^2} \right) \quad (2.40)$$

At any point having no free charge $\rho = 0$, it is called Laplace's equation.

$$\nabla^2 V = 0 \quad (2.41)$$

2.2.15 Method of images

There are some solution approaches for electrostatic problems. One of them is method of images used for particle velocity in pneumatic coal injection systems by Woodhead [6]. There is a class of electrostatic problems with boundary conditions that requires the solution of Poisson's or Laplace's equation directly, but the conditions on the bounding surfaces can be set up by appropriate image (equivalent) charges, and the potential distributions can then be determined in a straightforward manner. In this approach, the bounding surfaces are replaced by appropriate image charges calculated by the solution of Poisson's or Laplace's equations. This method is called the method of images [5]. Point charge and grounded plane conductor are presented in Figure 2.3

There are some rules to be followed:

1. At all points on the grounded conducting plane, the potential is zero; that is, $V(x, 0, z) = 0$

2. At points very close to Q the potential approaches that of the point charge alone; that is $V \rightarrow \frac{Q}{4\pi\epsilon_0 R}$, as $R \rightarrow 0$

where R is the distance to Q .

3. At points very far from Q ($x \rightarrow \pm\infty, y \rightarrow +\infty, z \rightarrow \pm\infty$) the potential approaches zero.

4. The potential function is even with respect to the x and z coordinates; that is, $V(x, y, z) = V(-x, y, z)$ and $V(x, y, z) = V(x, y, -z)$

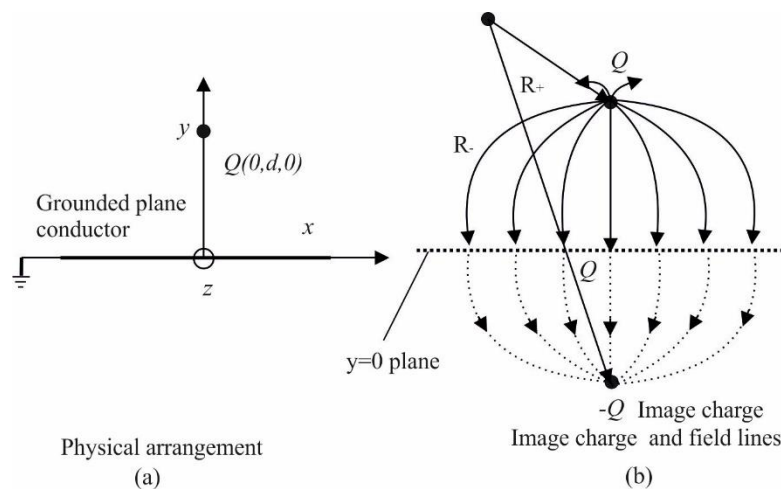


Figure 2.3 Point charge and grounded plane conductor [5].

$$V(x, y, z) = \frac{Q}{4\pi\epsilon_0\sqrt{z^2+(y-d)^2+z^2}} + \frac{1}{4\pi\epsilon_0} \int_S \frac{\rho_s}{R_1} ds \quad (2.42)$$

The method can be used for point charge and perpendicular conducting planes, as depicted in Figure 2.4

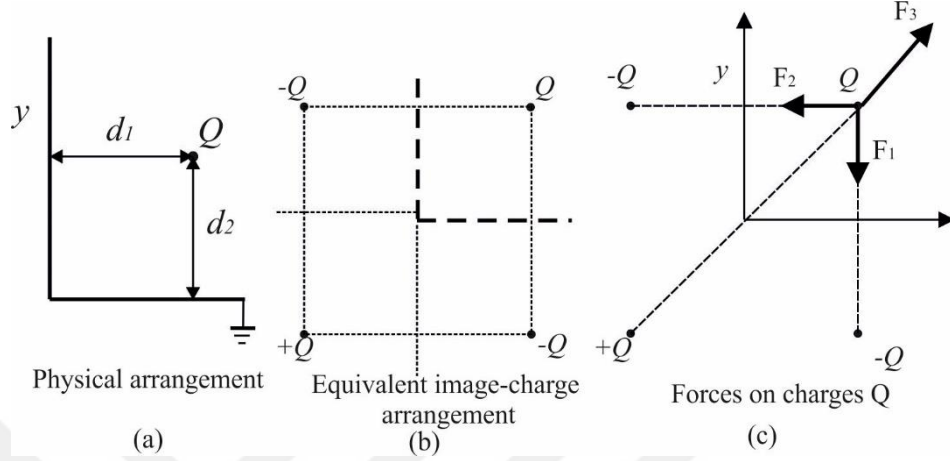


Figure 2.4 Point charge and perpendicular conducting planes [5].

Net force on Q is given as follows

$$F = F_1 + F_2 + F_3 \quad (2.43)$$

$$= \frac{Q^2}{16\pi\epsilon_0(2d_2)^2} \left\{ a_x \left[\frac{d_1}{(d_1^2 + d_2^2)^{\frac{3}{2}}} - \frac{1}{d_1^2} \right] + a_y \left[\frac{d_2}{(d_1^2 + d_2^2)^{\frac{3}{2}}} - \frac{1}{d_2^2} \right] \right\} \quad (2.44)$$

$$F_1 = -a_y \frac{Q^2}{4\pi\epsilon_0(2d_2)^2} \quad (2.45)$$

$$F_2 = -a_x \frac{Q^2}{4\pi\epsilon_0[(2d_1)^2 + (2d_2)^2]^{\frac{3}{2}}} \quad (2.46)$$

$$F_3 = \frac{Q^2}{4\pi\epsilon_0(2d_2)^2} (a_x 2d_1 + a_y 2d_2) \quad (2.47)$$

The potential at this point

$$V = \frac{q}{4\pi\epsilon_0} \left(\frac{1}{R_+} - \frac{1}{R_-} \right) \quad (2.48)$$

$$R_- = \sqrt{z^2 + (y-d)^2 + z^2} \quad (2.49)$$

$$R_+ = \sqrt{z^2 + (y+d)^2 + z^2} \quad (2.50)$$

It appears that it is mathematically difficult to construct a solution for V that will satisfy all of these conditions.

2.3 The Measurement of Charge

One of the well-known methods of measurement of charge, as presented in Figure 2.5, involves Faraday Cage, namely Faraday Pail. It is simply a shielded metal cup that is wired to a grounded electrometer in other words Coulomb meter. When the charged material is placed into the container, it induces an equal but opposite charge on the surface of the cup which flows to ground through the electrometer. The electrometer indicates the current flowing through it in order to determine the total charge that moved from ground and thus the charge of the material placed into the cup [7].

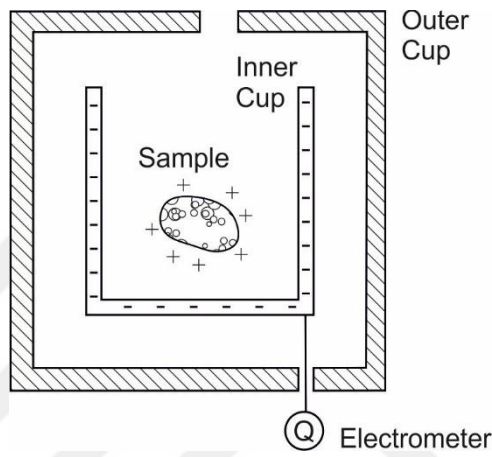


Figure 2.5 A Faraday cage to measure the induction charge [7].

Additionally, as shown in Figure 2.6 some methods of measuring the charge on an insulator are presented [8].

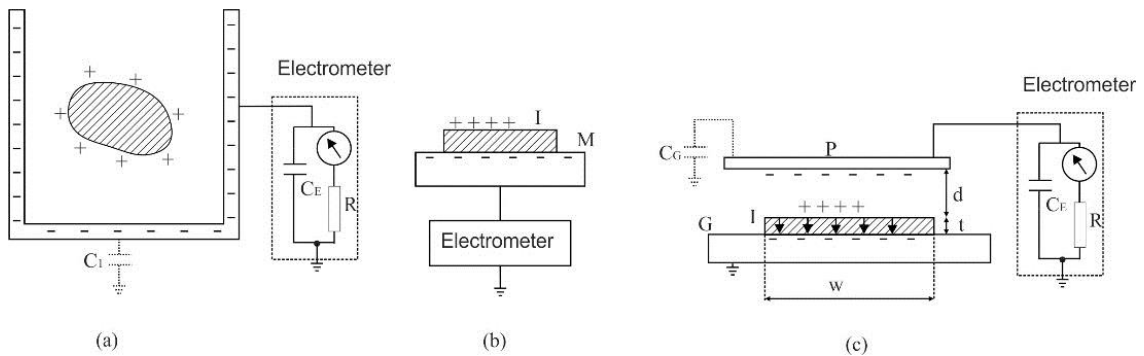


Figure 2.6 The methods of the measuring [8].

2.4 Conductors in Electrostatic Equilibrium

A good electrical conductor includes charges, i.e. electrons, which are not attached to any atom and freely moving within the material. In electrostatic equilibrium there is no net motion of charge within a conductor. A conductor in electrostatic equilibrium has some properties. First, the electric field is zero everywhere inside the conductor, whether the conductor is solid or hollow. Second, if charges are carried by the insulated conductor,

they remain on its surface. Third, the electric field at a point, just outside a charged conductor is perpendicular to the surface of the conductor and has a magnitude given by the formula σ/ϵ_0 , where σ is the surface charge density at that point and ϵ_0 is permittivity of free space. The last, the surface charge density is accumulated at locations where the radius of curvature of the surface is smallest, on an irregularly shaped conductor [9].

2.5 Charging of Materials

Materials can be either charged or neutral state. A Solid, gas, liquid or mixed type of materials can be charged by means of some methods or phenomena. There are three basic charging methods; corona charging, induction charging and contact charging, i.e. tribocharging in transporting, separating and depositing processes and/or sub-processes. There also are different methods for charging by nuclear or ultraviolet (UV) radiation.

2.5.1 Tribocharging and contact charging

When two different materials are brought into contact and then separated, an electric charge is usually transferred from one to the other. This phenomenon is often named contact electrification or contact charging. When they are rubbed against each other, it is named as frictional electrification or tribocharging, and short contact for materials are impact charging [10]. The mechanical systems produce charged materials in situations such as sliding, rolling or milling, impact, vibration of the surface contacts, separation of solid-solid, solid-liquid and liquid-liquid surfaces, and deformation. The relative speed of the particles and the pressure between them determines the outcome of charging. More contact pressure leads to an increased contact point number. In some situation, the surface charge density rises up to 2×10^{13} electrons/m².

There are many unclear effects associated with surface charges and some inconsistent results have been reported. In this part, the basic concepts and theories of charge transfer between solid surfaces will be explain below by formulating a description of particle charging caused by repeated impacts on a wall.

When there are not relative movements between two or more material surface, tribocharging and triboelectric effect can be observed. Contact charging, can also be classified into three categories according to the contacting materials, namely metal–metal contacts, metal–insulator contacts and insulator-insulator contacts.

2.5.1.1 Metal-metal contacts

The mechanism of electrification of metals is a well-known phenomenon. Due to low resistivity and high conductivity of electrons in conductors let electrons to move

freely throughout the materials. After separation, electron surge stops if the space between two surfaces surpasses 1 nanometer. Since charge relaxation time is very short, metal contacts will be neutral quickly. Figure 2.7 shows two metals with different work functions ϕ_1 and ϕ_2 in contact. Charged conductors do not typically retain charge because the excess charge usually flows to ground. However, charges on the conductor will not leave after contact charging if the conductors are separated from ground. The difference in chemical potentials between the two materials lead to some electron transfer. It determines the contact potential difference (CPD) at the point V_c is defined as the difference in the surface potential of the conductors [10]:

$$V_c = \frac{\phi_2 - \phi_1}{e} \quad (2.51)$$

where V_c , ϕ_2 and ϕ_1 are the contact potential, work functions of metals respectively.

The capacitance depends on the state of the contacting part and the charge exchanged by tunneling between the two contacting surfaces can be expressed as:

$$Q = C_{21}V_c \quad (2.52)$$

where C_{21} is the capacitance between the bodies at the critical separation distance.

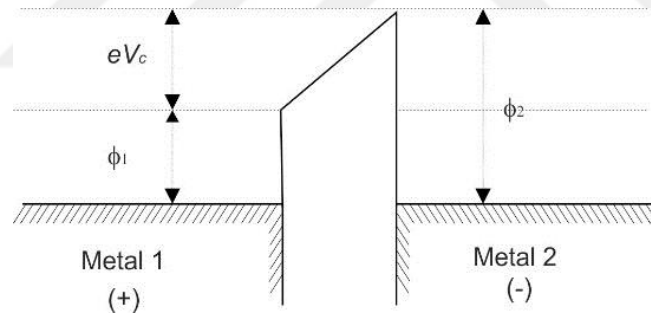


Figure 2.7 Electron potential energy at a metal–metal contact [10].

When two metals are separated from each other, reverse flow of electrons takes place due to tunneling. The tunneling stops when the distance between two surfaces exceeds 1×10^{-9} (nano) m. This distance is varied depending on the surface roughness, impurities, oxidized layer, separation speed, etc. In Figure 2.8, the experimental and theoretical consequences are depicted for the charge after contact [11].

The driving forces of the control parameters; the nature of charge carriers, i.e. electrons, ions and materials, work function, tunneling, energy states, surface state density, formation of contact, area, friction, particle-particle tribocharging.

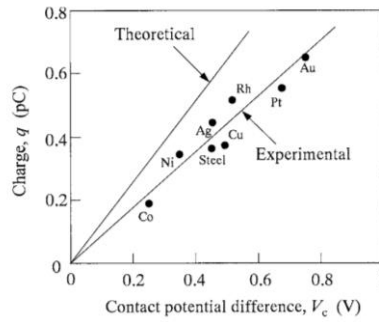


Figure 2.8 Charge on a chromium sphere, 4 mm in diameter, in contact with another metal sphere, 13 mm in diameter, as a function of the CPD of chromium against each metal [11].

Energy bands

The energy bands concept is an important concept to explain electron motion in a charging process. It is supposed that each electron of an insulated atom has a quantum energy depending on its orbit around the nucleus. Each orbit has a discrete energy level, and an electron moving on the orbit possesses that energy level. For solids, there are intense electron exchanges among atoms. The exchange of electrons residing on inner shells does not often happen, but outer shell electron exchanges happen intensely. Figure 2.9 shows that electrons in the conduction band determine the energy level [2].

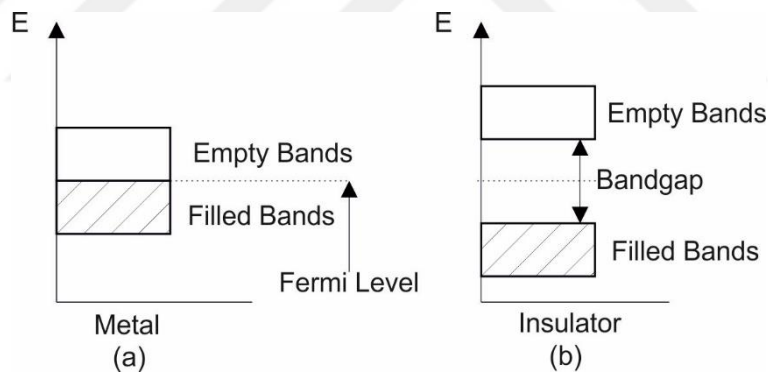


Figure 2.9 The Fermi energy level of metal and insulator [2].

2.5.1.2 Metal-insulator contacts

The concept of contact charging between metals can be utilized to examine charging for metal-insulator contacts [10]. But, experimental data are often distributed widely and inconsistent results are also registered. The linearity constant in this relationship mainly depends on the characteristics of the insulator. Since a linear relationship between the transferred charge and the work function can be attained empirically, the charging probably occurs via the electron transfer and the following relationship can be applied to the electrostatic characterization:

$$Q = C_{MI} \frac{(\phi_M - \phi_I)}{e} \quad (2.53)$$

where C_{MI} is the capacitance between metal and insulator, ϕ_M, ϕ_I are the work functions of the metal and the apparent work function of the insulator, respectively. The proportionality constant in this relationship depends on the characteristics of the insulator. Figure 2.10 shows the linear relationship obtained experimentally by Davies [12]. In order to develop charging characteristics of a powder, charge control agents (CCAs) are used on the powder surface or applied to the bulk powder processes. CCAs used in processes are generally fumed silica or carbosil and kyner, which is a highly fluorinated polymeric material or polyvinylidene fluoride. Bulk charge control agents are added into the polymer

The energy bands for metals and insulators are shown in Figure 2.11.

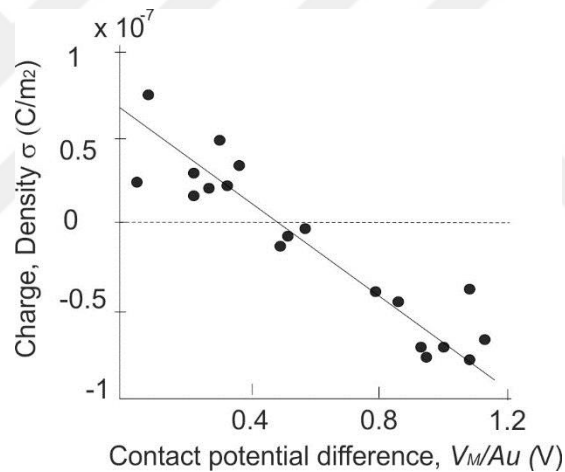


Figure 2.10 Charge density of nylon no: 66 by contacting with various metals. The horizontal axis is the CPD of each metal against a gold reference $V_M=Au$ [12] where the CPD is defined as $V_{Au/M}$ [12].

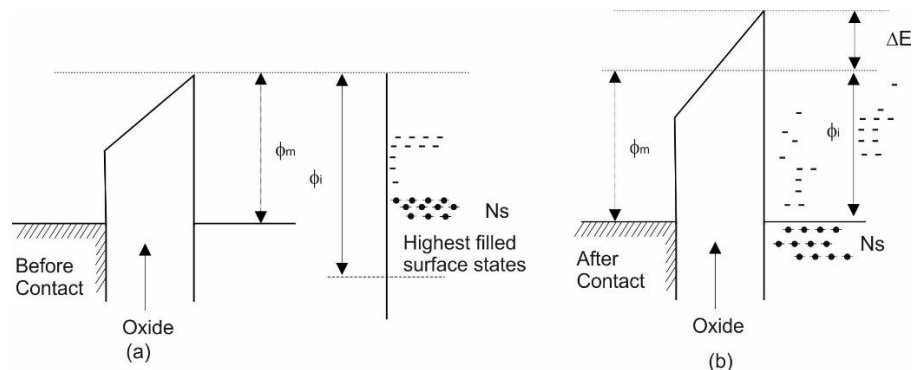


Figure 2.11 Contact charging between coal and metal surface [2].

2.5.1.3 Insulator-insulator contacts

The trend of the charging between insulators can be evaluated using by means of

triboelectric series, where insulators are ordered in a line such that a material is located up and always charge positive when rubbed with a material lower down. But, the results may not be always correct since there is not any formula describing the triboelectric series and only experimental values are available.

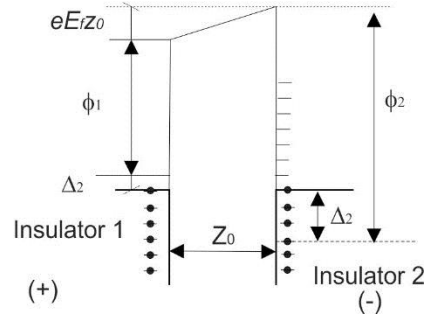


Figure 2.12 Energy level diagram for insulator-insulator contact [10].

Several models have been reported to describe the contact charging between insulators. All of the models are derived considering metal-insulator contact mechanism with limited transfer of electrons or ions in the material. Figure 2.12 shows a contact charging model that accounts for the effect of an electric field if the insulators come in contact. When the contact occurs, charges flow from the filled surface state of the first insulator to the empty surface state of the second insulator. It is supposed that the system stays in equilibrium state during tunneling until the surfaces are separated by a critical distance. The expression for the energy level including the effect of the electric field E_f is given as [10]:

$$\phi_1 + \Delta_1 + eE_f z_0 = \phi_2 - \Delta_2 \quad (2.54)$$

where Δ_1 and Δ_2 are the energy level shifts caused by the charge transfer.

Current flow can be generated by means of ion, electron, and charged material transfer in some electrostatic processes. Some important transfers are explained below.

Electron transfer

Dissimilar metals discharge or charge the surface states of the insulator in metal-insulator contact charge interaction. The phenomenon relies on the position of the surface work function of the insulator in connection with the Fermi level of the metal. There exist various external factors affected in contact charging under ambient conditions. For instance, on a metal oxide layer, the particles are also often coated with an oxide layer or other contaminants may take effect. The contact charge exchange density σ on the insulator can be calculates as follows [2]:

$$\sigma = eN_s(\phi_i + \Delta E - \phi_m) \left(1 + \frac{e^2 N_s d}{\epsilon}\right)^{-1} \quad (2.55)$$

where ϕ_i is the surface work function of the insulator, ϕ_m is the Fermi level of the metal surface, ΔE is the energy gap created by the oxide layer, N_s is the surface state density, eV/m², e is the electronic charge, d is the thickness of the oxide layer, and ϵ is the permittivity of the oxide layer. In the boundary of low surface state density, $e^2 N_s d / \epsilon \ll 1$ and if we include a factor f to symbolize the fraction of geometric area that makes close contact, then Eq.(2.52) can be simplified as:

$$\sigma = f e N_s (\phi_i + \Delta E - \phi_m) \quad (2.56)$$

Above expressions display that contact charging also depends on the surface oxidation and on the density of the surface states. Equations (2.52) and (2.52) exhibit two boundary situations. Low surface density and high surface density conditions are often taken into consideration in the surface state theory of charge transfer. In the first situation, the amount of charge exchanged between the metal and the insulator is equal to the number of surface states, and is low enough that the electric field between the metal and insulator does not cause a significant shift in the insulator energy levels. As the large number of surface states occupied, there is a strong electric field between the metal and insulator that increases the energy levels of the insulator surface states limiting further charge transfer [2]. Role of water is important factor in contact charging [4]. Almost all surfaces are covered with a thin layer of water molecules when exposed to atmospheric environment. The adsorption of water contributes to the surface conductivity and likely affects contact electrification. Moreover, the monolayers of water can act as a connection between the surfaces increasing the effective area of contact.

Ion transfer

Several researchers have suggested that contact charging between a metal and an insulator may be due to the transfer of ions [10]. Insulators may contain ions in the body or on the surface. These ions can be transferred by diffusion, relative acidity, affinities and the kinetic effect based on shearing off. When there are excess levels of ions, ion transfer affects contact charging. However, when the ions are few, electron transfer will limit the contact charging. In the ion transfer model, u_i represents chemical potential. Ion transfer depends on the difference in affinities of two contacting surfaces for specific ions. Harper's model, as discussed by Schein [13] estimates the surface charge density after contact as

$$\sigma_s = N_i e \left(-\frac{u_1 - u_2}{kT} \right) \quad (2.57)$$

where N_i is surface density of ions, and u_1 and u_2 are the potential energies of the two surfaces or their closeness for the ions in the ions transfer process, respectively.

Ion interchange can happen across the contacting double layer, but approximately 10 μ m thick adsorbed water layer may prevent the transmission of electrons. A direct observation of ion transfer in contact charging between a metal and a polymer has been reported in the literature [10].

Material transfer

The collision or friction may transfer some amount of material to the other. For instance, a metal rod sliding over polymer may capture some polymer molecules. The transferred polymer can carry charge and then change the effective contact potential difference between two materials. Additionally, if brittle particles impact on a metal wall, elements of particles can be transferred on the metal surface [10].

Effect of the separation state on charging

The state of separation may lead to particle charging. When the charge transferred to the surface of the insulator move into the metal, in turn, the net charge is decreased. This reduction is influenced by properties of particles such as conductivity, the separation state and the speed of sliding or rolling. Furthermore, the separation process may cause releasing a gaseous discharge during transfer [10].

Friction charging

In addition to the contact process, temperature differences between the contact points are known to be an additional factor affecting triboelectrification. The exchange of charge q can be related to the force F of contact as follows [2]:

$$Q \propto F^\alpha \quad (2.58)$$

where α is a factor range from 0.3 to 1 that varies the type of contact.

Gidaspow et al.[14] considered the impact velocity V and computed the charge exchange following a model developed by Chang and Soo [2] K_1 and K_2 are mechanical properties of the materials with respect to Poisson's ratio and Young's modulus and varies the ratio of the rebound speed to the incoming speed

$$Q = K_1 K_2 |V|^{0.6} d_p^2 \rho_p^{0.8} (\phi_i - \phi_m) \frac{N_i N_m}{N_i + N_m} \quad (2.59)$$

where K_1 and K_2 constants d_p and ρ_p are the particle diameter and density, V is the velocity, ϕ_i and ϕ_m are the work functions of the insulator and metal, respectively, and N_i and N_m are the related surface state densities.

Charge decay

Charge drain in a conductor is very fast, on the other hand, leak-off charge in an insulator material is very slow. The rate of charge decay depends on the resistivity of insulator material. If resistivity of materials are nonlinear, charge decay relies on the voltage across it [2]. The charge-decay q_0 across the dielectric capacitor can be expressed as follows:

$$q = q_0 e^{-\frac{t}{\tau}} \quad (2.60)$$

where ϵ_r material's dielectric constant ϵ_0 the permittivity of free space, ρ material's resistivity and $\tau (= \epsilon_0 \epsilon_r \rho)$ is time constant.

The charge decay time constant can be determined by an experiment.

Current Flow

The flow charge rate means the current:

$$i = \frac{dq}{dt} \quad (A) \quad (2.61)$$

In electrostatic processes, ions, electrons, and charged materials can generate a current flow. The whole current flow can be expressed as follow

$$i_t = i_i + i_p + i_e \quad (2.62)$$

where i_i , i_p , i_e are currents by ions, particles and electrons, respectively.

This equation valid for, such as in a conventional electrostatic powder spray process, all the ions charges the powder particles in the medium.

If the current flows over the surface, the current flow density J (A/m^2) occurs, which is important parameter of electrostatic process. The current is given as

$$i = - \iint J \cdot dA \quad (2.63)$$

where A is the area of surface.

The whole current density can be expressed as follows [2]:

$$J = \sum J_i = \sum n_i q_i \mu_i E = \sigma E \quad (2.64)$$

where n_i , q_i , μ_i are the density-number, charge-magnitude and carrier type mobility. E is the value of electric field. The symbol σ is the conductivity of material.

2.5.2 Induction charging

A conductive material connected to ground is exposed to an electric field and then, is disconnected from ground, it still stays in the presence of this field. This process may cause the charging of particles and then the particles with the electric charges induces conductor. This net induced charge is the opposite in sign to the polarity of the inducing field. The energy requirements for this charge separation can be achieved by the mechanical energy, not the electrical field itself. This method of charging may be used with either liquids or solids. Charging an object by induction does not require contact with the object [2].

As illustrated in Figure 2.13, a spherical conductor is neutral before entering between two parallel charged plates (A). As it comes to close the lower plate (B), it is induced negatively. In the further position, positive charges of the conductor flow to ground (C). Forth, as it approached the ground plate, the sphere is inducing negatively (D). In the last position, the negatively charged sphere moves in the field without electric potential. (E) [2].

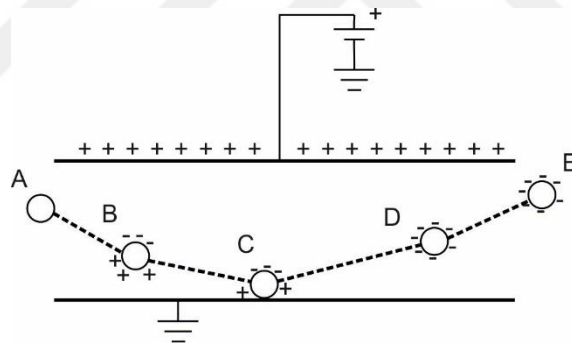


Figure 2.13 Representation of induction charging of neutral metal sphere [2].

In addition to particles, droplets are charged with either the same or the opposite to the polarity of induced electrode, however, mostly contrast charge induction is used. As depicted in Figure 2.14, the droplets are charged by induction [2].

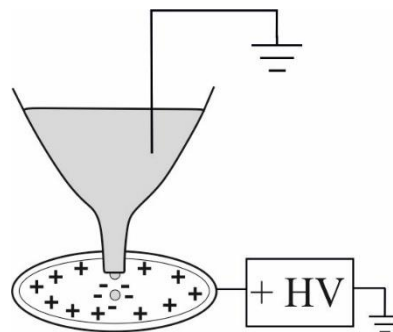


Figure 2.14 Induction charging of a conducting liquid.[2].

In induction charging, the substance needs sufficient surface or volumetric conductivity to obtain necessary leakage charge before the separation from the charged electrode. When the particles showing high resistance is charged, it requires a longer time. For instance, an ideal isolator, which has no free electrons, has molecular dipoles along the electric field direction. However, the total net charge is the same before the application of the electrical field. Induction charging is generally not suitable for the dry powder coating process because of its high resistivity, but this method is usually used in spray painting with liquid

2.5.3 Corona discharging

Corona discharge is a type of discharge mechanism happening when a fluid, e.g. air, surrounds a charged conductor. As shown in Figure 2.15, the current flows through a high voltage region. This mechanism creates a plasma region around the electrode. The value of high voltage determines the ionization behavior. The corona discharge mechanism can be composed of one or more discharging electrodes. If the energy intensity of the electrons is high enough to generate electron-ion pairs, the neutral gas molecules are ionized. After the ionization process, the corona glow occur, which is a high electric field region appearing as a bluish light around the conductor .The corona process can be either positive or negative ionization process [2].

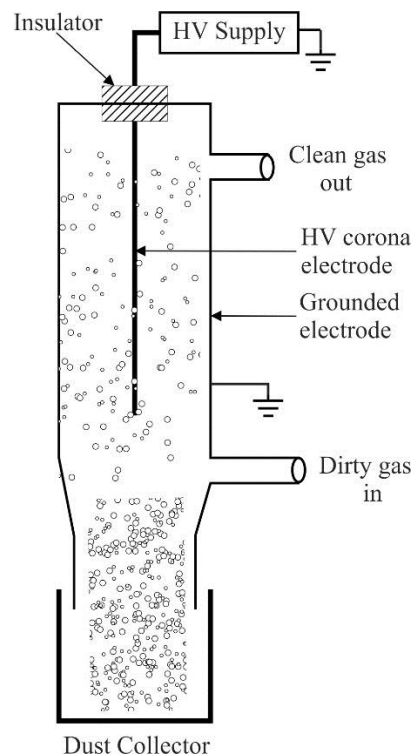


Figure 2.15 A type of an electrostatic-precipitator [2].

While the ions move to ground plate, most of them collide with each other and is exposed to the neutral gas molecules. However insufficient energy may cause ionization energy, then, momentum of ionized air molecules result in an ion wind, typically range from 1 m/s to 2 m/s velocity. This phenomenon is called *ion wind*

Diffusion charging originates from thermal movement of ions and random impacts between ions and tiny particles. When particles bigger than 2 μm in diameter the major charging mechanism in diffusion charging, but particles smaller than 1 μm in diameter, diffusion charging becomes more important. It does not depend on electric field intensity (E) Both diffusion charging and field charging can be used in corona-charging [2].

When a particle is subjected to any ion concentration N_0 (ions/ m^3), it will achieve in charging time- t , charge- $q(t)$ as follows

$$q(t) = \frac{4\pi\epsilon_0rkT}{e} \ln\left(\frac{rN_0e^2ut}{4\pi\epsilon_0kT} + 1\right) \quad (2.65)$$

where r is the radius of particle, k is Boltzmann's constant, T is the absolute temperature in kelvin, e is the unit electronic charge, and u is the mean thermal velocity of ions (approximately 240 m/s). When the charges of ions excess one electric charge, n_1 the ionic charge must be used instead of e -unit charge. Diffusion charging is widely employed for submicron particles. For instance, size classification of ultrafine particles is possible by mobility analyzers [2].

As referred Ren et al. [15] the charging process of particles over time can be represented by the Equation (2.63), where q_p is the charge of the particle, d_p is the diameter of the particle, k is the Boltzmann constant, T is the temperature, e is an electronic charge, v is the mean particle velocity, N is the concentration (number of particles), and t is time

$$q_p(t) = \frac{d_p kT}{2e^2} \ln\left(\frac{d_p v \pi e^2 N t}{2kT} + 1\right) \quad (2.66)$$

Based on the analysis above and Equation (2.62), the charging characteristic of particles is related not only to the concentration of electrons and ions but also to the size of the particles

Boltzman distribution is

$$\frac{n}{N - n} = e^{\left(\frac{-nde^2}{\epsilon_0 kT}\right)} \quad (2.67)$$

One of main industrial practice of diffusion charging is *charge neutralization*. It is generally used in semiconductor industry. By using bipolar ions, corona discharging can

be used to generate an ac voltage, whose rated values are 5kV and 60Hz.

Another technique to generate bipolar ions is based on krypton-85 and polonium-210. The advantage of the method is the fact that it is not using high voltage, which generally creates side effects such as sparks.

2.5.4 Particle charging by repeated impacts on a metal wall

2.5.4.1 Charge transfer

When some particles hit on a metal wall, each of them obtains an equal charge with opposite polarity. The quantity of charge transferred is subject to the total potential difference V between the contact bodies. The potential difference is composed of two parts: V_c related to the surface work function and V_e stemming from image charge, which is induced in the wall by an external charge. These are related as follows [16].

$$V = V_c - V_e \quad (2.68)$$

The potential difference V_e is approximated by:

$$V_e = k_0 q \quad (2.69)$$

where k_0 is a constant and q is the charge on the particle before impact.

Figure 2.16 shows the deviation in the charge on a rubber sphere by repeated impacts [16]. The transferred charge caused by an impact decreases with the number of collisions and the charge comes close to a boundary value. The boundary value tends to decrease as the interval between collisions rise due to increasing charge relaxation with elapsed time. The dotted-lines in Figure 2.16 are the results calculated. These calculated values correspond to the experimental results.

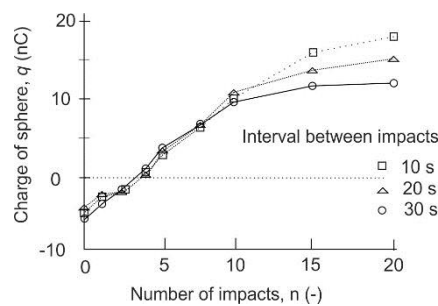


Figure 2.16 Variation in the charge of the sphere by repeated impacts (rubber sphere, drop height: 0.4 m, relative humidity: 41–43%) [16].

2.5.4.2 Effect of elasticity

When a particle hits on a hard plate, the particle is deformed and a contact area is produced. If the particle is a sphere with a smooth surface then the contact deformation can be approximated the maximum contact area S during the impact is represented by:

$$S = 1.36 k_e^{\frac{2}{5}} \rho_p^{\frac{2}{5}} D_p^2 v_i^{\frac{4}{5}} \quad (2.70)$$

where k_e is the elasticity parameter, ρ_p is the density of the sphere, D_p is the particle diameter and v_i is the impact (incident) velocity. If the particle is not spherical form, the particle shape should be taken into account [17].

2.5.5 Charging in gas-solids pipe flow

In gas–solids pipe flow, particles are charged as a result of the collisions with the wall; the charged particles form an electric field and the electric field influences the total potential difference V ;

$$V = V_c - V_e - V_b \quad (2.71)$$

where $V_b(=k_3q)$ is the potential difference stemming from the electric field, called the space charge effect. If a electrically isolated metal pipe is grounded, the charge transferred from the particles to the wall flows through earth. The charge transferred per unit time is identified as electric current [18].

3. PNEUMATIC TRANSPORT

Some materials in solid form may be transported within industrial plant by means of mechanical, hydraulic or pneumatic conveying, while pneumatic conveying has become the dominant method for a long time. The mechanical transportation of solids in pipelines is a primary requirement of many industrial processes. The benefits include comparative mechanical simplicity, fully enclosed operation and the ability to deal with a wide variety of solids. Pneumatic conveying of powdered and granular materials is utilized extensively in some industries such as coal pulverizing, flour making, cement production, and fertilizer processing. These applications involve moving bulk solids and in power generation pulverized fuel (p.f.) is supplied to burners by means of pneumatic transport [19, 20].

Generally, all particles become electrically charged during pneumatic transportation, which can be hazardous for industrial environment. As determined Section (2.5), the primary sources of electrification are frictional contact charging between particles, particles and the conductor facility, charge transfer from one particle to another and charge induction [21]. However, the development of on-line instruments for measuring the gas-solids flow rate which should be reasonably accurate, safe, economical and reliable has encountered many challenging problems which are not associated with single phase flows. For a single-phase flow, the medium is continuous so that the flow rate can be measured by simply measuring the flow parameters related to the mean flow velocity, since the conveyed fluid completely fills the pipe. However, for gas solids flows, due to the discontinuous nature of the suspension, measuring the solids velocity alone is not sufficient to give the required mass flow rate. The mass flow rate is obtained by simultaneously measuring the solids velocity and the solids concentration, or alternatively, it should be measured by detecting flow signals directly related to the mass flow rate.

3.1 Characteristics of Pneumatically Conveyed Gas-Solids Flow

As expressed by Zhang [22] gas-solids flows can undertake an infinite variety of complex regimes due to inhomogeneous concentration and velocity distributions within a given cross sectional area. These complex flow profiles vary with the conveying velocity, particle size, humidity, temperature and pipe obstructions such as pipe joints modified by bends, flanges and pipe geometries. The roping flow regime is an example of inhomogeneous distribution where the solids concentrate into a rope. The 'roping'

phenomenon usually appears near pipe bends and obstructive objects such as orifices, valves and pipe-size conversion parts. It can also be caused by imperfections in the pipe wall.

Huber reported experimental results on particle concentration distributions in dilute phase pneumatic conveying [23]. The profiles are shown in Figure 3.1 and Figure 3.2 derived from their published paper. Z is the vertical axis, d is the diameter of the pipe and X is the distance from the outer wall. The above profiles show that both the particle velocity and the concentration distributions were not uniform seventeen diameters downstream of the elbow, upstream of which the original flow was uniformly distributed.

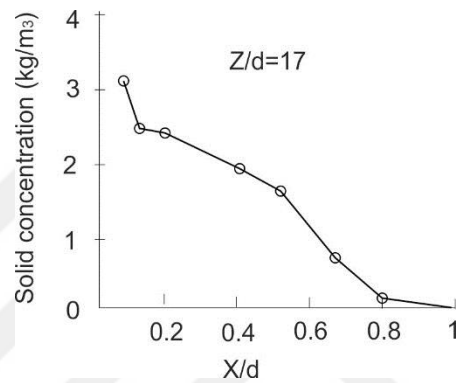


Figure 3.1 Solids Concentration Profile in a Vertical Pipe [23].

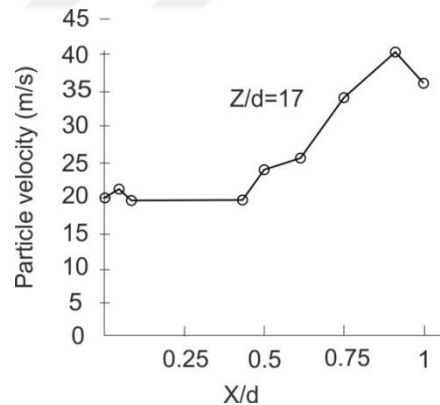


Figure 3.2 Solids Velocity Profile in a Vertical Pipe [23].

The factors influencing the solids distribution can be attributed mainly to the following; pipe orientation, solids concentration, particle size, pipe bends fittings, pipe wall roughness, particle distribution over the pipe cross-sectional area in a horizontal pipeline, in general, a more inhomogeneous particle distribution can be expected in horizontal pipes compared with vertical pipes. The degree of accumulation is also associated with several other practical conditions such as the conveying velocity, gas pressure, pipeline diameter, pipe wall roughness, particle size and moisture content. Particle size is also another factor which influences the solids distribution, the finer the

powder the more homogeneous will be the solids distribution. Usually any flow with such a solids distribution is called roping flow. Roping is found in both vertical and horizontal pipelines usually at positions located closest to bends. It is known that pipe-wall roughness has a considerable influence on the development of the particle distribution in a horizontal pipeline. In vertically upwards flow, for a dilute phase of fine particles suspended in air, a more homogenous solids distribution can be expected at a reasonably long distance from a pipe bend. For this reason, it is preferable to site measuring instruments at such locations. The level of solids concentration varies widely depending on the nature of the processing industry. The description of the solids density used in pneumatic conveying has been divided into lean-phase, called dilute-phase, or lightly loaded and dense-phase conveying. There is no strict boundary between these two categories but usually phase densities above 40 kg solids/kg air is recognized as the dense-phase type and that below 20kg solids/kg air (0.3-6% by volume) as the lean-phase type [24]. In power generation, the pneumatic conveyors are large diameter pipes, usually 250 mm to 600 mm and lean phase conveying is used where the solids volumetric concentration is of the order 0.2 % to 1%. The small volume of solids in such large diameter pipes presents additional measurement problems. Consequently, it can be concluded that lean-phase conveying can achieve a relatively more uniform particle distribution in both horizontal and vertical pipes than dense-phase solids conveying. Operational flow conditions and its properties of fuel particles in pneumatic conveyors are presented in Table 3.1

Table 3.1 Operational flow conditions and properties of fuel particles [24].

Parameter	Range
Mass flow rate	0.3 to 3 kg/s
Conveying air velocity	30 to 40 m/s
Solids distribution	inhomogeneous
Pipe diameter	25 to 1000 mm
Pipe orientation	horizontal/vertical
Line temperature	50 to 160 °C
Line pressure	wide range
Coal grade	3 to 18 %
Ash content	1 to 30 %
True density coal	1300 kgm ⁻³

Triboelectrification may be considered as a complex form of contact electrification in which there is transverse motion when two substances impose or are rubbed together. The transverse motion can in turn emphasize the charge transfer. Contact electrification occurs not only in pneumatic conveying, but also in milling, grinding, sieving and screw feeding. Particles can share charges when they hit to each other, or one particle is settled on another. Charge sharing is more obvious between conductive particles [21].

Electrostatic charge can be recombined, for example via the earth or by contact with an object holding opposite charge. However, charge on non-conductive particles can be retained and the relaxation time depends on the volume resistivity of bulk solids. material's conductivity.

Table 3.2 shows the level of charge accumulation in particles, where the charge carried by unit mass of particle is given for solids of medium volume resistivity emerging from different processes. If the volume resistivity is high, the charge could be retained even if the solids are in an earthed container. For particles suspended in pure gases as in pneumatic conveying, particles can remain charged for a long period of time irrespective of the particle

Table 3.2 Charge build up on powder [25].

Operation	Mass charge density ($\mu\text{C}/\text{kg}$)
Sieving	$10^{-3}-10^{-5}$
Pouring	$10^{-1}-10^{-3}$
Scroll feed transfer	10^1-10^{-2}
Grinding	$10^{-1}-10^{-1}$
Micronising	10^2-10^{-1}
Pneumatic conveying	10^3-10^{-1}
Triboelectrical powder coating	10^4-10^3
Fluidized bed (Bubbling freeboard)	$10^{-3}-10^{-1}$
Aerosol spray can	$10^{-3}-10^{-1}$
Fog: supersonic nozzle	$10^{-3}-10^{-1}$

When the charged particles are suddenly discharged to earth or another body, producing a high energy density for ignition source, it can lead to be hazard. The discharges of particles can be categorized as spark, brush, corona, propagating brush, cone and lighting like discharges. Amid them, spark, brush and lighting like discharges may happen in pneumatic conveying. The discharge-incendivity is determined by the

energy stored and the minimum ignition energy (MIE). Therefore, the hazardousness of discharge depends on the area categorization related to zones and gas group of process environment. Electric potential on metal materials like pipelines, flanges, bolts and etc, can be avoided by means of earthing. If non-conductive pipes and hoses must be used for pneumatic transport, the maximum possible energy stored must not exceed the MIE value. Without using air in the pipe, it can be made use of the dense phase conveying to reduce the risk of ignition inside pipe. More details can be found in British and CENELEC Standard PD CLC/TR 50404:2003, “Electrostatics—code of practice for the avoidance of hazards due to static electricity” [25].

The velocity of solids in a pneumatic pipe system must be controlled to consider safety and efficiency. An extremely high solids velocity may bring about too much energy costs because of frictional losses due to higher pressure drops, solids degradation and pipe internal wall wearing. On the other hand, too low velocity may lead to solids settlement and irregular operation, or even to a pipe blockage. The on-line measuring and controlling the solids velocity must be realized to operate at higher efficiencies and under safer conditions. One of the important flow parameters is mass flow rate. An unbalanced mass flow rate in turn, an irregular coal distribution among the tuyeres would lead to unfinished combustion giving rise to a loss of efficiency.

The description of the solids density used in pneumatic conveying can be divided into lean-phase and dense-phase conveying. There is no strict boundary between these two categories but usually phase densities above 40kg solids/kg air is recognized as the dense-phase type and that below 20kg solids/kg air (0.3-6% by volume) as the lean-phase type [24]. In power generation, the pneumatic conveyors are large diameter pipes, usually 250mm to 600mm and ‘lean phase’ conveying is used where the solids volumetric concentration is of the order 0.2 % to 1%. The small volume of solids in such large diameter pipes presents additional measurement problems physical and chemical properties of the solids moisture, accumulation of particulates within a pipe

As shown in Figure 3.3 concentration profiles (a), (b) and (c) are identical since they will induce the same charges on a circular electrode, so also are profiles d and e. In addition, an equivalent concentration ring can be found with inner radius r_1 and outer radius r_2 as shown in profile (f), which induces the same charges as (d) or (e)

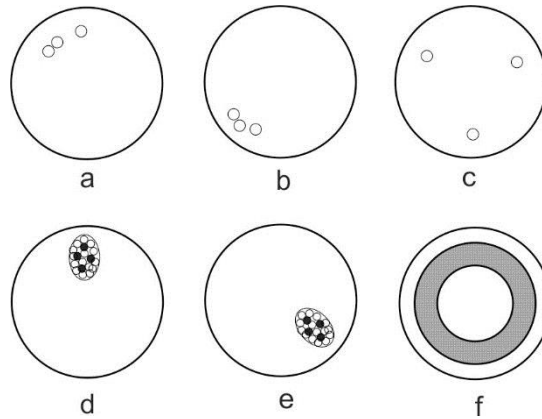


Figure 3.3 Concentration profiles [22].

3.2 Some Challenging Features of Solids Flow in Pneumatic Pipelines

Despite the growing importance of pneumatic conveying, for instance cement, gypsum, micronization and pulverized coal for electric power generation plants, some important problems encountered in solids flow measurement are not normally associated with gas or liquid flows [26]. Because obstructive techniques are undesirable for pneumatic conveying due to the very abrasive character of fast flowing particles, non-obstructive flow metering approaches must be presented.

3.2.1 Nonuniform flowing solids distributions

The solids distribution in a pipeline by pneumatic transport, generally inhomogeneous, can be determined by the pipeline positioning, metering location, solid phase loading, velocity of mixture of air and solid and properties of the solid material such as particle size, moisture content, cohesiveness and adhesiveness. Some typical solids distribution types are presented in Figure 3.4. Especially, the most difficult type of inhomogeneous distribution is the roping of conveying system, where some conveying particles are collected a little segment of pipe cross-section for numerous causes.

3.2.2 Fluctuating velocity in the pipe

Owing to the inhomogeneous distribution of solids-air mixture, there can be a range of velocities over the cross section of pipe; certain samples are illustrated in Figure 3.4. As phase loadings rises, the irregular velocity profile will increase and horizontally conveying air-solid particles at the top of the pipeline are faster than particles below

3.2.3 Irregular particle size in the pipe

The particle size used in pneumatic conveying can be started from a few micrometers for instance pulverized coal, wheat flour, continued to a few centimeters, for example micronizing particles in mining industry. The deviation of particle size may be

limited to control the process system and efficiency.

3.2.4 Moisture content of particulate materials

The moistures of particulate materials range from 1% to 30%, which is subject to material source, storage conditions and process requirements. Materials, containing high moisture content, can only be conveyed at high temperatures. Namely, solids flow sensors should not be sensitive to humidity of the material.

3.2.5 Other flow parameters

Besides four irregular values, other parameters may also affect the metering performance, such as material type and the grade of deposit of fine particles. Some of which may be unviable to keep under control or estimate and certainly show wide range between different conveyors and types of solid materials. To compensate effects of uneven solids distribution and irregular velocity profiles on the measurement the flow sensor should usually be mounted on a vertical pipeline to meter upwards flow.

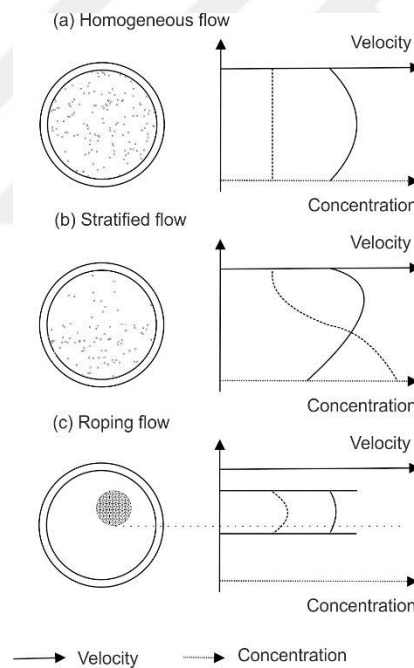


Figure 3.4 Dimensional characteristic distribution and velocity changes for solid-air mixture in pipe cross-sectional area [26].

Consequently, due to the need for automatic control of pneumatic conveying systems, the factors influencing the solids distribution can be attributed mainly to the following; pipe orientation, solids concentration particle size, pipe bends fittings pipe wall roughness [27].

4. THE METHODS AND APPLICATIONS

4.1 Background

According to report by Zheng and Liu [28], air-filled solid (pneumatic) transport is usually employed to convey solids to be granular shaped or pulverized solids in a lot of industry related to mass solid processing. In terms of efficiency, the importance in power generation, raw materials-handling, waste management, ecologic laws and directives a precise, on-line, continuous non-obstructive measuring of pipeline-flow parameters of two-phase-solids have steadily been increasing. Both the researches at universities and applications in various industries have been risen the measuring of flow parameters of pneumatic conveying. Several types of techniques for measuring two phase solid flow parameters have been suggested and developed over the past four decades. However, each method exhibits its own pros and cons under diverse application conditions. Each application area requires rework in order to optimize the accuracy, the reliability, the robustness and the sensitivity of the instruments.

Even if all pneumatic pulverized solids systems present practical parallelism regardless of matters, the pulverized solid materials for electrical energy and steel production plant play an important roles for flow parameters, such as velocity, uneven distribution of pulverized coal and unburned combustive material ash [26]. Identifying and modeling these challenges will help research and related practices.

4.2 Mass Flow Rate Measurements

Pneumatic transport systems deliver some flexibility of pipeline transport for particulate mass solids. Variables, such as the volumetric flow rate, volumetric concentration, solids' velocity and the mass flow rate of the solids, are important characteristics that are often required to be measured and controlled to achieve efficient utilization of energy and raw materials. Operators in industrial processes are most likely to be interested in the metering of solids' mass flow rate in pneumatic transport pipelines.

Pneumatic transport structures deliver some flexibility and holding of pipeline conveyance for the mixture of air-solids. The efficiency all the industrial processing systems related to them, the parameters of mass flow metering are important, such as the mean solid velocity, the concentration and distribution of solids, volume loading

Flow sensors in pneumatic pipes may be classified as either restrictive, called obstructive, invasive or intrusive or nonrestrictive. Restrictive flow sensors can have an impact matter such as an orifice plate, a venturi tube, a coriolis tube, an impact plate or a

turbine. Their major problem is wearing due to the abrasive nature of fast-moving particles and diversion and constriction of flow lines. Pneumatic transport has been widely utilized in some handling and conveying systems such as food processing, cement, micronization and mining industry, pharmacy sector and convey mixture solids, granules and beans.

Various measuring techniques are summed up in Table 4.1 with regard to all known the state-of-the-art measurement methods. The techniques of measuring mass flow rate of solids in a pneumatic pipeline may be primarily classified as indirect, namely inferential measurements and direct measurements. A direct metering instrument has a detecting head that reacts immediate by means of the detector. An inferential instrument must specify the mass flow rate of solids over pipeline by inferring from both the immediate volumetric concentration and velocity of solids. Sensor can provide users with three parameters, the velocity, concentration and mass flow rate of solids [26].

$$M_s(t) = \rho_s A V_s(t) \beta_s(t) \quad (4.1)$$

where $V_s(t)$ and $\beta_s(t)$ are solids velocity and the immediate cross-sectional mean volumetric concentration respectively, ρ_s the real density of the flowing solids material and A the cross-section of the pipe.

The solids concentration β is described as

$$\beta = \frac{A_0}{A} \times 100\% \quad (4.2)$$

where A_0 is the effective cross-sectional area occupied by the particles, and A is the inner cross-sectional area of the conveying pipe.

Therefore, the solids flow rate can be calculated as follows;

$$M = A \beta \rho_s v \quad (4.3)$$

where v the mean solids velocity.

Suppose that the local particle density contained in the area $dx dy$ can be expressed. The sensing systems used in the flow meters can be classified micro and macro sensing types. The first type of mass flow meter uses an array of sensors each of which is influenced by solids within a small volume of the pipe cross section, so that a more precise description of the solids distribution can, can be called flow imaging With a macro sensing system, the overall solids concentration and mean solids velocity are derived from signals produced by sensors influenced by solids within a sensing volume which may extend over the entire pipe cross-sectional area.

Table 4.1 Measurement methods of two phase solid flow parameters

Volumetric Concentration and Velocity Measurements of Solids.			
Category		Method	Sensing Technique
Concentration Measurement Mass Flow Rate Measurements	Direct Methods	Mechanical Method	Coriolis and Gyroscopic Measurement
		Thermodynamics Method	Heat Transfer Measurement
		Electrical Methods	Active Charging Measurement
	Passive Charging Measurement		
	Indirect Methods	Electrical Methods	Capacitive Measurement Electrostatic Measurement
		Attenuation and Scattering Methods	Radiometric: γ Rays, X-Rays Microwave Measurements Optical Measurement Acoustic and Ultrasonic Measurements
		Resonance Methods	Magnetic Measurement Microwave Measurement Acoustic Measurement
		Flow Tomography Methods	Electrostatic Measurement Capacitance, Resistance Measurement Optical Measurement Radiometric: γ Rays, X-Rays Measurement
		Digital Imaging Method	Laser Sheet and CCD Camera
	Velocity Measurement		Cross Correlation Methods
Doppler Methods			Laser Doppler Measurement Microwave Doppler Measurement
Spatial Filtering Method			Capacitive Electrostatic Measurement Microwave Measurement Optical Measurement
Electrical Sensors and New Signal Processing Methods			Electrostatic Sensor and Wavelet Analysis Capacitive Sensor and Fourier Transform

4.2.1 Direct measurements

The direct approach of solids' mass flow measurement is a more straightforward way and easy to measure compared with indirect (inferential) measurement.

4.2.1.1 Coriolis and gyroscopic mass flowmeters

By Medlock and Furness[29], Fundamental features of coriolis mass flowmeters have been defined the mass flow rate of the solids relies on the measurement of the Coriolis force, which is experienced by the particles when they move through a sensing tube vibrated. Because of fluid motion, the tube vibrating give rise to twist the tube a torque T_q which is directly proportional to mass flow \dot{M}_s , as followed:

$$T_q = k\omega\dot{M}_s \quad (4.4)$$

where ω is the angular velocity with which the sensing tube is vibrating and k is a constant.

The method used in gyroscopic flow meter very similar to the coriolis flow meter. The only difference between them is plane of vibration proportional to the plane of causing torque

4.2.1.2 Thermal methods

Thermal techniques used to detect heat difference between input and output of pipe system. The fundamental equation:

$$\dot{M}_s = \frac{H}{C_p\Delta T} \quad (4.5)$$

where H the value of heat input, C_p the special heat coefficient $\Delta T(=T_{c1} - T_{c2})$ difference of the heated sensing section, T_{c1} and T_{c2} are the temperatures of inlet and outlet of the meter

4.2.1.3 Electrical methods

There are dual kinds of instruments to measure electrostatic charge sensing. In the first, the generator created externally charges all the particulate materials (active method), however, in the second, measures the inherent charge on the particulate materials (passive method) The former is known as passive that measures the charges naturally carried by particles due to particle-particle interaction, particle pipe wall impacts and friction between particles and air stream in gas-solids flow. The latter is called the initiative or active method which uses two chambers. A charging chamber is used to initiate or charge up the solids and measuring chamber for detecting the charges on the solids

Active charging-sensing methods

The active charging-sensing instrument consists of two chambers, an electrostatic charge and a measurement section. The particles moving through the charging section is charged by a high voltage source, usually ranging from 100 to 500 V. The particulate materials moving through the measurement chamber induce an electrical charge in the wall and lead to generate an electrical current I_0 , which is in direct proportion to the solids' mass flow rate.

$$M_s = cI_0 \quad (4.6)$$

where c is a calibration coefficient of the instrument with related to the solids material

Passive sensing methods

When charged particles impact to inside wall of metal-pipe, it can give rise to electric charge transmission.

In passive charge detecting approach, the quantity of charge transferred from particles in non-dense air-solid flow to a metallic pipe is with related to the mass flow rate of solids. Since the moving particles through chambers are charged due to frictions and impacts, the total charge of conveying materials in direct proportion to the amount of solid materials. Thus, the quantity of charge can be measured an appropriate instrument like electrometer. The total measured charge are composed of both initial charge and induced charge thanks to conveying particles.

The currents I_0 and I_1 , generated in the two detecting chambers, are determined by means of an electrometer. Then the mass flow rate of solids can be calculated with regard to the equation

$$M_s = aI_0 - bI_1 \quad (4.7)$$

where a and b are constants, which rely on the electrostatic characteristics of the particles and compartments.

4.2.2 Indirect measurements

4.2.2.1 Electrical sensors for measuring concentration of solid

Electrical methods, related to dielectric or electrostatic characteristics of particles, have been interested in by a good many of researchers to measure solids' volumetric concentration in conveying system to measure solids concentration. Some inferential (indirect) measurement methods based on capacitive or electrostatic principles are low-cost and simple to implement, but it is reports that these instruments are quite sensitive to

moisture content, particle size and chemical composition. The electrodynamic or induction method can be differ from in terms of zero capacitive effect.

Capacitance sensors

The capacitance value of simple capacitor, composed of two simple plates is

$$C = \frac{\varepsilon_0 \varepsilon_r A_p}{d} \quad (4.8)$$

where $\varepsilon_0, \varepsilon, A_p, d$ are the permittivity of free space, the relative permittivity of the dielectric material, the area of the parallel plates and distance of two plates respectively.

The capacitance method of solids concentration measurement rely on presence of solids within a capacitive sensing volume, which will increase the measured capacitance C due to the increased relative permittivity ε_r

The methods by means of capacitance metering is based on the variation of ε_r , which changes proportionally according to air parameter ε_0 . As the value of ε_r risen, the capacitance C is increased. The suitable electrical signal is extracted from i.e, current, voltage or frequency, the capacitor related to proper electronic circuit. There have been substantial studies on capacitive flow sensors over the past decades. The capacitive sensing probes can be composed of plates, plates more than two, ring-type, semi-ring type, quarter-ring type, rod-type, pin-type and in addition sensor array of some types of probes and some can be installed inside of pipe and the others outside of an insulated segment of the pipe. The value of capacitance may be linked either directly or indirectly to the particulate solid material concentration. The former, the most commonly used capacitance technique and has a wide range of applications, is coined steady-state capacitance measurement and the latter is dynamic capacitance measurement. The low expenditure and simplicity are the main benefits of a capacitive sensor for metering particulate concentration. The effect of solid deposition in the pipe section can be compensated by use of a dynamic measurement technique. Volumetric concentration of solids can be determined by measuring the capacitance of the sensor when solids are flowing through the sensing field, which is a commonly used capacitance sensor for the concentration measurement of gas–solid flow in pneumatically conveyed pulverized fuel at power stations

Electrodynamic sensors

According to detecting technology, the term electrostatic have the same meaning the other renowned terms triboelectric and electrodynamic. A certain amount of net

electrostatic charges have been occurred owing to impacts between particulate materials, between solid materials and internal pipe wall, and friction between solid materials and air stream. Their charge densities range from 10^{-7} to 10^{-3} C/kg over the pipeline. The charge on the particulate materials can be detected by a shielded and isolated electrode along with a proper charge sensing circuit.

Because of similarity of the electrodes in capacitance and electrodynamic sensors, the sensing techniques seem to be identical. Indeed, while an induction or triboelectric detector sense the variation of the natural electrostatic charge on the flowing solids, a capacitive probe make use of the dielectric characteristics of the solid particulate materials. The charge sensing circuit may be planned to use either AC, called dynamic measurement, or DC method to measure the magnitude of the charge signal. Additionally, in AC method, the data can be processed as bandwidth and frequency components. The AC techniques have been provided useful and repeatable results recently. According to experimental result, the main characteristic of electrodynamic sensor can be its high sensitivity for concentration metering, but the fact that he obtained signal depends on the physical properties of the particles like size, shape, distribution, conductivity, permittivity, chemical composition, moisture content and conveying conditions for example pipe size, pipe wall roughness, line temperature can be considered some important disadvantages

In addition to capacitive probe, the electrostatic sensing electrodes can be composed of plates, fully ring-type, semi-ring type quarter-ring-type, rod, pin-type, sphere, semi-sphere type even various sensor array types either rods or ring types.

The electrodynamic probe being main focus of this thesis will be comprehensively explained in chapter 6

4.2.2.2 Attenuation and scattering methods

According to the Lambert–Beer law, the attenuation of a monochromatic electromagnetic wave or a sound wave is transmitted through a medium having solids particles as followed.

$$I = I_0 e^{-\mu x} \quad (4.9)$$

where I_0 and I are the amplitudes of the incident and reflected electromagnetic or sound waves respectively. x is the effective wideness of the medium passing through the wave and μ is a fixed number related to the linear attenuation coefficient.

In accordance with this fundamental principle, various detecting techniques, such

as radiometric, optical and acoustic sensing, have been developed to measure solids concentration by transmitting one or more electromagnetic or sound waves through a pneumatic pipe. The information of the flowing solids concentration is deduced from the measured attenuation by the fluidal solids-air-mixture medium. Electromagnetic waves for this purpose can be visible light, a laser beam, some spectrum of microwaves, γ -rays or x -rays. On the other hand, a sound wave can be produced using a suitable acoustic or ultrasonic sensor for its measurement. A scattering electromagnetic wave can also be transmitted to measure the solids concentration of gas–solids flows.

Radiometric sensors

In the flow metering by using radiometry method, some ionize radiating waves, especially γ -rays or x -rays, are employed in order to investigate the on-line particle flow medium.

The line attenuation of a radiation rays passes through in a medium relies mainly on the total effective mass per unit area of the particulate solids material and it does not change in conjunction with the particulate materials distribution. Almost, there is no moisture effect certain spectral range. The radiometric attenuation technique can be high cost and exhaustive operation conditions. however it is useful for calibrating and validating other inexpensive and simple instruments either on-line or off-line process.

The one of the challenging troubles of radiometry method in the solids flowing pipeline is irregular solid distribution over the pipe cross-sectional area. So, instead of single beam-geometry, multiple track line attenuation geometry is used to approach real values. Some density scanning devices is useful, it can be used only off line processes.[26]. The system used a parallel beam guidance array with two orthogonal sensing directions of gamma radiation to generate multiple, parallel interrogation beams of small cross-sectional area. This configuration almost eliminated the geometrical errors associated with more conventional divergent-beam interrogation. Experimental results were obtained off-line using idealized flow models, and on-line using a pneumatic conveyor. The system was proved reliable and stable in operation throughout the on-line trials on the pneumatic conveying test facility.

Microwave sensors

Microwave instrument by using of attenuation techniques can be employed to detect the particulate solids concentration in pneumatic pipeline conveying Solids particles over the pipe absorb microwave energy and increase the attenuation of the

incident and transmitted microwave energy source. For a fixed microwave path length, the greater the solids concentration, the larger will be the attenuation

Optical sensors

Some light attenuation and scattering techniques may be employed to detect mean solids concentrations in two phase air–solids flows. The theoretical fundamental of the metering is based on the Mie theory which is deduced from the Lambert-Beer equation. As expressed in the equation, the amplitude of light is exponential-proportional to a lean two-phase air-solid particulates. Not only laser beam can be used as a light source, but also light emitting diode (LED) or similar light sources can be used. The photo-detector units can be employed to detect the sources. One of the problems must be taken careful is to provide the minimal thermal drift in the sensing unit and haphazard light sources around the sensor.

It is considered that one of the main advantages of optical detector can be almost no effect on the device output in terms of variation in chemical composition and moisture content and it is supposed that all the solid particulates are opaque matter. There can be some disadvantages in optical metering systems such as contamination and drift of alignment between input and output lenses which give rise to misleading signals and incorrect readings. In order to provide accurate and reliable measurement, air-cleaning is utilized in the complicated systems

Acoustic and ultrasonic sensors

Two phase solid concentration can be approximately deduced from aerodynamic flow noise being generated by flowing particulates. The detecting part may be a simple microphone fastened to the outer surface of a pipeline. It has been determined that this technique may be well suitable for defining on-off conditions for flow, but not for real analogue measurement of solids concentrations because the sound level is changed by the velocity and size of the particles.

Some other techniques can be used to realize the consistent readouts, one of them is to detect the attenuation between the incident and transmitted sound energy over the pipeline. The main difficulty is considered the coupling of sound transmitter to detect flowing acoustic noise. In order to solve this problem, the frequency source having the rate of 100 kHz can be used. Optimum frequency which is proportional to particle size range from 30 kHz to 400 kHz

4.2.2.3 Resonance sensors for measuring concentration of solids

Stimulation or injection of external energy can lead to take place physical resonance inside a particulate material under conditions. By means of several sensing techniques such as using magnetic, microwave and acoustic sensors in conjunction with the resonance principle have been examined.

Magnetic resonance sensors

When an electromagnetic field which has proper frequency implemented to a material with a net magnetic moment, the atomic nuclei of this material may absorb energy from the field at their Lamor frequencies and it is coined nuclear magnetic resonance (NMR). The electron magnetic resonance (EMR) is similar to NMR. EMR detects the free or unpaired electrons whereas NMR detects the nuclei of a chosen species of a material. In both methods, the sample material influenced by a static magnetic field has been used. Detection is achieved by identifying the effects of interactions between an applied electromagnetic field and the magnetic moments of sub-atomic particles of interest in both cases. The magnitude of the NMR response is related to the number of suitable nuclei per unit volume and number of unpaired electrons is related to that of EMR. In order to obtain the some flow parameters and physical properties of solids which involve concentration, velocity, mass flow rate and moisture content, the NMR and EMR methods have been employed.

Microwave resonance sensors

By using the frequency shift of the resonance, one of the microwave metering being a microwave cavity is used to sense flowing solids concentration. A unit of cylinder-shaped dielectric matter wrapped with conductor metal pipeline can compose a microwave cavity resonator.

The cavity coupled to a microwave system by means of an aperture can lead to generate considerable power from the microwave system at certain different frequencies called as resonant frequencies. The major marker of the system is dielectric properties of solids particulates. Once, the frequency value is determined for empty cavity and the frequency shift of cavity is proportional to the flowing dilute solids concentration.

Acoustic resonance sensor

In the flowing solid pipeline, the density of the particulate solids is related to the velocity of sound wave pass through the medium. When compared to only gas or air in

the pipeline, the speed of sound waves in the two-phase solid material decreases. The resonant frequencies of the sound waves will be directly related to the sound speed when suitable geometries acoustic resonance is applied. The achieved acoustic resonant frequencies deduce from a measure of sound speed and then it is calculated the solids concentration. The mean solids concentration can be obtained by using the frequency of a single acoustic resonance. Unfortunately, there are no real test results about acoustic resonance studies.

4.2.2.4 Tomography methods for measuring concentration of solids

Process tomography methods are originated the medical tomography systems. The findings in the medial field have been transferred and implemented two-phase solid handling processes Such as electrical, radiation and nuclear tomography, acoustic capacitance and electrostatic tomography, there are various tomographic techniques. Process tomography essentially is composed of two parts, multiple sensors around the object and image reconstruction using data from them. In process tomography, the kind of sensing and is not restricted.[30]. Process tomography is akin to medical tomographic scanners in many aspects except that industrial process images. Process tomography is coined in industries to achieve images of processes in pipelines, process tanks. Additionally, process tomography is less costly, faster, and more robust, compared to many medical tomography applications.[31-33]. Process tomography is a measurement method demonstrating a further approach to sensing the concentration of solids in pneumatic transport. Early initiated with medical computed tomography scanners, a lot of effort has been made during the last few years to attain cross sectional distributions of components as visual image. All the experiences of tomography method to solids-gas flows over a wide range of operating conditions have met with only limited success owing to inadequate resolution and little sensitivity of the instruments [26].

Electrostatic Tomography

Electrostatic tomography (EST) is a non-intrusive technique to detect charge distribution. The electrostatic sensors play an essential part in the electrical charge of tomography system. It may be made of several parts, for instance an electrode (probe), an amplifier, a rectifier and a low-pass filter. The aim of the electrostatic sensor is to convert the electrical charge into the transported various material through the metal electrode. The electrical flow noise detected by the probe will be converted into a voltage and sent to the image reconstruction system through the data acquisition system (DAS).

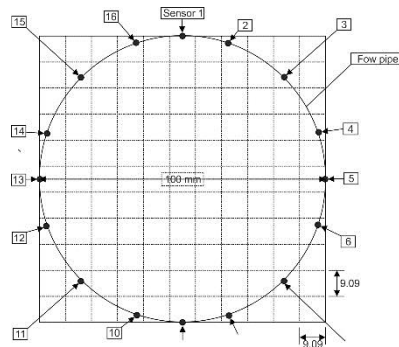


Figure 4.1 11×11 rectangular array with the cross-section of the pipe mapped onto it showing sensor positions [32].

Electrical Capacitance Tomography

In a tomography system to be made of capacitance sensors, most important components are capacitance sensors. Data acquisition system aimed at sensor stimulation and successive impedance metering reads the data of multiple electrodes located on a part of electrostatically transparent dielectric pipe. The capacitance measurement may be achieved between any two of the probes in all possible combinations by using a charging-discharging phases. The distribution of solids across the pipe sections is shown by the subsequent two-dimensional images.

Optical Tomography

Optical fibre instruments using for process tomography have recently been studied by some researchers endeavoring to determine the flow of pneumatically transported pulverized materials such as coal. In order to investigate the measurement both in the horizontal and in the vertical direction, there may be some cross sensitivity owing to the optical hole of the transmitting fibre and light scattering by the particles. The light sends out constantly and any particulate solids moving though the medium investigated by an optical fibre sensor is sensed as a difference in the level of brightness of the sensor.

Radiometric Tomography

By means of the same parallel beam technique, radiometric sensors can also be used to attain images of solid particle flows. In this case, the radiometric sensors are beneficial in that the line attenuation of a narrow radiation beam depends mainly on the total effective mass per unit area of material crossed along the beam trajectory and is not dependent of the solids distribution along the beam line. A low-energy radioactive strip source in combination with a collimator generates a set of parallel radiation beams scanning the entire pipe cross section. A multi-element photodiode array detecting the

transmitted beams provides attenuation measurements. The data for flow imaging and solids concentration measurement is represented by the outputs of detector arrays in the two dimensions.

4.2.2.5 *Digital image method*

The digital image measurement system is essentially made up of a semiconductor based laser for lighting and an inexpensive CCD camera to acquire process image of flowing solid particles by means of the same detection unit using dissimilar exposure time and various image processing techniques, the velocity, volumetric concentration and solids particles can be measured. A net image and a moving fuzzy picture are attained individually by adjusting the exposure time of the camera. It can be applicable for dense phase flows by using a combination of electrostatic and digital imaging sensors to measure the solids' velocity, size and concentration. The speed of solid particulates can be identified from a moving fuzzy picture. All the particles flowing through a pipeline can be lightened using a laser page to focus a slice through the flow. Images of that segment can be obtained using a charge-coupled device (CCD) camera. The basic concept and sensing arrangement are depicted in Figure 4.2. Once the images have been acquired, digital image-processing techniques can be applied to obtain information like particle size distribution and flowing solids concentration.

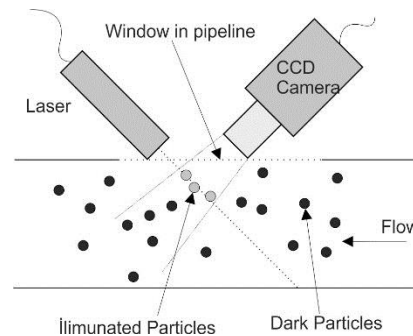


Figure 4.2 *General imaging sensor arrangement* [34].

All the steps must be processed to extract the necessary information. The general sequence of operations is illustrated in Figure 4.3

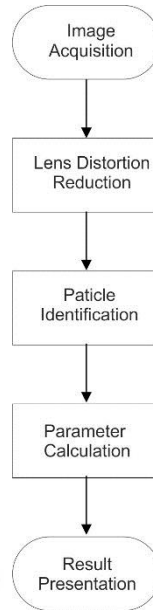


Figure 4.3 *Sequence of operations* [34].

4.3 Measurements of Solids' Velocity

Both solids' concentration and solids' velocity must be measured simultaneously for on-line and non-intrusive mass flow metering of particulate solids. Individual solid particle in the pipeline is moving instantaneously at different velocity because of some specifications of the matter such as size, location, uncertain collision each other, axis of moving etc. The velocity of all the solid-particles can be represented the mean velocity value of the flowing solid particles. Several methods have been improved to measure solids' velocity in a conveying pipeline. Various sensors, such as optical, electrostatic and capacitance sensors have been used in conjunction with correlation analysis or spatial filtering method to accomplish solids' velocity measurement.

4.3.1 Cross correlation

As the speed of the vehicle between the two distances can be calculated with the information of distance and transport time, the speed of the two-phase solid in the pipeline can be computed by the same approach.

Two same sensors are axially mounted a distance L aside from each other. The transit-time τ_m of the particles moving from the first sensor to the second sensor is metered by means of cross correlation, where the two signals have software with a digital signal process algorithm As determined below, the solids velocity V_s is then evaluated from the known sensor spacing L and the transit-time τ_m :

$$V_s = \frac{L}{\tau_m} \quad (4.10)$$

Both flowing noise signals are not identical, but the second signal is a time-lagged and little modified version of the former, the cross correlator can be able to figure out the relations between the two signals statistically. The average transit time can be obtained from a peak value of flow noise, but there is an intrinsic systematic error in the velocity measurement which depends on the detection configurations and correlation process algorithms

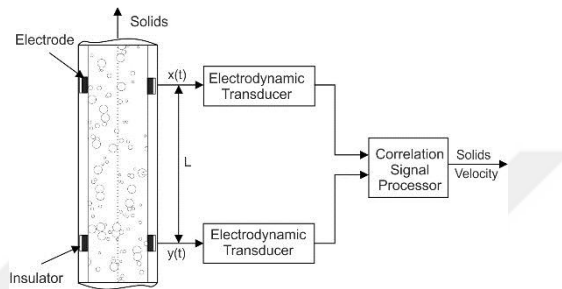


Figure 4.4 Cross correlation solids velocimeter using electrodynamic sensors.

Cross correlation, firstly, independent of the variations in particle properties including particle size, shape, moisture content, chemical composition, conductivity, etc. Secondly, independent of the variations in conveying conditions like pipe size, pipe material, wall roughness, pipeline' temperature etc. Thirdly, appropriate for either extremely dilute phase or very dense phase conveying systems. Finally, independent of solids distribution including roping flow regimes provided the particle velocity is unchanged.

4.3.1.1 Optical sensor

The transit time of two-phase solid flow can be determined with two optical fiber probe by using cross correlating the two signals and then the known axial distance divided by the transit time. The essential points in this method are to identify and calibrate the distance between both probes and determine effects on the correlation coefficient and the measurement accuracy of the transit time

4.3.1.2 Radiometric sensors

The small scale x-ray generator producing low grade radiation fields and paired photosensitive arrays are employed to detect flowing solids velocities by cross-correlator, which correspond to of signals from photosensitive array pairs. A perfect type of system can be constructed using parallel radiation beams and photo-diode arrays in combination

with correlation signal processing.

4.3.1.3 Acoustic sensors

The measurement of two phase solid particles by means of sound attenuation is challenging method because of high attenuation of sound caused by solid particles and either impact noise of particles each other or between particles and pipeline, the cross-correlator can be used a industrial spectrum analyzer. The investigated spectrum of acoustic waves are useful to calculate flowing solid concentration, but is not enough accurate, for example approximately 30%.

4.3.1.4 Electrostatic sensor

The impact or rubbing of solid particles each other and pipeline can lead to charge on particle, in addition previous charge of particles can be sensed appropriate probe. The induced charge is conditioned by an amplifier circuit and send data processing unit.

Ring-type probes are more suitable than other types such as pin-type, rod-type, quarter-ring type etc due to higher spatial sensitivity. The ring-type probes having cross correlator and digital signal processing units are presented in Figure 4.4. The experimental study is comprehensively reported in a paper by Yan *et al* [35], involving the electrostatic detecting system, the spatial sensitivity and spatial filtering properties of the instrument in addition to available correlations to metering accuracy and the effects of solids velocity profiles.

4.3.1.5 Capacitive sensor

The cross-correlator instrumentation by using capacitive sensing have been increasing importance either in terms of studies or experiment. Laboratory experiments or field tests of systems have been limited to small-scale test rigs. The solids velocities measured by cross correlation have been compared with those measured by high speed photography. Considerable divergences between the two velocities were noticed at higher velocities 15–25 m/s.

4.3.2 Spatial filtering methods

All the flow sensors show various spatial filter effects on the flow noise signal owing to physical size and geometrical shape of detecting unite. A spatial filter with suitable frequency on any flow sensing method is related to the solids velocity. The acquired signal of the filter may be similar to a bandwidth-limited white noise or includes a periodic component hidden in a background noise with respect to the construction and

structure of the device.

The autocorrelation method is advantageous method to investigate the spectrum of signal. All the frequency component of signal can be showed by means of autocorrelation methods needing to only one measuring point. One of the measurement challenges for applying spatial filtering methods is the distribution of velocities in the pipe. In order to identify bandwidth of the filtered signal is used and then the solids velocity may be extracted from it by means of autocorrelation function analysis. In the solids velocity measurement by means of spatial filtering methods such as capacitive and electrostatic, optical and microwave sensors, autocorrelation signal processing techniques together with have been widely studied in recent years.

4.3.2.1 Capacitive and electrodynamic sensors

Because of the electrode in a capacitance and electrostatic sensor behaves as low-pass filter to the flow signal. All the studies have shown that the bandwidth of the filtered signal B_W is correlated to the axial width of the electrode W and the mean solids velocity V_s via the relationship [26].

$$B_W = \frac{D K_b V_s}{W} \quad (4.11)$$

where K_b is a dimensionless constant connecting to the solids distribution over the pipe cross-sectional area, velocity profile, particle size and distribution in the fluid. K_b is any constant under flow conditions and can be experimentally identified. As the solids flow signal approach to a bandwidth-limited white noise, B_W can be projected from the first zero crossing point of the auto-correlation function of the signal.

4.3.2.2 Microwave sensors

The microwave resonance device provides to meter solids' flow velocity by means of spatial filtering technique. The axial length of the resonator L_m must be few times the wavelength of the standing-wave λ . If particles travel in the axial direction, the resonant frequency shift varies periodically and the shifting frequency f_0 is related to the solids velocity.

$$f_0 = \frac{V_s}{\lambda} \quad (4.12)$$

In order to identify the periodic-frequency-component of signal, the first zero-crossing point of the auto-correlation function must be employed

4.3.2.3 Optical sensors

The using of spatial filters in optic is originated from aircraft speed measurement in the 1960s, an optical-spatial filter including many identical sensors designed in order to utilize the same principle for solids velocity measurement. Parallel light beams radiated from a set of regularly located infrared light emitting diodes move through a part of transparent pipeline and then attain an array of photodiodes of the same wavelength as light emitting diodes. The signals extracted from the photo-diodes are united in a differential mode, so letting the frequency of the spatial filter f_0 to be correlated to the solids velocity by

$$f_0 = \frac{2V_s}{L_0} \quad (4.13)$$

where L_0 is the spacing between an end-to-end pair of the light emitting diodes

4.3.3 Doppler velocimetry

While the electromagnetic energy source having the frequency f_t is transferred to the two-phase solid-gas flow, some of the sources will be reflected by the frequency- f_r . With respect to the Doppler shift method, the frequency difference between the transmitted and received signals is directly related to the V_s solids velocity.

$$f_r - f_t = \frac{2V_s f_t \cos\theta}{c} \quad (4.14)$$

where c is the velocity of electromagnetic energy; and θ is the viewpoint angle of the reflected energy to the flow. The velocity of solids can be evaluated by measuring the Doppler frequency $f_r - f_t$. Using the Doppler shift principle, a particle velocimetry system can be formed as an energy source as a laser or microwave energy generator.

4.3.3.1 Laser Doppler velocimetry

The improvement and practice of laser Doppler velocimetry (LDV) system have been the main investigation of academy and industry over the past four decades. The principal reason for this is that the method is able to acquire non-intrusive velocity metering of suitable dimensional resolution and very high accurateness without calibration.

The LDV can be employed to meter flowing solids velocity either the reference beam mode or differential Doppler mode. In the former, the laser light beam scattered from particles moving through the little lightened region is mixed with a reference light beam and then fixed through a small hole onto a photoelectric sensor that senses the

frequency shift between transmitted and reflected light. The latter employs the spread light from two focused incident beams which converge on the moving particles from different directions. The more particles move through the crossover region of the beams, the greater scatter light from each beam resulting in two Doppler-shifted frequencies. The divergence between the two frequencies, which can be detected by a photo sensor, is correlated to the velocity of the flowing two-phase solids particles.

4.3.3.2 Microwave Doppler sensors

The microwave Doppler solids speedometer may be arranged both in bistatic-form and in monostatic-form. The detection configuration of the bistatic form are used for transmission and reception of the microwave signals by means of the transparent windows. By the coinciding beams of the spreading a receiving antennae the detecting unit is characterized. But, the monostatic form employs a microwave transceiver instead of a separate transmitter and receiver. Insulation between the spreading and receiving waves is delivered by a ferrite circulator, so just one antenna is required in this form. The advantages are lower cost and easier installation than the former, though the latter gives a more clearly defined detecting section.

4.3.4 Soft computing and new signal processing methods

By Chuanlong et al. [36], due to the mechanical vibration of the pipeline, pulsation of the particle flow and electrical disturbance, the output signal of the electrostatic sensor contains much noise. The representations of the noise in the power spectrum characteristic curve are that it is not smooth and the indistinctive peak frequency f_{\max} may be even submerged by other local peaks, which influences the measurement accuracy of f_{\max} and hence the mean particle velocity. A multi-scaling Wavelet analysis based filtering method for the power spectrum was introduced to extract its trend term, which effectively overcomes the above interference mentioned and improves the accuracy of the mean particle velocity measurement. The output signal of the electrostatic sensor is processed in two steps. The power spectrum of the sampled and discrete signal is estimated using Welch method and then the power spectrum is divided into a smooth trend and a local detail term by wavelet analysis. Finally, the peak frequency can be determined accurately from the extracted trend term. The raw acquired signal and its processing result are shown in Figure 4.5 (a) illustrates the raw output signal of the electrostatic sensor with 1 s interval. And obviously, it is very difficult to determine the peak frequency f_{\max} from the power spectrum curve with a number of local peaks shown in Figure 4.5 (b). But the

filtered power spectrum curve is smooth with distinctive peak Figure 4.5 (c), the corresponding frequency to which is 36 Hz. In this paper, the 3-order Debechies's orthonormal wavelet basis is used in the filtering method, and the scale function $\varphi_3^D(t)$ and Wavelet function $\psi_3^D(t)$ are given by

$$\varphi_3^D(t) = \frac{1+\sqrt{3}}{4\sqrt{2}} \varphi_3^D(2t) + \frac{3+\sqrt{3}}{4\sqrt{2}} \varphi_3^D(2t-1) + \frac{3-\sqrt{3}}{4\sqrt{2}} \varphi_3^D(2t-2) + \frac{1-\sqrt{3}}{4\sqrt{2}} \varphi_3^D(2t-3) \quad (4.15)$$

$$\psi_3^D(t) = \frac{1-\sqrt{3}}{4\sqrt{2}} \varphi_3^D(2t+2) - \frac{3-\sqrt{3}}{4\sqrt{2}} \varphi_3^D(2t+1) + \frac{3+\sqrt{3}}{4\sqrt{2}} \varphi_3^D(2t) + \frac{1+\sqrt{3}}{4\sqrt{2}} \varphi_3^D(2t-1) \quad (4.16)$$

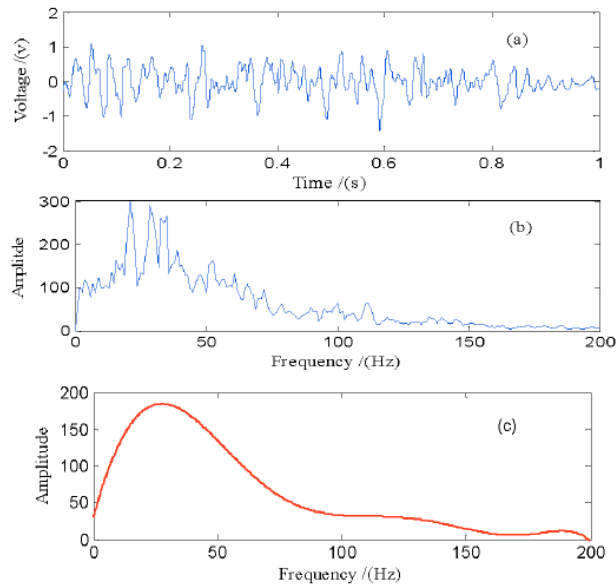


Figure 4.5 Output signal of electrostatic sensor and processing results [36].

In terms of known problems existed with cross correlation techniques, Zhang et al. [37] studied on a wavelet-based method for measuring particulate velocity by an active electrostatic sensor to deal with the distortion of the output waveforms and the variance of the output pulse width from the detecting electrode of the sensor.

Fuchs and Zang [38] demonstrated a development of a capacitive flow sensor and an algorithm based on Fourier transformation for the determination of the slug length and the slug velocity in pneumatic dense phase conveying. The measurement system has been theoretically and experimentally conducted to validate the applicability of both the capacitive flow sensor and the algorithm in pneumatic dense phase conveying. For each of slugs, the slug velocity was calculated by Fourier transformation as 1.46 m/s while the cross-correlation approach resulted in an estimated slug velocity of 1.44 m/s

In recent years, with the rapid development of computer hardware and machine learning, soft computing techniques have been applied in many engineering disciplines, including indirect measurement of multiphase flow [39].

4.4 Particle mean-size measurement

The basis of this detection system relates to the principle that particles of different sizes induce signals with different bandwidths. For a given electrode dimensions, the signal waveform and the corresponding signal bandwidth are fundamentally dependent upon the time that particles remain within the sensing volume. Therefore, larger particles remain within the sensing volume for a longer time corresponding to a narrower signal bandwidth than that produced by smaller particles moving at the same speed.

According to the results described in the analysis of the signal spectrum and its relation to velocity, electrode dimensions and particle location, in order to obtain the most significant change in signal bandwidth with size of particle, the electrode width needs to be comparable with the particle size. There are two reasons for such a requirement

It has been shown that the signal bandwidth is particle location dependent. To make the sensor less dependent on particle distribution, the particle-sizing electrode should be very narrow so that it can only sense particles within a region close to the electrode.

If the electrode is much wider than the particle size, the sensing zone becomes large reducing the higher-frequency signal components due to the longer sensing region. Small differences in particle size can only be detected if extremely narrow electrodes are used having a correspondingly limited sensing region.

4.5 Relative measurement

An signal of solids loading can be attained by measuring the mean electrostatic charge in the fluid [24]. The very large amount of electrostatic charge in pneumatic lines permits high sensitivity in dilute-phase solids loading metering. The average electrostatic charge relies on both solids loading and on particle properties, velocity and other flow conditions. Usually, solid velocity is distinctly measured and the other parameters are usually similar in different pipes so the meter output is independent of the solids distribution, the meter could then provide a measure of relative loading. Such relative information in conjunction with velocity data expressed would be useful for balancing purposes between pipes in a pneumatic transport system.

5. HISTORICAL LITERATURE REVIEW

The studies on electrostatic sensor, called triboflow, tribo effect, triboflow electrodynamic or flow noise sensor, are based on a broad and complex knowledge domain. They are developed along with not only the primary fields such as electronic, electrostatic, powder and particle technology, sensor and measurement technology, computer-software, digital signal processing, random processes, electrochemistry but also the secondary fields such as energy production, combustion efficiency, maintenance, atmospheric studies and environmental technologies. The development of the electrostatic sensor method for measuring the electric charge, which has a 60-year historical evolution for measuring electric charge with electrostatic method, can be considered as one of the basic information field for the sensor.

5.1 Before 1980

Instruments and methods for investigating atmospheric electricity, was a book written by Imyanitov in 1957, refer to the review of Gajewski [40] presents some technics of measurement of electric charge of particles in the atmosphere. Principally, as shown in Figure 5.1, this method might have been comprehensively explained for the first time.

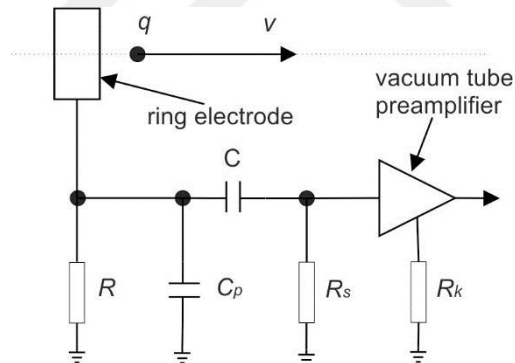


Figure 5.1 The ring type-electrode and vacuum-tube-preamplifier [40].

The technique is based on the electrostatic-induction and expected to make use of the measurements of electric charge of single raindrop in the atmosphere. It was studied on elaborately, but the mathematical model was not determined. The measured charge values on ring range from the order of 10^{-16} to 10^{-15} C. Q_i induced charge is a portion of the raindrop-charge q . It is related to the ring-geometry, and if 50 mm in and 20 mm in diameter and width respectively, if $\tau_0 \ll \tau$ has to be satisfied, then the division will be about 0.25. In Figure 5.2 to measure both the value and sign of the charge carried by the single drops. Where τ_0 and τ are time constants of droplet-pulse and probe with wires. If the system transmits 90% of the energy of signal, the band with ought to be $0.26/\tau_0$. It is

measured by means of the ring preamplifier-system voltage U , proportional to the induced charge of ring Q_i and the drop charge.

$$q: U \propto Q_i \text{ and } U \propto q (Q_i \propto q) \quad (5.1)$$

It can be acquired for a total system capacity range from 10 to 20 pF, a leakage resistance of wires ranges from 10 to 100 G Ω and linear velocity of raindrop (v) 1 m/s.

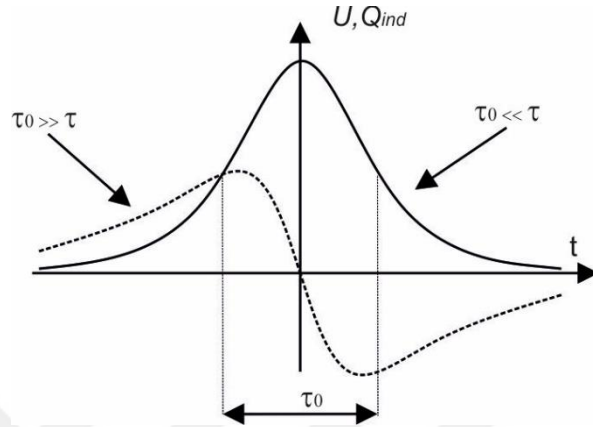


Figure 5.2 Representation the voltage and charge induced on the ring electrode [40].

A model of the correlations between the probe current and flow parameters for electrification of liquids in motion, was presented by Cooper [41], Hignett [42] and Hignett et. al [43]. General relation of the current of the probe was determined as below;

$$I = f_n(\epsilon, K, V, d, \rho, M, A_p) \quad (5.2)$$

where ϵ , K , the electrical permittivity and conductivity of particle, d the particle diameter, V the flow velocity in the region of the probe, ρ the density of air M the mass flow rate or flux of particle flow, and A_p the cross-sectional area of probe

Consistent with Pi Theorem [44], these variables may be stated as four dimensionless groups such that

$$\left[\frac{I^2}{\epsilon d^2 \rho V^4} \right] = f_n \left[\left(\frac{\epsilon v}{K d} \right), \left(\frac{d^2}{A_p} \right), \left(\frac{M \epsilon}{K d \rho} \right) \right] \quad (5.3)$$

Since only V and M vary, other parameters are supposed to be constant, the following function can be determined as;

$$\left(\frac{I^2}{V^4} \right) = f_n(M) \quad (5.4)$$

King, referred to as [40], had been used semi-ring and pin probes in tests whose outcomes were reported in 1973. He pointed out that the square root of the solid mass flow rate value M related to I . As shown the values, the pipe streaming current I_s , rms noise \hat{V}

$$\hat{V} \propto \sqrt{M} \quad (5.5)$$

$$\hat{V} \propto \sqrt{I_s} \quad (5.6)$$

Law [45] conducted an experiment with the toroidal metal circular induction probe to measure aerial agricultural particles' charge. The test rig is depicted in Figure 5.3. Firstly, Law determined the mathematical relationship between the probe voltage U and charge Q , ($= CV$) which is point charge q indicating the charged particle traveling along axis x .

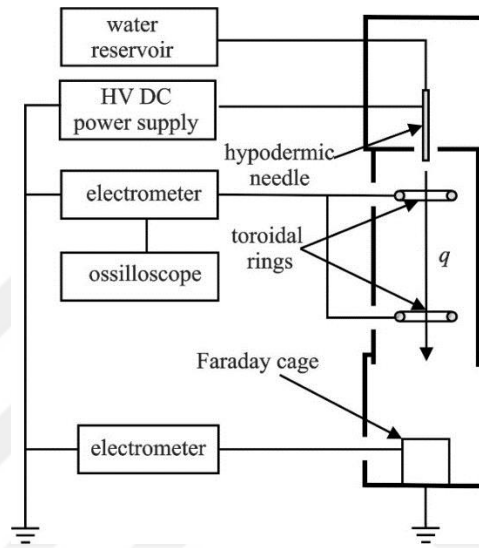


Figure 5.3 The basic representation of the test rig to measure the charge [45].

$$U = -\frac{q}{4\pi\epsilon} \frac{1}{\sqrt{(r^2 + vx^2)}} \quad (5.7)$$

$$U = -\frac{q}{4\pi\epsilon} \frac{1}{\sqrt{(r^2 + v^2t^2)}} \quad (5.8)$$

$$Q = \frac{Cq}{4\pi\epsilon} \frac{1}{\sqrt{(r^2 + v^2t^2)}} \quad (5.9)$$

where C is related to the probe-geometry; r is radius, ϵ permittivity and v is the droplet velocity and $x(=vt)$ is the path. The induction current $i(t)$:

$$i(t) = \frac{dQ}{dt} \quad (5.10)$$

$$i(t) = \frac{Cq}{4\pi\epsilon} \frac{v^2t}{\sqrt{(r^2 + v^2t^2)}^3} \quad (5.11)$$

Experimental consequences exhibited that the signal would have been proportional to the solids flow rate if it had been under 250kg/hr. Solids concentrations have also been measured by Coulthard [22, 27].

5.1.1 1980-2000

This period contributes to the ongoing progress of the technique, especially the mathematical modeling is important, despite rather limited printed papers on the laboratory and industrial applications. In this phase, the first study related to the model of Gajewski and Szaynok [46] employ various techniques in conjunction with that of Imyanitov and Law to determine net charge and the initial rate of charge accumulation in the flux are strongly dc large on solid particles. It was showed that the resultant charge dependent on the velocity of the air suspension, which causes that the dust particles are slip from the metal surface of the into feeder. As followed equation;

$$V_p(t) = \frac{C C_p}{C + C_p} R \frac{q}{4\pi\epsilon\epsilon_0} \frac{-x(t)\dot{x}(t)}{\sqrt{(x(t)^2 + r^2)^3}} \quad (5.12)$$

where C_p is the self-capacitance of probe; C is the capacitance of the measuring device and connecting wires; R is the resistance of the ring, measuring device, and connecting wires; q is the point charge $x(t)$ is the path when the flow velocity v is not a constant, $\dot{x}(t) = v(t)$ is the flow velocity; r is the probe radius; and ϵ and ϵ_0 are the relative and free space permittivity.

Further experiments [47], carried out the influence of dust volume, particle diameter, and of an instantaneous velocity of the discontinuous dust fluxes, shown that resultant charge is found to be strongly dependent on the velocity, however less on the dust particle diameter and even less on the volume. In 1984, Gajewski reported that exhibits a novel mathematical model for the single point charges [48]. Both point charges q_1 and q_2 brought into line and disconnected by the constant distance d are considered when these flow one after another and rectilinearly along the geometrical axis of the metal-ring probe at the constant velocity v in Figure 5.4. The potential $u(t)$;

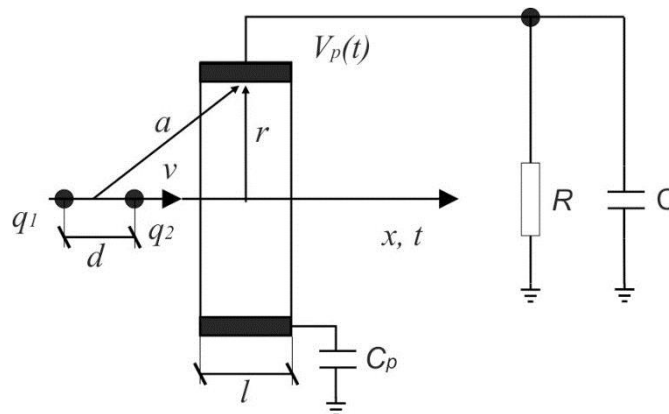


Figure 5.4 The illustration of ring shaped probe and its wires and measurment connection [48].

$$u(t) = \frac{CC_p}{C + C_p} R \frac{1}{4\pi\epsilon\epsilon_0} \left[(q_1 + q_2) \frac{-x(t)\dot{x}(t)}{\sqrt{(x(t)^2 + r^2)^3}} - \frac{1}{2} (q_1 - q_2)d \frac{(-2x(t)^2 + r^2)\dot{x}(t)}{\sqrt{(x(t)^2 + r^2)^5}} \right] \quad (5.13)$$

where the symbols used are the same as for (5.12). If, for instance, q_2 and d are equal to zero, then (5.13) is the same as (5.12).

Referred to as Woodhead [6], five papers were sourced by Dechene and Averdieck. The first paper, published in 1985, reports the use of a single electrostatic sensor to detect an increase in dust level in a duct, such as may be caused by the failure of a bag filter. A diagram of the installation was reported. The dust concentrations reported were of the order of 3.0×10^{-5} grains/m³, which corresponds to approximately 2.0×10^{-9} kg/m³. Typical air velocities past the probe were reported as 18m/s. Dust particle sizes were reported as around 10 μ m. As reported by Dechene installation of dust sensor for the failure of a bag of jet pulse type of dust collection fabric filter. It was aimed to obtain when a threshold of dust concentration. There was not linear information of the sensor.

Beck and Plasskowski, referring to [40] show that for ring probes, the voltage due to flowing charged particles V_2 and its sensing volume voltage V_a are expressed as follows:

$$V_2 = \int_{\omega_l}^{\omega_u} \left| \frac{C_c C_p}{C_c + C_p} V_a(\omega) \right| d\omega \quad (5.14)$$

where C_c is the coupler capacity between a charged particle flux and the probe; C is the overall capacitance of the probe, wires, and operational-amplifier; and ω_u and ω_l are the upper and lower-cutoff angular frequencies of operational-amplifier

A further study on mathematical model for fully ring electrostatic metal probe by Gajewski et al. [49, 50]. The employed this probe around of dielectric flow pipe, which does not affect electric field by generated particle flow noise. In Figure 5.5 and Figure 5.6, the metal measuring head which protects probe and its measuring amplifier provides an electromagnetic screen for zero potential.

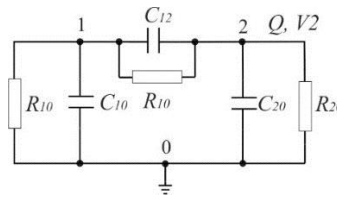


Figure 5.5 The schematic representation of ring sensor [49].

$$V_2(s) = \frac{sRC}{sRC + 1} \dot{V}_2(s) \quad (5.15)$$

$$V_2(t) = \frac{q}{4\pi\epsilon\epsilon_0} \frac{1}{\sqrt{(r^2 + v^2t^2)}} \quad (5.16)$$

The other report by Gajewski [51], according to the Poisson equation;

$$U_{out} = \frac{sRC_p}{sR(C + C_p)} \Phi_p(s) = \begin{cases} sRC_p \Phi_p(s), & \text{for } sR(C + C_p) \ll 1 \\ \frac{C}{C + C_p} \Phi_p(s), & \text{for } sR(C + C_p) \gg 1 \end{cases} \quad (5.17)$$

$$\Phi_p(t) = -\frac{q_v^d(t)}{4\pi\epsilon\epsilon_0} r_p^2 = -\frac{q_v^d(t)}{4\pi\epsilon\epsilon_0} \sigma(t), \quad \text{for } \sqrt{y^2 + z^2} < r_p \quad (5.18)$$

Yan et al. [24] investigated charge induction based on free space electrostatic field theory. They model the full-ring-shaped metal electrode that is only separated from the pipe wall but not from the flow; it is flush with the inner pipe wall. They showed a relationship real current $I_s(t)$ with the charge q

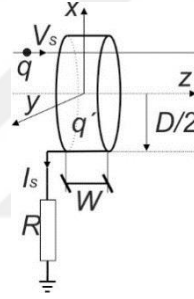


Figure 5.6 Basic schematic of ring-probe [40].

$$I_s(t) = \frac{DqV_s}{4\pi} \int_0^\pi \left(\frac{\frac{1}{2}D - x\cos\theta}{\sqrt{[(V_s t - \frac{1}{2}W)^2 + F^2(x, \theta)]^3}} - \frac{\frac{1}{2}D + x\cos\theta}{\sqrt{[(V_s t + \frac{1}{2}W)^2 + F^2(x, \theta)]^3}} \right) d\theta \quad (5.19)$$

where $I_s(t) = d\dot{q}/dt$ D is diameter of the ring; q and \dot{q} are the point-charge and the total charge induced on ring, respectively; V_s is the point-charge linear velocity; θ is an angle between the radius and a given location of the point charge; W is the axial length ring(width); and $F(x, \theta)$ is a certain function of x and θ .

$$\dot{q} = \frac{Dq}{4\pi} \int_0^\pi \frac{\frac{1}{2}D - x\cos\theta}{F^2(x, \theta)} \left(\frac{z + \frac{1}{2}W}{\sqrt{[(V_s t + \frac{1}{2}W)^2 + F^2(x, \theta)]}} - \frac{z - \frac{1}{2}W}{\sqrt{[(V_s t - \frac{1}{2}W)^2 + F^2(x, \theta)]}} \right) d\theta \quad (5.20)$$

where the symbols used are the same as for (5.19). If for instance, q_2 and d are equal to zero, (5.20) is the same as (5.19). Not only (5.19) but also (5.20) can be solved using just numerical techniques. They also employed *Gauss law* and considered the rectilinearly travelling point charge as a impulse input of the ring-probe, the consequences supported

Law's study [45].

It seems that the impulse response $h(t)$ can be approximated to a triangular waveform, as illustrated in Figure 5.7. From this approximation the frequency response corresponding to this wave form can then be derived using equation, so that

$$H_S(f) = [j4nA_p\tau^2 f \text{Sinc}(2\pi ft) \text{Sinc}^2(\pi ft)] \quad (5.21)$$

This amplitude frequency response is plotted in Figure 5.8.

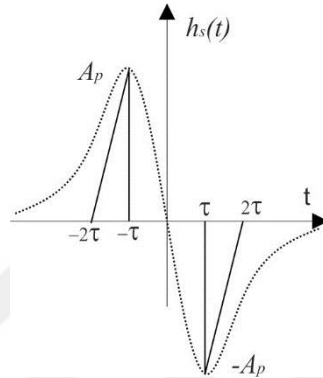


Figure 5.7 Estimated illustration of the impulse response [24].

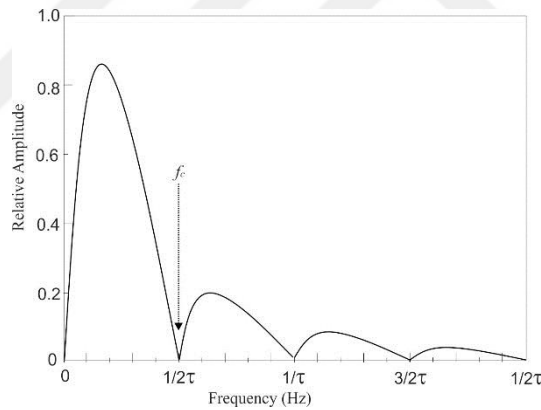


Figure 5.8 Estimated frequency response of the ring sensor [24].

They find that, in the case of electrostatic sensors, the full-ring electrodes have the best homogeneity characteristics [35] and conclude that the ratio of (W/D) is a crucial parameter influencing the homogeneity of the sensor

Gajewski [52] suggests a different novel approach for measurements of solids concentration and axial solids velocity in gas–solid two–phase flows, it is presented in Figure 5.9.

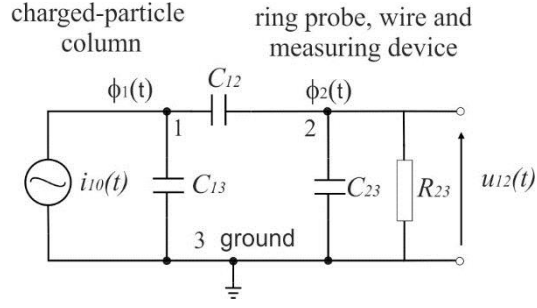


Figure 5.9 Model for the charged-particle, ring probe, wire and device for measurement [52].

$$\Phi_2(s) = \frac{C_p}{C_{23}} \frac{\tau s}{\tau s + 1} \Phi_{21}(s) + \frac{\tau s}{\tau s + 1} \Phi_2(0) \quad (5.22)$$

where $\Phi_2(s)$ and $\Phi_{21}(s)$ are the Laplace parameters.; $\phi_2(0)$ is the initial voltage value; C_p is the electrode self-capacitance C_{23} is the total capacitance of the electrode, wiring, and amplifier input; $\tau = R_{23}C_{23}$ is the system time constant; and R_{23} is the total resistance that consists of the probe leakage resistance. The voltages the steady state:

$$\begin{cases} \Phi_2(t) = aKq_{v1}(t) + k_{c1}q_{v1}(0) = \\ bKq_{v1}(t) + k_{c2}q_{v1}(0), & \text{for } \tau s \gg 1 \\ \Phi_2(t) = aT \frac{dq_{v1}(t)}{dt} + bT \frac{dq_1(t)}{dt}, & \text{for } \tau s \ll 1 \end{cases} \quad (5.23)$$

where $T = R_{23}C_p$ is also the time constant, and a , b , K , k_{c1} , C , and $k_{c2}C$ are, respectively,

$$\text{the other coefficients: } a = \frac{R^2}{4\epsilon\epsilon_0} \ln \frac{\sqrt{R^2 + (\frac{1}{2}L)^2 + \frac{1}{2}L}}{\sqrt{R^2 + (\frac{1}{2}L)^2 - \frac{1}{2}L}} = k_l \frac{R^2}{4\epsilon\epsilon_0}, b = k_l \frac{1}{4\epsilon\epsilon_0} \frac{1}{L}, K = \frac{C_p}{C_{23}}, k_{c1} =$$

$$k_{c2}V = \frac{V}{C_{12}(C_{12}C_{12} + C_{12}C_{12} + C_{12}C_{12})}$$

According to frequency-response of the full-ring-metal electrode potential $\Phi_2(t)$ to rectangular pulse as a point-charge $q_1(t)$ [53] and for the same equivalent circuit diagram, as that in Figure 5.5, is acquired below,

$$|\Phi_2(j\omega)| = 2kq_1\tau \frac{|\sin \omega \frac{b}{2v}|}{\sqrt{\omega^2\tau^2 + 1}} \quad (5.24)$$

where ω is angular frequency of the electrode $q_1 = q_1(t)$ is the point-charge; $\tau = \frac{1}{R_{23}C_{23} + R_{23}C_{12}C_{13}(C_{12} + C_{13})}$ is the time constant; k is a constant related to flow parameters and dimension; b is the probe width; and v is the mean flow velocity

$$\omega_c = 2\pi \frac{v}{b} \quad (5.25)$$

$$0 < \omega \frac{b}{v} \leq \frac{2}{5} \quad (5.26)$$

where ω_c is cutoff angular frequency.

The method of images is employed for the travelling point of charge on an grounded flat, finite, and conductive plane, modeling an internal wall of a cylindrical electrode [54], The approach is built on the idea of only finite conductor plane suggested by Murnane et al. [55] who have further advanced it a form that uses four finite planes organized as a square-section electrode. The general form of a relationship between the point charge Q and the charge induced on the plane Q_{IND} is as follows:

$$Q_{IND} = -\frac{Qh}{2\pi} \iint_{x_1 y_1}^{x_2 y_2} \frac{1}{\sqrt{(x^2 + y^2 + z^2)^3}} dx dy \quad (5.27)$$

$$Q_{IND} = -\frac{Qh}{2\pi} \left[\arctan\left(\frac{x_2}{h} \frac{y_1}{\sqrt{(y_1^2 + x_2^2 + h^2)}}\right) - \arctan\left(\frac{x_2}{h} \frac{y_2}{\sqrt{(y_2^2 + x_2^2 + h^2)}}\right) - \arctan\left(\frac{x_1}{h} \frac{y_1}{\sqrt{(y_1^2 + x_1^2 + h^2)}}\right) + \arctan\left(\frac{x_1}{h} \frac{y_1}{\sqrt{(y_2^2 + x_1^2 + h^2)}}\right) \right] \quad (5.28)$$

where x, y are the coordinates on the plane; x_1, x_2 and y_1, y_2 are the limits to the length and width of the plane, respectively; and h is the height of the charge Q above $z=0$.

The potential $V_{OUT}(t)$ at the amplifier-output is acquired by integrating the current $I(t)$ is expressed by

$$V_{OUT}(t) = H \frac{1}{\tau} \int I(t) dt \quad (5.29)$$

where H is the amplifier gain; τ is the amplifier time constant; and $I(t)$ is the induced current.

The consequences of all studies for full ring shaped conductor probe is employed in the mass flow rate and particle size measurements, frequency analysis

The ring type probe has a linear-static feature. Its evidence is given by some experimental studies [56],[57]. Some amplitude and frequency characteristics of probe, charge amplifier and measuring system is presented by Gajewski [58].

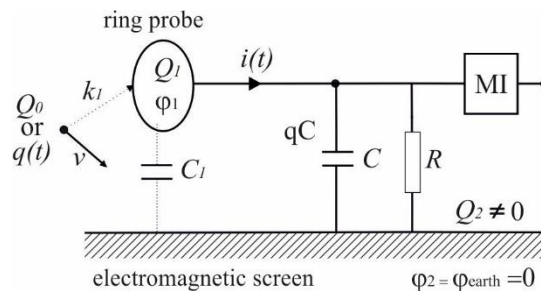


Figure 5.10 Model of ring-probe and measuring instrument for a point-charge [59]

The current-output of electrode is expressed as follows:

$$i(t) = -C_1 \frac{d\phi_1}{dt} - C_0 \frac{dk_1}{dt} \quad (5.30)$$

where C_1 is the capacitance between ground and node 1; $\phi_1 = \phi_1(t)$ is the total probe potential C_1 and C_0 ; Q_0 is the point charge; and k_1 is a certain coupling factor that depends on the point-charge velocity.

$$\Phi_1(s) = \frac{s\tau}{s\tau + 1} Q_0(s) + \frac{s\tau}{s\tau + 1} A(0) \quad (5.31)$$

where R is the total resistance, including leakage, insulation, wiring and the input resistances.

The Laplace transform of the probe potential $\phi_1(t)$ has the following form:

$$\Phi_1(s) = \alpha \frac{C_1}{C^*} \frac{s\tau}{s\tau + 1} \rho(s) + \frac{s\tau}{s\tau + 1} \varphi_1(0) \quad (5.32)$$

$$\Phi_1(s) = \beta \frac{C_1}{C^*} \frac{s\tau}{s\tau + 1} q(s) + \frac{s\tau}{s\tau + 1} \varphi_1(0) \quad (5.33)$$

where $\varphi_1(0)$ is the initial condition

According to the continuation of study on fully circular electrostatic sensor probe obeying electrostatic theory by using data resulting from finite-element analysis by Cheng [27], the one of the most important parameter is ratio wide to diameters of the ring sensor (W/R). In Figure 5.11, Induced charge and related a.c signal is expressed the sensitivity distribution of the electrode relating to the stream line along moving charge passes through the sensor. The spatial sensitivity of a.c signal is the derivative of the spatial charge of particles.

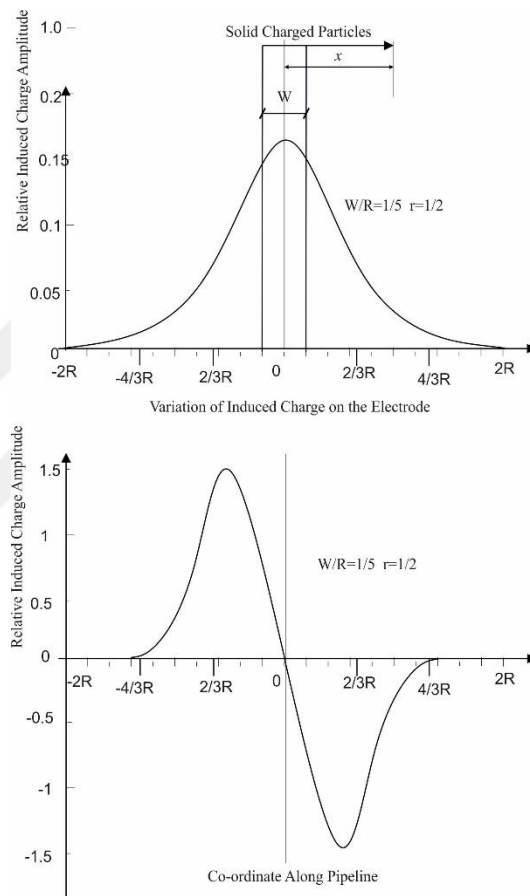


Figure 5.11 Basic ac signal representation the probe interaction with single point [27].

The results of the study show that the charged particle on the axial line nearer (r larger) to the pipe wall, causes a higher level of induced charge on the electrode than that on the central axial line where $r=0$ and some critical properties of sensing may vary narrow ($W/R < 1/2$) and wide ($W/R > 1$). Although one sensing volume is widened with respect to large (W/R) in narrow sensor, two sensing volume of wide sensor having dead zones in Figure 5.12. The sensing volume of narrow electrode is larger with the size of the electrodes

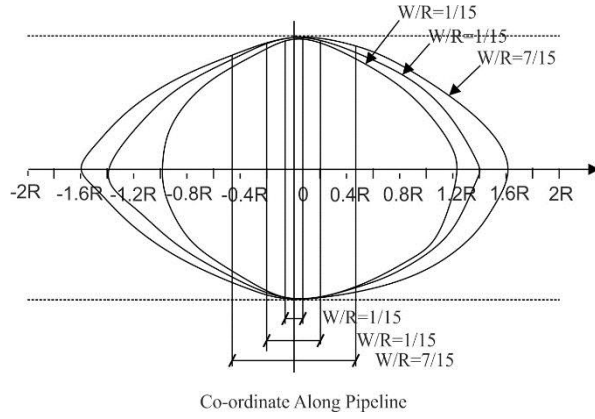


Figure 5.12 Sensing levels of narrow probes [27].

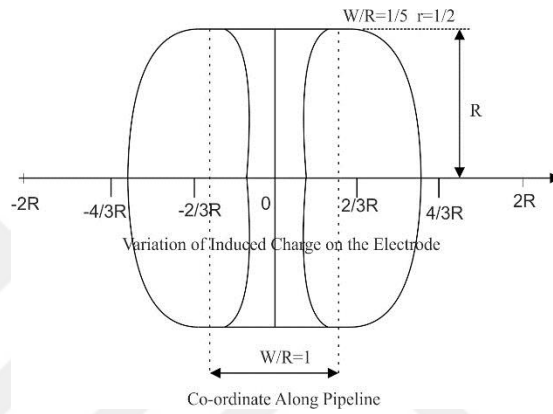


Figure 5.13 Sensing levels of narrow probes ($W/R=1$) [27].

It is desired to express the signal waveforms mathematically so that a more comprehensive analysis of the sensor characteristic can proceed. From observing the two curves shown in Figure 5.11, it was obvious that the data resulting from finite-element analysis can be fitted to curves defined by the equation below;

$$Q = Ae^{-kx^2} \quad (5.34)$$

where x is representing the distance from the center line of the electrode to the source charge. A and k are two parameters determined by a combination of conditions reliant on the electrode dimensions and the axis along which the particle passes through the sensor. The a. c. current signal can be expressed in the form;

$$I(x) = -2kAx e^{-kx^2} \quad (5.35)$$

If $kx=X$ a constant, then

$$I(x) = -2kv^2 e^{-kv^2 t^2} \quad (5.36)$$

where $x=vt$, $I(x) = dQ/dt$ by substituting the relation in equation (5.34) the following expression for the current signal was obtained;

As for signal model for multiple particles, since the electrostatic system is linear

due to the vectorial properties of an electrostatic field, the multiple-particle signals will be the sum of all the individual signals and this can be stated as below;

$$I_{\Sigma}(x) = \sum_{i=-N}^N I(x + i\lambda) \quad (5.37)$$

The effect of electrode geometry is shown Figure 5.14

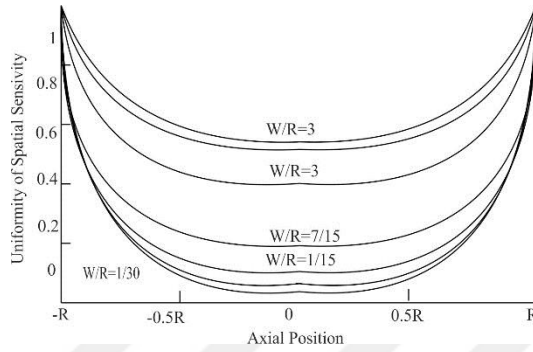


Figure 5.14 Probe geometry affecting on spatial-sensitivity [27].

$$I_{\Sigma}(x) = \sum_{i=-N}^N -2A(x + i\lambda)ke^{-k(x+i\lambda)} \quad (5.38)$$

Both narrow and wide ones width ratio of the two electrodes for a presented electrode dimensions, the spatial sensitivity function can be written as $U(r)$. If the scaling ratio for the two signals is γ , As UA-undercompensated $\gamma = 0.3$ UB-overcompensated $\gamma = 1.0$ in the Figure 5.15, the combined signal spatial sensitivity will be as follows;

$$U_c(r) = U_1(r) - \gamma U_2(r) \quad (5.39)$$

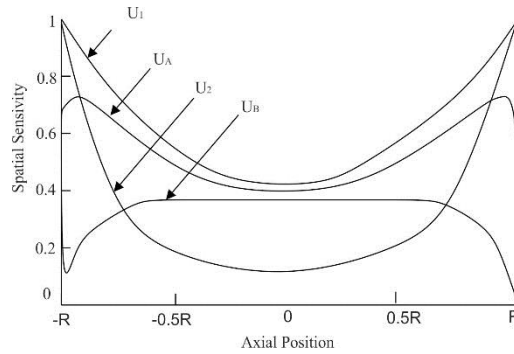


Figure 5.15 The resultant signal [27].

The signal spectrum for a circular electrode will be affected mostly by the resulting factors: solids distribution within the sensing volume, the geometrical ratio of width W to the inner radius R of the electrode and solids velocity, particle size. Result from Cheng's study

$$A(\omega_L) = A(\omega_H) = A_m/\sqrt{2}, \quad \omega_L \approx 0.6954\sqrt{k}, \omega_H \approx 2.2981\sqrt{k}, B_f \approx$$

$0,2551\sqrt{k}$

$$\frac{B_{\omega 1}}{B_{\omega 2}} = \frac{\sqrt{k_1}}{\sqrt{k_2}} = \frac{v_1}{v_2} \quad (5.40)$$

This proposed system by Cheng and Coulthard was incorporated into the prototype commercial systems at the Scottish Power generating plant, Methil Power Station in Fife Scotland. The principle formed the basis of British Patent Application No. 9525067.6 [27].

5.1.2 Since 2000

According to Zhang's study [22], taking into consideration complex flow profiles vary with the conveying velocity, particle size, humidity, temperature and pipe obstructions such as pipe joints and are modified by bends, flanges and pipe geometry for vertical and horizontal conveying pipes, the mass flow rate F_m can be expressed by the expression

$$F_m = \iint_A V(u, v)C(u, v)dudv \quad (5.41)$$

where $C(u, v)$ is the concentration defined on the plane u, v , and $V(u, v)$ is the velocity of the fluid within the pixel at the location u, v .

$$F_m = \iint_A V(u, v)Con(u, v)dudv = \overline{Con_A} \cdot A \cdot \frac{\iint_A V(u, v)C(u, v)dudv}{A} = \overline{Con_A} \cdot A \cdot \overline{V_A} \quad (5.42)$$

The mass flow rate can be derived as shown in the following equation

$$F_{mA} = \overline{Con_A} \cdot A \cdot \overline{V_A} \quad (5.43)$$

$\overline{V_A}$ in the equation is the average velocity over the cross section of the conduit. For certain flows, $\overline{Con_A}$ is a known constant so that by combining equation with the general expression

That means the flow is modulated by flow noise, which is considered as a stationary and ergodic stochastic process. In the electrostatic method, it is assumed that the 'net charge' carried by the solids is directly proportional to the mass flow rate or to the solids concentration.

The relationship between concentration and charges carried by particles.

$$Con(t) = \frac{\pi}{6} \int_{D_{min}}^{D_{max}} N(t) \cdot f(D, t) \cdot \rho_m \cdot D^3 dD \quad (5.44)$$

D_{min} and D_{max} are the minimum and maximum diameters of the particles ranged

D_{min} to D_{max} . $N(t)$ is the number of the particles in unit volume. $f(D, t)$ is the probability density function of the particles with size D . The density, ρ_m , is constant throughout the sensing volume, defined as the mass per unit volume of the solids.

Any arbitrary function $F(t)$ a stochastic process, is composed of two components $\overline{F(t)}$ represents the average of function, $f(t)$ represents the fluctuation about the mean of function $N(t) = \overline{N(t)} + n(t)$, $Con(t) = \overline{Con(t)} + con$, $Q(t) = \overline{Q(t)} + q(t)$, $Vol_p(t) = \overline{Vol_p(t)} + vol_p(t)$, $A_p(t) = \overline{A_p(t)} + a_p(t)$,

, respectively number of particles, concentration, charge, volume and cross sectional area

$$Q(t) = \pi \cdot Vol \cdot \int_{D_{min}}^{D_{max}} N(t) \cdot f(D, t) \cdot \beta \cdot D^2 dD \quad (5.45)$$

where β is the particle surface charge density

$$\frac{Q(t)}{Con(t)} = \frac{6\beta Vol \int_{D_{min}}^{D_{max}} f(D, t) D^2 dD}{\rho_m \int_{D_{min}}^{D_{max}} f(D, t) D^3 dD} = \frac{\beta Vol \overline{A_p(t)}}{\rho_m \overline{Vol_p(t)}} \quad (5.46)$$

For spherical particles of constant diameter D the relationship between $Q(t)$ and $Con(t)$ is as follows

$$\frac{\overline{Q(t)}}{\overline{Con(t)}} = \frac{6\beta Vol}{\rho_m \overline{D}} \quad (5.47)$$

If the particle size has a Gaussian distribution in the range (D_{min} and D_{max}), which does not vary with time i.e.

$$f(D, t) = f(D) = \frac{1}{\sigma_D \sqrt{2\pi}} e^{-\frac{(D-\overline{D})^2}{2\sigma_D^2}} \quad (5.48)$$

Then following conclusion can be drawn

$$\frac{\overline{Q(t)}}{\overline{Con(t)}} = \frac{6\beta Vol}{\rho_m \overline{D}} \left[\frac{1}{\overline{D}} - \frac{2\sigma_D^2}{\overline{D}(\overline{D}^2 + \sigma_D^2)} \right] \quad (5.49)$$

$$q_{rms} = F \left[\overline{Q(t)} \right] = G \left[\overline{Con(t)} \right] \quad (5.50)$$

G expresses the functional relation between $q_{rms}(t)$ and $\overline{Con(t)}$. F and G are generally considered as linear functions. The stationary stochastic process is called an ergodic process. The $q(t)$ is usually considered as an ergodic one. Therefore, the probability function is given by

$$F \left[q_{rms}(t) = \lim_{T \rightarrow \infty} \frac{1}{T} \int_0^T q^2(t) dt \right] = 1 \quad (5.51)$$

In practice, calculations are time limited to obtain the statistical parameters. The time limited average is still a random variable. It is referred to as the 'evaluation' of the true average value. 'Evaluation' is denoted using symbol '^' here.

$$\frac{1}{T} \int_0^T q^2(t) dt = \hat{E}[q^2(t)] = \hat{q}_{rms}^2 \quad (5.52)$$

$$\hat{q}_{rms}^2 = \frac{1}{M} \sum_{j=1}^M q_j^2 \quad (5.53)$$

$$\hat{q}_{rms} = \sqrt{\frac{1}{M} \sum_{j=1}^M q_j^2} = F[\overline{Q(t)}] = G[\overline{Con(t)}] \quad (5.54)$$

$Q(t)$ expresses the functional relation between $q_{rms}(t)$ and $\overline{Con(t)}$. F and G are generally considered as linear functions

As for power spectral density function of $q(t)$, if $q(t)$ is considered as a stationary and ergodic stochastic process then according to the Weiner-Khinchine formula, its auto (power) spectral density function $S_{qq}(f)$ is the Fourier transform of its auto-correlation function $R_{qq}(t)$, i.e.

$$S_{qq}(f) = \int_{-\infty}^{\infty} R_{qq}(\tau) e^{-j2\pi f\tau} d\tau \quad (5.55)$$

In practice, it is more convenient to work with the spectra defined over the nonnegative frequency region. This is called a one-sided spectral function.

$$S_{qq}(f) = 2 \int_0^{\infty} R_{qq}(\tau) e^{-j2\pi f\tau} d\tau, \quad \text{for } f \geq 0 \quad (5.56)$$

Since auto-correlation functions are always even functions of τ , the power spectrum is entirely real.

$$S_{qq}(f) = 4 \int_0^{\infty} R_{qq}(\tau) \cos(2\pi f\tau) df \quad (5.57)$$

Conversely the auto-correlation function is given by the inverse transformation

$$R_{qq}(\tau) = 4 \int_0^{\infty} S_{qq}(f) \cos(2\pi f\tau) df \quad (5.58)$$

Both the power spectral density and the auto-correlation function can be analyzed online or off-line, provided that $q(t)$ can be separated from the overall signal.

Mathematical modeling of the charge induced on an isolated circular electrode owing to a single charged particle has been developed by many researcher mentioned

previously. The mathematical expression by using Finite Element Method (FEM) [22, 27] for the charges induced due to a single unit point charged particle below;

$$s(r, W, x) = A(r, W)e^{-k(r, W)x^2} \quad (5.59)$$

According to the analyses Cheng [27], when the width of the circular electrode is less than $\frac{1}{2}$ radius of the pipe, the relationship between $A(r, W)$, $k(r, W)$ and r , W can be obtained by curve fitting as follows;

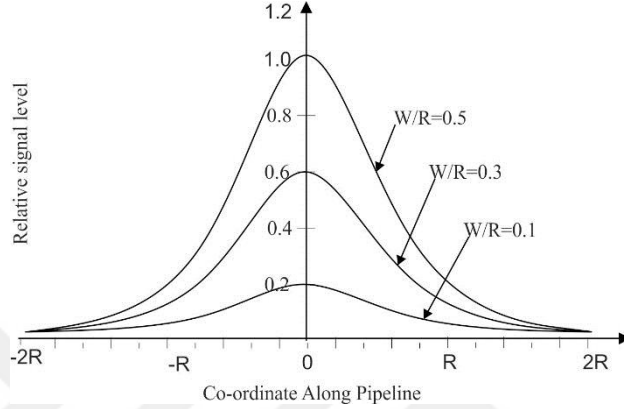


Figure 5.16 Representation of charge variation with different widths [27].

Combining with equation (5.59) with the assumption made previously

$$s(r, W, x) = \beta\pi D^2 A(r, W)N(r, x)e^{-k(r, W)x^2} \quad (5.60)$$

where p and D are the surface charge density and the diameter of the particle respectively.

The total induced charges produced by particles within whole sensing volume can be derived from following equation

$$S = \iint_{Vol} 2\beta\pi^2 r A(r, W)N(r, x)e^{-k(r, W)x^2} \int_{D_{min}}^{D_{max}} D^2 f(D) dD dr dx \quad (5.61)$$

the concentration can be expressed as follows

$$Con(t) = \frac{\pi}{6Vol} \iint_{Vol} dr dx \int_{D_{min}}^{D_{max}} N(r, x) \cdot f(D) \rho_m D^3 dD \quad (5.62)$$

With combining equations

$$\frac{S}{Con(t)} = \frac{\iint_{Vol} 2\beta\pi^2 r A(r, W)N(r, x)e^{-k(r, W)x^2} \int_{D_{min}}^{D_{max}} D^2 f(D) dD dr dx}{\frac{\pi}{6Vol} \iint_{Vol} dr dx \int_{D_{min}}^{D_{max}} N(r, x) \cdot f(D) \rho_m D^3 dD} \quad (5.63)$$

where β , D , $N(r, x)$ and $f(D)$ are the surface charge density, the diameter of the particle, the particle number in a unit volume at that position and the particle size distribution probability density respectively. Vol represents the sensing volume.

As for static characteristics of the electrode when particles are uniformly distributed

over the whole sensing volume, if particles in the sensing volume are evenly distributed, then the number of particles in a unit volume is constant. If $N(r, x) = N = \text{constant}$ the concentration therefore is

$$Con = \frac{\rho_m}{6} N \pi \int_{D_{min}}^{D_{max}} D^3 f(D) dD \quad (5.64)$$

When the particles are spherical and of uniform size having a diameter \bar{D} , it follows that

$$\int_{D_{min}}^{D_{max}} \pi D^2 f(D) dD = \pi \bar{D}^2 \quad (5.65)$$

$$\frac{S}{Con} = \frac{12\beta\pi^2 R^2 B}{\bar{D}\rho_m \sqrt{1 - k_1 \frac{W}{R}}} \frac{W}{R} \quad 0 < \frac{W}{R} < \frac{1}{2} \quad (5.66)$$

Particles having a Gaussian distribution

$$\frac{S}{Con} = \frac{12\beta\pi^2 R^2 B}{\bar{D}\rho_m \sqrt{1 - k_1 \frac{W}{R}}} \frac{W}{R} \left[1 - \frac{2\sigma_D^2}{(\bar{D}^2 + 3\sigma_D^2)} \right] \quad (5.67)$$

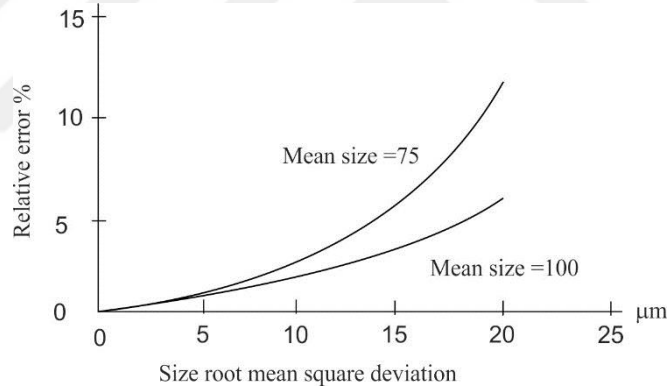


Figure 5.17 Relative error owing to particle size [22].

Static characteristics when the flow forms a 'rope'

$$S = \int_{r_1}^{r_2} 2\beta\pi^2 r A(r, W) dr \int_{L_1}^{L_2} N(r, x) e^{-k(r, W)x^2} dx \int_{D_{min}}^{D_{max}} D^2 f(D) dD \quad (5.68)$$

In this equation, r_1 , and r_2 are the inner and outer radii of the ring shaped roping stream. L_1 , and L_2 are the sensing volume dimensions along the pipeline. D_{min} and D_{max} are the diameters of maximum and minimum particle.

$$\begin{aligned} S &= h(t) = \frac{12\beta\pi\phi R^2}{\rho_m \bar{D}} \iint_{Vol} \frac{r}{R} A(r, W) \delta \left[t - \frac{\dot{x}}{V} \right] e^{-k(r, W)\phi^2 \dot{x}^2} d \frac{r}{R} \\ &= \frac{12\beta\pi\phi R^2}{\rho_m \bar{D}} \int_0^1 \frac{r}{R} A(r, W) d \left(\frac{r}{R} \right) \int_{-\infty}^{\infty} \delta \left[t - \frac{\dot{x}}{V} \right] e^{-k(r, W)\phi^2 \dot{x}^2} d \dot{x} \end{aligned} \quad (5.69)$$

Because $\int_{-\infty}^{\infty} \delta \left[t - \frac{\dot{x}}{v} \right] e^{-k(r,W)\varphi^2 \dot{x}^2} d\dot{x} = e^{-k(r,W)\varphi^2 \dot{x}^2}$

The dynamic response of the electrode

$$h(t) = \frac{12\beta\pi\phi R^2}{\rho_m \bar{D}} \int_0^1 \frac{r}{R} A(r, W) d\left(\frac{r}{R}\right) e^{-k(r,W)\varphi^2 \dot{x}^2} d\frac{r}{R} \quad -\infty < t < \infty \quad (5.70)$$

Frequency response characteristics of the electrode Applying Fourier transformation to equation 3.32, the frequency response characteristic of a circular electrode is as follows

$$\begin{aligned} H(\bar{\omega}) &= \int_{-\infty}^{\infty} h(t) e^{-j\omega t} dt \quad () \\ &= \frac{12\beta\pi\phi R^2}{\rho_m \bar{D}} \int_{-\infty}^{\infty} e^{-j\omega t} dt \int_0^1 \frac{r}{R} A(r, W) e^{-k(r,W)V^2(\varphi t)^2} d\frac{r}{R} \quad (5.71) \end{aligned}$$

$$= \frac{12\beta\sqrt{\pi^3}R^2}{\rho_m \bar{D}V} \int_0^1 \frac{r}{R} \frac{A(r,W)}{\sqrt{k(r,W)}} e^{-\left[\frac{(\bar{\omega})^2}{4V^2} \frac{1}{k(r,W)}\right]} d\frac{r}{R}$$

$$A(r, W) = a_0 \left(\frac{W}{R}\right) \left[1 + a_1 \left(\frac{r}{R}\right)^2\right] \quad 0 \leq r < \frac{6}{10} R$$

$$k(r, W) = k_0 \left[1 - k_1 \left(\frac{W}{R}\right)\right] \left[1 + k_2 \left(\frac{r}{R}\right)^2\right] \quad 0 \leq r < \frac{6}{10} R \quad (5.72)$$

$$A(r, W) = a_2 \left(\frac{W}{R}\right) \left[a_3 \left(\frac{r}{R}\right)^2 - 1\right] \quad 0 \leq r < R$$

$$k(r, W) = k_3 \left[1 - k_1 \left(\frac{W}{R}\right)\right] \left[k_4 \left(\frac{r}{R}\right)^2 - 1\right] \quad 0 \leq r < R$$

$H(\bar{\omega})$ does not converge to an analytical expression but it is clear that $H(m)$ has low pass filtering characteristics which are also related to velocity. Although an analytical solution cannot be obtained, the frequency response characteristics of the electrode at a given radius r still can reveal its intrinsic frequency dependent nature.

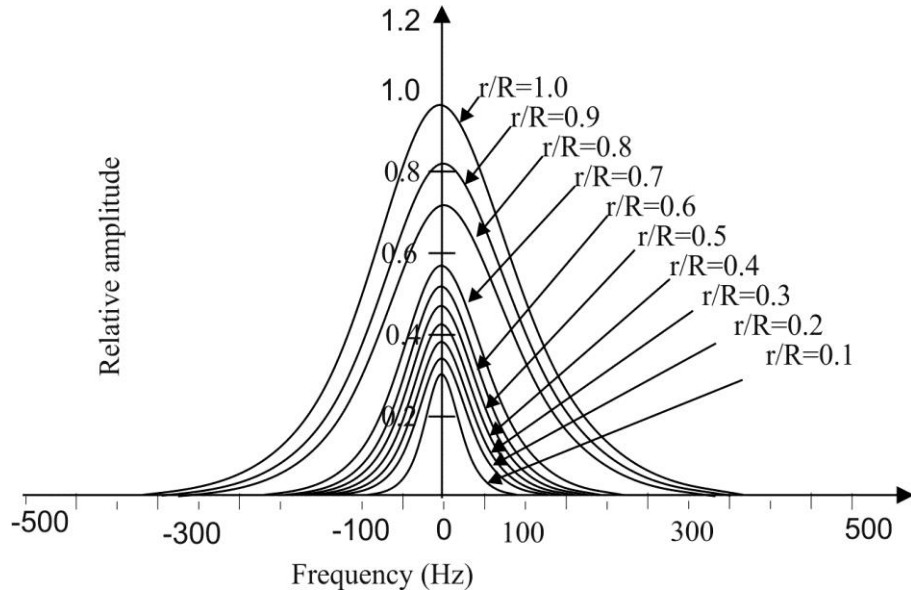


Figure 5.18 For values $R=150$ mm, $V=15$ m/s, $W/R=0.5$, spatial sensitivity in frequency domain [22].

Equivalent circuit of the circular electrode is below;

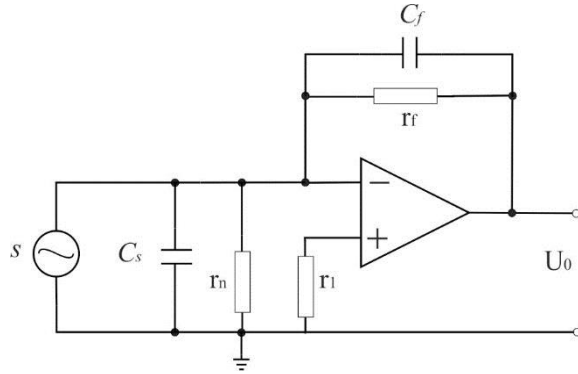


Figure 5.19 The charge Amplifier [22].

The amplitude-frequency characteristics of the sensor

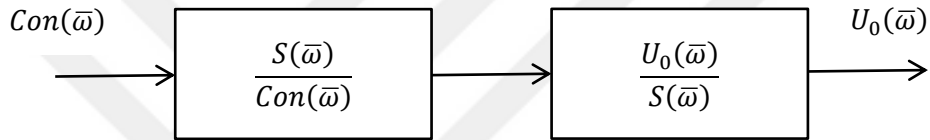


Figure 5.20 The transfer function of ring probe [22].

$$H(\bar{\omega}) = \frac{S(\bar{\omega})}{Con(\bar{\omega})} = \frac{12\beta\sqrt{\pi^3}R^2}{\rho_m \bar{D}V} \int_0^1 \frac{r}{R} \frac{A(r,W)}{\sqrt{k(r,W)}} e^{-\left[\frac{(\bar{\omega})^2}{4V^2} \frac{1}{k(r,W)}\right]} d\left(\frac{r}{R}\right) \quad (5.73)$$

The transfer function of the ac coupled preamplifier circuit as shown in Fig.4.2a is a second-order filter that can be expressed as follows

$$P(\bar{\omega}) = \frac{U_o(\bar{\omega})}{S(\bar{\omega})} = \left(1 + \frac{r_2}{r_1}\right) \frac{-\bar{\omega}^2 C_d r_d r_n}{1 + j\bar{\omega}(C_n r_n + C_d r_d + C_d r_n) - \bar{\omega}^2 C_d r_d C_n r_n} \quad (5.74)$$

The tranfer function of the ac coupled preamplifier circuit as shown in Fig.4.2a is a second-order filter that can be expressed as follows

$$T(\bar{\omega}) = H(\bar{\omega}) * P(\bar{\omega}) \quad (5.75)$$

$$= \left[\frac{12\beta\sqrt{\pi^3}R^2}{\rho_m \bar{D}V} \left(1 + \frac{r_2}{r_1}\right) \frac{-\bar{\omega}^2 C_d r_d r_n}{1 + j\bar{\omega}(C_n r_n + C_d r_d + C_d r_n) - \bar{\omega}^2 C_d r_d C_n r_n} \right] \cdot \left[\int_0^1 \frac{r}{R} \frac{A(r,W)}{\sqrt{k(r,W)}} e^{-\left[\frac{(\bar{\omega})^2}{4V^2} \frac{1}{k(r,W)}\right]} d\left(\frac{r}{R}\right) \right]$$

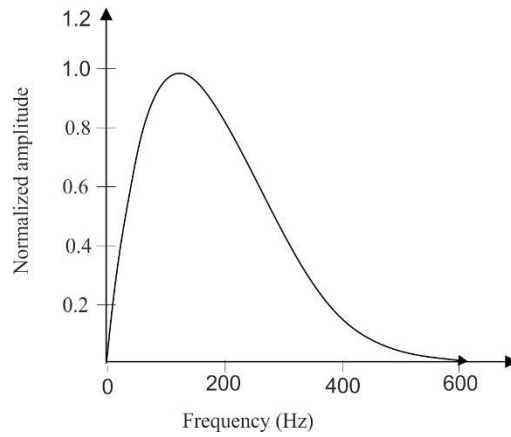


Figure 5.21 For values $R=150$ mm, $V=25$ m/s, $W=40$ mm frequency characteristic of the probe [22].

Results of amplitude frequency characteristic of the sensor at a velocity 25 m/s for diameter =300mm, $r_n=1\text{M}\Omega$, $C_n=1.47\text{nF}$, $r_d=0.1\text{M}\Omega$, $C_d=1\mu\text{F}$ [22]

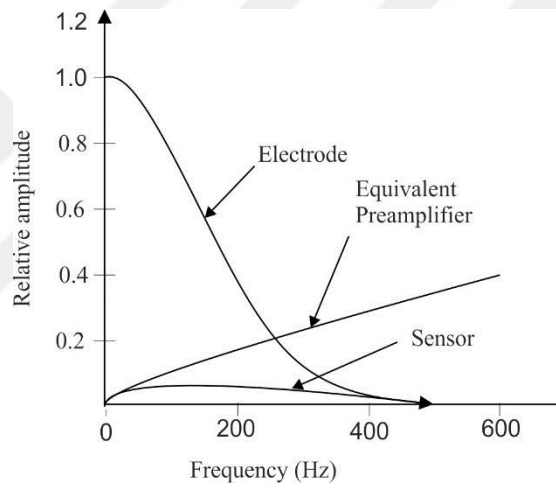


Figure 5.22 For values $R=150$ mm, $V=25$ m/s, $W=40$ mm frequency characteristic of the probe sensor [22].

The following analytical expression via curve-fitting is derived based on the related data [60, 61]. A double Gaussian equation offers high fitting accuracy,

$$S(r, z) = A(r)e^{-B(r)z^2} + C(r)e^{-D(r)z^2} \quad (5.76)$$

where A, B, C, D are determined by the geometric shape of the electrode and radial position r of a charged particle inside the pipe. Combining equations, we have,

$$U_i = \frac{1}{C} Q(t) = \iiint_{\Omega_r} q(r, \theta, z, t) [A(r)e^{-B(r,z)z^2} + C(r)e^{-D(r,z)z^2}] d\Omega \quad (5.77)$$

Poisson equation and boundary conditions:

$$\left\{ \begin{array}{l} \nabla \cdot (\varepsilon \cdot \nabla \Phi) = -\rho \\ \Phi(r, \theta, z)|_{(r, \theta, z) \in \Gamma_p} = 0 \\ \Phi(r, \theta, z)|_{(r, \theta, z) \in \Gamma_s} = 0 \\ \Phi(r, \theta, z)|_{(r, \theta, z) \in \Gamma_e} = c \end{array} \right. \quad (5.78)$$

$$s(z) = ae^{-bz^2} + ae^{-bz^2} \quad (5.79)$$

$$q = \iint i(z, r)s(z, r) dz dr \quad (5.80)$$

$$\begin{aligned} H(f) &= \int h(t)e^{-j2\pi ft} dt = \left(\int \int SS(f_z)e^{-j2\pi f_z vt} df_z \right) e^{-j2\pi ft} dt \\ &= \frac{1}{v} SS\left(-\frac{f}{v}\right) = \frac{a\sqrt{\pi}}{v\sqrt{b}} e^{-\frac{\pi^2 f^2}{bv^2}} + \frac{c\sqrt{\pi}}{v\sqrt{d}} e^{-\frac{\pi^2 f^2}{dv^2}} \end{aligned} \quad (5.81)$$

where $SS(f_z)$ is the spatial Fourier transform of $s(z)$ and equal to $S(2\pi f_z)$.

The total amount of the induced charge q on it can be calculated using the following equation due to the axis-symmetry of the measuring head. The induced charge $q(t)$ can then be determined by

$$q(t) = \iint i(z + vt, r)s(z, r) dz dr \quad (5.82)$$

The autocorrelation function of $q(f)$ is defined as

$$\begin{aligned} \Phi_q(\tau) &= E[q(t)q(t + \tau)] \quad (5.83) \\ &= E \left[\iint i(z + vt + v\tau, r)s(z, r) dz dr \iint i(\alpha + vt + v\tau, \beta)s(\alpha, \beta) d\alpha d\beta \right] \\ &= \iint \iint i(z - \alpha + v\tau, r - \beta)s(z, r)s(\alpha, \beta) dz dr d\alpha d\beta \end{aligned}$$

where $\langle j \rangle_t(z, r)$ is the autocorrelation function of electrostatic flow noise $i(z, r)$. According to Wiener Khintchine theorem, the power spectrum of $q(t)$ is expressed as

$$S_q = \int_{-\infty}^{\infty} \Phi_q(\tau) e^{-j2\pi f\tau} d\tau \quad (5.84)$$

$$\begin{aligned}
&= \iiint \iiint S_f(f_z, f_r) e^{-j2\pi f_z(-\alpha+v\tau)-j2\pi f_r\beta} S_f^*(f_z, f_r) s(\alpha, \beta) e^{-j2\pi f\tau} df_z df_r d\alpha d\beta d\tau \\
&= \frac{1}{v} \int S_i\left(\frac{f}{v}, f_r\right) \left| S_i\left(\frac{f}{v}, f_r\right) \right|^2 df_r
\end{aligned}$$

where $S_j(f_z, f_r)$ is the power spectrum of electrostatic flow noise $i(z, r)$, $S(f_z, f_r)$ is the Fourier transform of the spatial sensitivity function $s(z, r)$, and $S^*(f_z, f_r)$ denotes the complex conjugate of $S(f_z, f_r)$. They are given respectively by

$$S_f(f_z, f_r) = \iint \phi_i(z, r) e^{-j2\pi(f_z z + f_r r)} dz dr \quad (5.85)$$

$$S_f(f_z, f_r) = \iint s(z, r) e^{-j2\pi(f_z z + f_r r)} dz dr \quad (5.86)$$

$$S^*(f_z, f_r) = S(-f_z, -f_r) \quad (5.87)$$

$$S(r, z) = A(r)e^{-B(r,z)z^2} + C(r)e^{-D(r,z)z^2} \quad (5.88)$$

where Ω , r denotes the sensing zone of the electrode. Due to the uncertainty of the charge distribution of particles, the electrostatic charge noise $q(r, \theta, z, t)$ is a stochastic variable function of time. $s(r, \theta, z)$ is the space sensitivity distribution function. From equation (11), the induced charge $Q(t)$ on the electrode is the weighted average of $q(r, \theta, z, t)$ by $s(r, \theta, z)$ which can be found using FEM mentioned above.

$$Q(t) = \iiint_{\Omega} q(r, \theta, z, t) s(r, \theta, z) d\Omega \quad (5.89)$$

where A , B , C , D are determined by the geometric shape of the electrode and radial position r of a charged particle inside the pipe. Combining equations (5) (10) and (12), we have,

$$U_i = \frac{1}{C} Q(t) = \iiint_{\Omega} q(r, \theta, z, t) [A(r)e^{-B(r,z)z^2} + C(r)e^{-D(r,z)z^2}] d\Omega \quad (5.90)$$

$$U_0 = \frac{k}{C} \frac{dQ(t)}{dt} = \frac{k}{C} \frac{\iiint_{\Omega} q(r, \theta, z, t) [A(r)e^{-B(r,z)z^2} + C(r)e^{-D(r,z)z^2}] d\Omega}{dt} \quad (5.91)$$

$$U_0 = \frac{k}{C} \frac{dQ(t)}{dt} = \frac{k}{C} \iiint_{\Omega} \left[\frac{\partial q}{\partial r} \frac{dr}{dt} + \frac{\partial q}{\partial \theta} \frac{d\theta}{dt} + \frac{\partial q}{\partial z} \frac{dz}{dt} + \frac{\partial q}{\partial t} \right] \left[\frac{\partial S}{\partial r} \frac{dr}{dt} + \frac{\partial S}{\partial z} \frac{dz}{dt} \right] d\Omega \quad (5.92)$$

where $\frac{\partial q}{\partial r}$, $\frac{\partial q}{\partial \theta}$ and $\frac{\partial q}{\partial z}$ are the distribution gradient along the radial, circumferential and axial coordinates of the charges carried by particles. $\frac{dr}{dt} = Vr$, $\frac{d\theta}{dt} = V\theta$, and $\frac{dz}{dt} = Vz$ are the particle velocity projections at the radial, tangential and axial directions. In real powder pneumatic conveyance, the charges carried by the particle q is one of principal sources contributed

to the detected signal, which is determined primarily by the solids concentration, $\frac{\partial S}{\partial r}$, $\frac{\partial S}{\partial z}$ the partial derivatives of the spatial sensitivity $s(r,z)$ are dependent upon the geometry of electrode and the location of particles. Besides, it can be seen that the output of the meter is affected by the velocities and the rate of change in charges carried by particles, because the output of the meter is proportional to the derivative of the charges induced on the electrode [61].

$$Q_{NET}^r = \sigma_p \pi D_p^2 N \int_{L_x} A(r, W) e^{-k(r, W)x^2} dx \quad (5.93)$$

where A and k in equation are replaced with $A(r, W)$ and $k(r, W)$ to represent their dependences on electrode width and position of the stream with respect to the center axis [22]. If we consider this roping particle stream wave travelling at velocity V as a delta function, i.e.

$$Q_{NET}^r = \sigma_p \pi D_p^2 N(t) = \delta\left(t - \frac{x}{V}\right) \quad (5.94)$$

At any given time, at only one point along the x direction where Q_{NET} , r exists, this point is $x=V*t$. Hence Eq. (5.94) becomes

$$Q_{NET}^r = h_{rd}(t) = A(r, W) e^{-k(r, W)x^2} \quad (5.95)$$

This equation describes the dynamic response of a ring-shaped electrode to a unit impulse of net charge carried by solid particles at radius r . The variable $h_{rd}(t)$ is sensitive to the stream spatial position. Applying Fourier transformation to Eq. (5.96), the spatial frequency-response characteristic of a ring-shaped electrode to a unit impulse of net charge carried by particles is,

$$H(\bar{\omega}) = \int h(t) e^{-j\omega t} dt = \int_{-\infty}^{\infty} A(r, W) e^{-k(r, W)V^2 t^2} e^{-j\omega t} dt = \frac{A(r, W)\sqrt{\pi}}{V\sqrt{k(r, W)}} e^{-\frac{\omega^2}{4V^2} \frac{1}{k(r, W)}} \quad (5.96)$$

6. ELECTROSTATIC SENSING TECHNIQUE

6.1 Electrostatic Method

The phenomenon of triboelectric charge generated in pneumatic conveying of solids has long been known and employed for measuring gas-solids flow. The measurement devices of this sort is referred to as the electrostatic flow meter. The electrostatic flow meter is based on the measurement of charges that are induced on the electrodes when the solids pass through the sensing volume. The RMS value of the charge fluctuations are proportional to the charges carried by the solids which, in turn, are related to the solids concentration or mass flow rate. The signals derived from this type of sensing system have been used for measuring mass flow rate, velocity and concentration of solids.

After the pioneering research carried out by Cheng and Zhang [22, 27], the electrostatic technique has become applicable to measurements of solids concentration in pneumatic conveying systems. This method is advantageous due to the following facts 1) there is no restriction in flow, 2) it is relatively low cost, 3) it is suitable for applications in very hostile environments, 4) it is free from radiation hazards, 5) it provides high sensitivity with low maintenance and 6) the data can be processed with digital signal processing techniques. The major disadvantage of this type of flow meter is that the detected signal is an output of multiple variables since the acquired electrostatic charge signals depend upon many factors, such as material type, moisture content and particle size. Therefore, measurements of solids concentration by electrostatic sensors can only offer a relative indication of mass flow rate, which can be used for balancing the distribution of solids between conveyors in applications where other parameters are identical.

The instruments that can be used of metering mass-flow rates must be robust, reliable and reasonably accurate [27]. It is presented that for complex flow regimes, like roping flow, the non-uniform spatial sensitivity of an electrostatic sensor would affect the sensor output. Also, electrode shape may change the sensor output. Additionally, simulations and experiments carried out on electrostatic sensors with ring-shaped electrodes showed that lower frequency components dominated the sensor output. Gas-solids flow can exhibit a variety of complex regimes due to inhomogeneous concentration and velocity distributions within a given cross sectional area. These complex flow profiles vary with the conveying velocity, particle size, humidity, temperature and pipe obstructions such as pipe joints are modified by bends, flanges and pipe geometry. As

given in Section 4.2.1.3, passive methods produce favorable results since active methods based on charging the passing by solid flow can lead to electrostatic hazards due to highly charged particles.

6.2 Signal Generation by the Electrostatic Sensor

Particles can be charged electrostatically by frictional contact charging, charge transfer from one object to another and charging of a conductor by induction due to the presence of charges within its sensing field. In case of a metal pipe wall, which is usually earthed and originally uncharged, flowing particles are charged by frictional contact between particles, and particles and the pipe wall, and particles and the conveying air. The resultant charge on the solids facilitates the monitoring of the charge level which, in turn, provides data on the flow process. It is difficult to predict the absolute amount of charge since it depends on many factors including the variable conditions of solids transportation, the type of material, the particle size and shape, the material comprising the conveying pipe walls, the roughness of the inner surface of the conveying pipe and the pipe diameter. Also, the polarity of the charge may vary depending on those conditions.

Another source charge method is induction. Charges can be induced on a conductor in an electrostatic field generated by charged particles. The field distribution is changed by this conductor. When conductor is isolated from the earth, the potential relies on the amount of charges, the permittivity of particles and particle positions relative to the conductor. The charge accumulated on the particles due to induction vanishes when the charged particle moves away from the vicinity or sensing volume of the conductor as in the case of pneumatic conveyance.

The sensing volume is defined as the entire region where a charged particle influencing the signal produced by the sensor. By changing the sensing volumes from few millimeters to few meters, the signal amplitudes can be increased largely. Generally, this is accomplished by integrating multiple pipes into the system. If the same flow conditions, as described in chapter 3, exists inside each of the pipes, it is expected that the total charge measured from every pipe is almost equal to the measure of the solids transported through each pipe. Therefore, the signal amplitude can be enhanced. It is known that, under 'lean phase' flow conditions, i.e. the solid flow density is low, as usually occur in power stations, this assumption is known to be valid. Therefore, a 'relative measurement' of solids loading by the electrostatic sensor is possible permitting a means of balancing the

solids flow by control of the distribution of pulverized coal through parallel pneumatic conveyors, each carrying the same material.

During the passage of charged particles through the sensing field, electrical charges will be generated on the electrode due to the following effects; the first, impact between particles and the inner surface of the electrode, the second, charge transfer which takes place during the subsequent separation of the particles from the contacting surface, the third, induced charge due to the presence of charged particles within the pipe [27]. The performance of the system depends fundamentally upon the characteristics of the signals. The signals consist of two main components; acquired from an electrostatic sensor is related to particles contacting with the electrode and the charge inducement which requires no contact with the electrode sensing volume.

There are various factors affecting the signal acquisition quality of the system. Low detection threshold and high sensitivity are some of the major issues that must be considered in the measurement system. High sensitivity is a factor that is generally used in choosing a suitable type of sensor to detect the lean flow, where the density of the solid is low. Electrostatic systems are generally noisy and yielding little signal amplitudes. Because of the acquisition of very low amplitude signals, low-noise amplifiers need to be used closely situated to the sensors to obtain the highest signal-to-noise ratios. Although the quality of the amplifier directly affects the output of the system, there are other factors affecting it. The acquired signal depends on the size of the electrode, the type of signal processing, the pipe diameter and the concentration of the conveyed solids. Since the speed of charged particles passing through the sensor is insignificant compared with the speed of light, electromagnetic effects are generally neglected. Shortly, the electrical field can be assumed to be entirely electrostatic and analysis of the problem can be carried out by the basic electrostatic field theorems.

6.3 Electrostatic Sensor

Electrostatic sensor is composed of different parts. In order to analyze the electrostatic flow probes mathematically and metrologically, various factors must be taken into consideration. Impedances of detectors, wires, and preamplifiers, amplifiers and other circuits directly affect the results. The capacitance plays a very important role in the electrostatic induction of both charge and potential on the electrostatic flow probes, sensors, etc., in any measuring system based on the method. The induction occurs if and only if the nonzero capacitance exists. Also, there are additional factors, such as sampling and signal processing algorithms. Therefore, for designing an electrostatic sensor, all the factors from the sensor to the other end may affect the system performance. Each must be dealt with in proper ways.

6.3.1 Mathematical model for charge induction

The flow noise is generated by the small, irregular, average flow of charged solid particles in pipes of pneumatic transport. The small irregular band-limited Gaussian variable fluctuation superimposed on the flow of charged solid particles in the sensing area [53].

As aforementioned in section 5.1, Law's model [45] complying with Coulomb's Law in Equation (2.26) was probably first mathematical model for electrostatic sensor. The further mathematical model by Gajewski is shown in Figure 6.1 and 6.2. After Gajewski [48] and Yan [24] study, Cheng [27] (Eq 5.34) and Zhang [22]. (Eq 5.59) developed a model fitted curve with FEM. The latest model by Xu [61]. (Eq 5.77) was a double Gaussian equation offers high fitting accuracy.

6.3.2 Electrostatic flow probe: the physical model

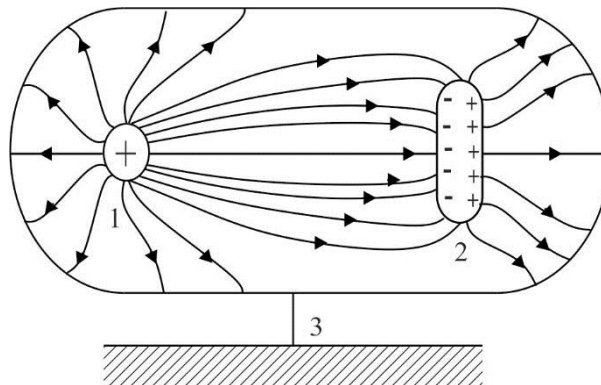


Figure 6.1 Three electrode system: the net electric charge of solid particle in the sensing zone (1), the metal ring probe (2), and grounded electromagnetic screen (3) [53].

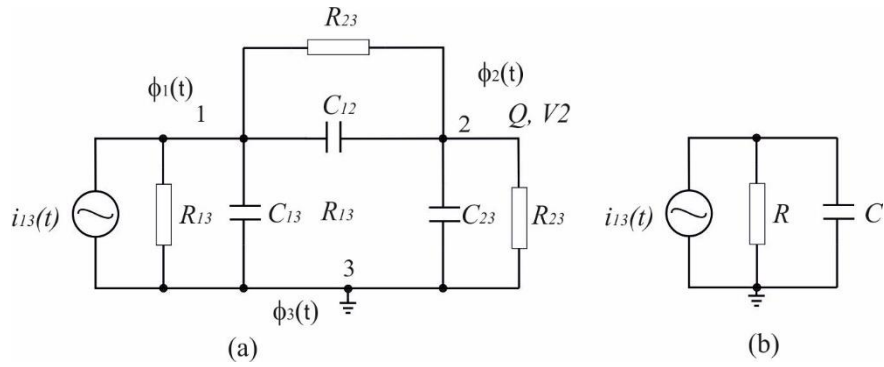


Figure 6.2 Full circuit diagram of the modeled source of a useful signal, and of the real electrostatic flow probe and measuring preamplifier (a) and simplified model

The most popular electrodes developed and used widely are full-ring-shaped ones. There are some theoretical considerations and practical laboratory experiments, and their results are presented and published widely where the single charged particles are taken into account. The charged particle or charged particles aligned can travel rectilinearly along the ring's geometrical axis or any other axis parallel to that geometrical one. Some of the electrode designs are not full-ring shaped. They can be different forms, such as split-ring probes, insulated probes inserted through the transfer pipe walls, quarter-ring probes, half-ring probes, pin electrodes, probes mounted flush with the pipe wall and hemisphere-shaped [62]. The form of full ring sensors can be a direct contact with the flowing charged solid particles. Common electrodes used in electrostatic flow sensor are presented in Figures (6.3), (6.4), (6.5) and (6.6).

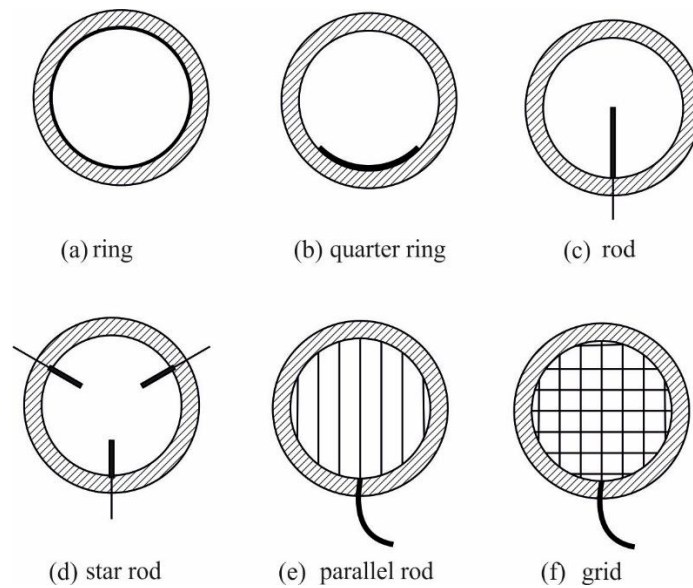


Figure 6.3 Common electrodes used in electrostatic flow sensor

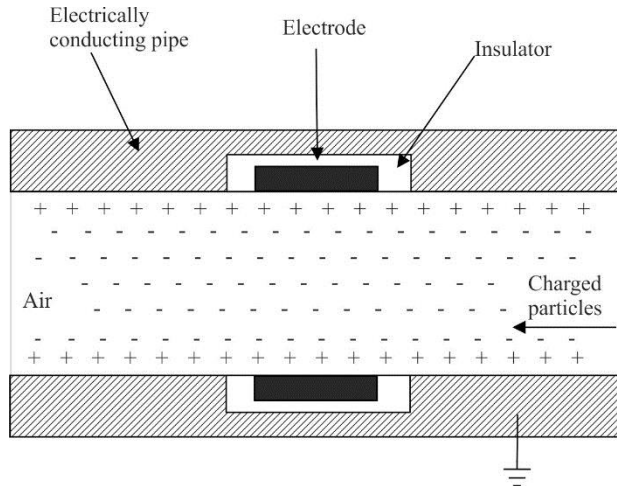


Figure 6.4 Fully ring sensor installed flush with pipe

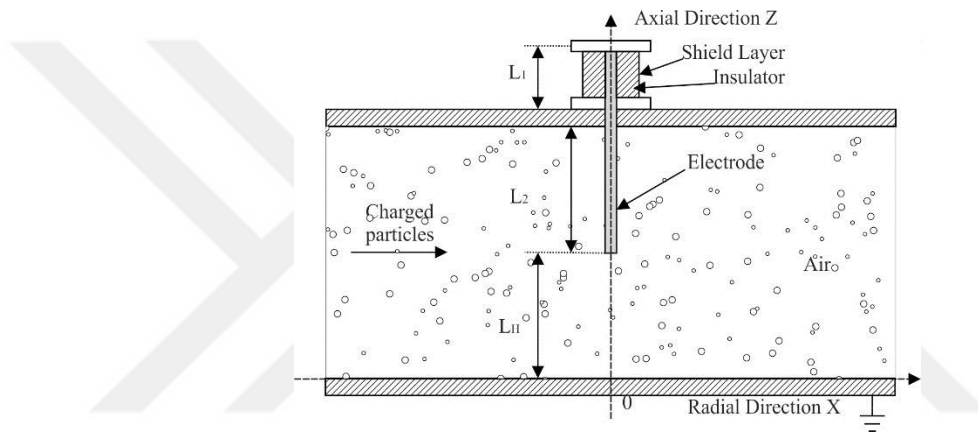


Figure 6.5 Measuring head cross-section of rod electrostatic sensor

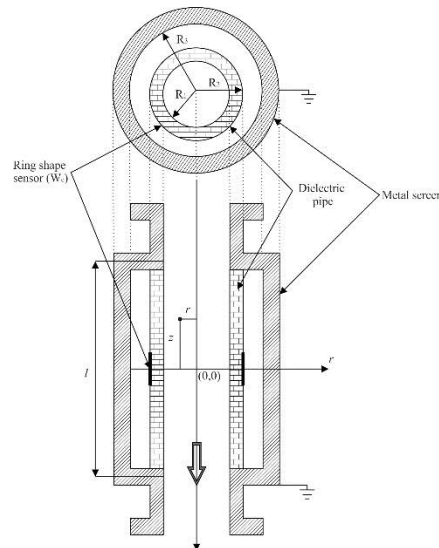


Figure 6.6 Measuring head cross-section of ring-shape electrostatic sensor

The optimum shape of electrodes appears to be the ring type, however other shapes such as pin type and quarter-ring type have also been proposed in some applications. Compared with full-ring electrodes, pin electrodes and quarter-ring electrodes have less

symmetrical sensing volumes corresponding to a more pronounced inhomogeneous spatial sensitivity Ring-shaped electrodes have certain advantages over other forms, since they are able to average the flow velocity circumferentially and have a higher sensitivity than the other types for the same axial length. In comparison with ring-shaped ones, the square-shaped electrodes are more difficult to be analyzed due to the four sharp corners in the geometry of the square-shaped electrode. Based on a mathematical model of the electrostatic sensor, induced charge on the electrode and hence the induced current can be derived, both sensitivity distribution and frequency response of the sensor can be identified. From this consideration, a pair of full ring-shaped electrodes should be more appropriate for acquiring data for cross-correlation signal processing in circular pipes.

The axial length of the ring electrode (W) is a crucial parameter influencing the performance of the sensing head As the axial length of the electrodes for velocity measurement are different from that for loading measurement, they are considered separately

6.3.3 Amplifier

The flow noise signal induced on the probe is usually connected to a measuring equipment via preamplifier. As shown in Figure (6.7), the input impedance of a preamplifier or a measurement equipment is very high, then the characteristics of the sensor comprising the electrode and the connected electronics depend not both the electronics and on the internal impedance of the electrode due to loading effect [21, 22]

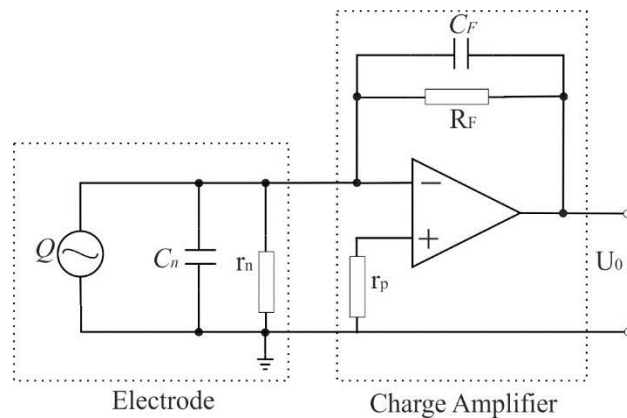


Figure 6.7 Sensing System: equivalent circuit and charge amplifier [21, 22].

According to Gajewski's study [58, 63] is shown Figure (6.8) and Figure (6.9). They also show and confirm that the actual probe preamplifier configuration is typical of a band-pass filter and the probe alone is a high-pass filter. Both the probe-preamplifier system and the probe do not transmit DC signals and within a range of useful frequencies

of 500 or even 3000 Hz they differentiate input signals, as generated by the electrostatic low noise. The frequency characteristics of such a type of measuring systems should be shaped individually according to real needs and requirements.

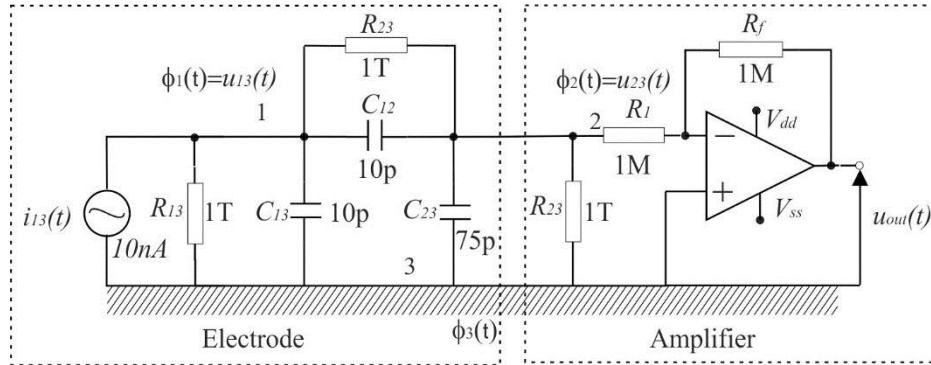


Figure 6.8 Equivalent circuit diagram of the active four terminal network made up of the alternating current generator, probe and preamplifier [64].

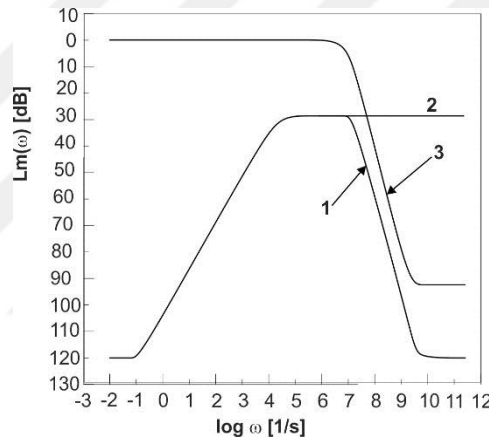


Figure 6.9 Simulated frequency characteristic of the whole four terminal network (1), probe(2), and preamplifier (3) for $\tau=750\mu\text{s}$ and $|k_u| = 1$ [58].

7. THE STUDY ON SENSOR

In this study, the basic properties of a measurement system have been examined both theoretically and experimentally. Because of limited standard calibration system, a theoretical study of the electrostatic sensor has played an important role understanding the system in addition to delivering useful engineering design data. The investigation in this thesis commences with a study of the response of the ring-shaped electrostatic system to induced signals. The signal induced on a circular electrode due to a single charged particle is starting point of our experiments. Since the fluid materials consist of a single particle, it may be a good start to understand the characteristics of a single particle to identify the properties of all solid flow parameters. The electrode dimensions of circular sensors on the system properties have important effects either concentration or velocity measurements.

In order to investigate the basic interactions between the particles and the sensor, a simplified physical model is proposed. The pneumatic conveying pipeline is assumed to be a perfectly conductive tube with its outside surface earthed. The air drag and gravity effects are neglected. However, despite these simplified assumptions the physical problem is still complex. The main difficulty may be the electrostatic field due to the charged particle within the sensing head is asymmetrically distributed in three dimensions. Consequently, the charge density distribution on the internal surface of the pipe wall and electrode is extremely complex. It is suggested that it can be solved only approximately using numerical methods. Since the integrals in equations (5.19) and (5.20), illustrated in Figure 5.11, cannot be solved analytically, the influences of these factors on the sensor output have to be determined using merely numerical methods.

The physical geometry of the electrode is taken into consideration in the modelling, because the geometrical dimensions strongly affect the performance of the sensing system. As indicated by Equation (5.19), the sensor output depends on the position of the point charge relative to the center of the electrode. Such a property is known as spatial sensitivity. The spatial sensitivity should respond to the amplitude of the sensor current as shown in Figure 5.11. Since the sensor current is not a constant, the total area under the either half curve in Figure 5.11 is the most adequate parameter.

In this simplified physical model, because the particle velocity is much less than the speed of light, relativistic distortion of the electrostatic field due to the movement of the charged particles is ignored. Electrostatic charge densities in pneumatic pipelines

range from 10^{-7} C/kg to 10^{-3} C/kg so the streaming current carried by the fluid is not greater than 3 mA, with a mass flow rate between 0.3 kg/s to 3 kg/s

7.1 Test Rig, Particles and Measurement

A new test rig is developed in this thesis work in order to measure electrostatically charged particles passing through a sensor. The main sensing element comprises an insulated metal ring, wrapped around the PVC the earthed pipe wall. The ring is connected to the input of a charge detector and then to related signal processing electronics. While the charged particles transport across the metal ring electrode, the charge carried on the particles will induce a particular amount of opposite charge on the inside surface of the ring. Since the ring is initially neutral, an equal amount of charge will be supplied to or from the earth through the input resistor depending on polarity. Because of the motion of the particles, the induced charge will fluctuate correspondingly, resulting in a voltage signal

The test rig is composed of a mechanical setup, ten different electrodes, highly sensitive measurement charge amplifier and oscilloscopes. The mechanical setup is designed to handle falling charged particles of various types. A wide variety of particles are obtained to simulate mass flows. Particles made of different materials such as glass, plastic, etc. with different sizes are used in the experiments. The test rig comprises a variety of circle shaped probes, ranging from 0.18 to 200 mm, on the electrostatically transparent PVC pipe and in addition to dc battery power supply for low noise, it is employed an electrostatic shield for noise reduction. It is shown in Figure 7.1 and Figure 7.2

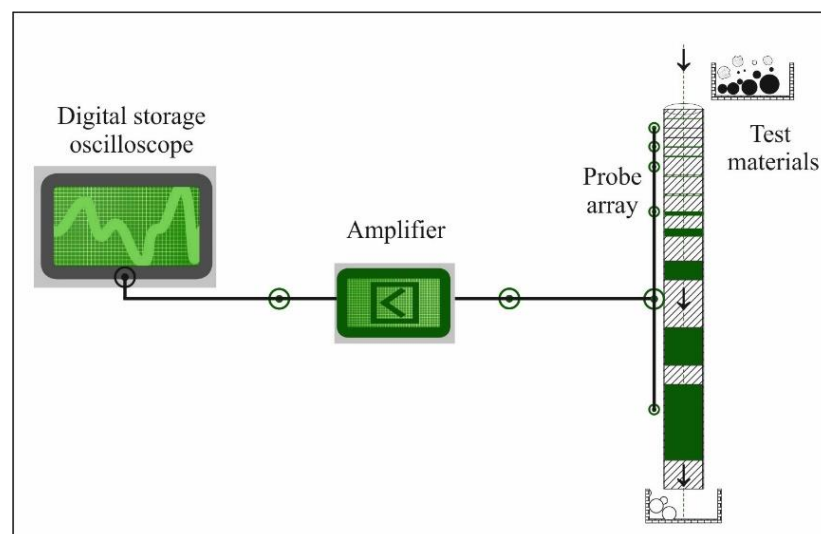


Figure 7.1 General diagram of the test rig

The electrostatically transparent plastic tube used in the test rig is approximately 100 millimeters in diameter and 1000 millimeters in length and composed of ten different electrodes. The electrode be made of copper plate with a thickness of 40 microns are wrapped over the pipe and the top is made of grounded aluminum foil.

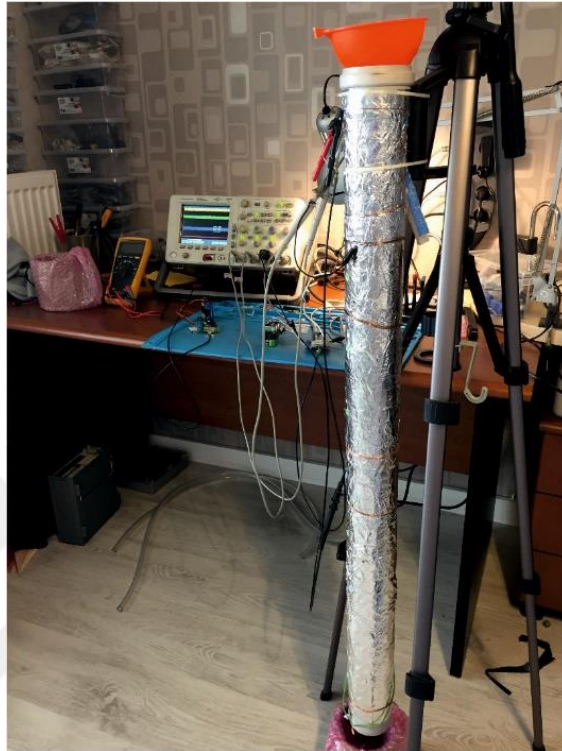


Figure 7.2 *The view of test rig*

All the test materials are composed of various materials, i.e., glass, polyamide, natural stone, wood, metal, metal and glass coated materials. They range from 500 μm to 30 mm in diameter, from few milligrams to few ten grams by weight

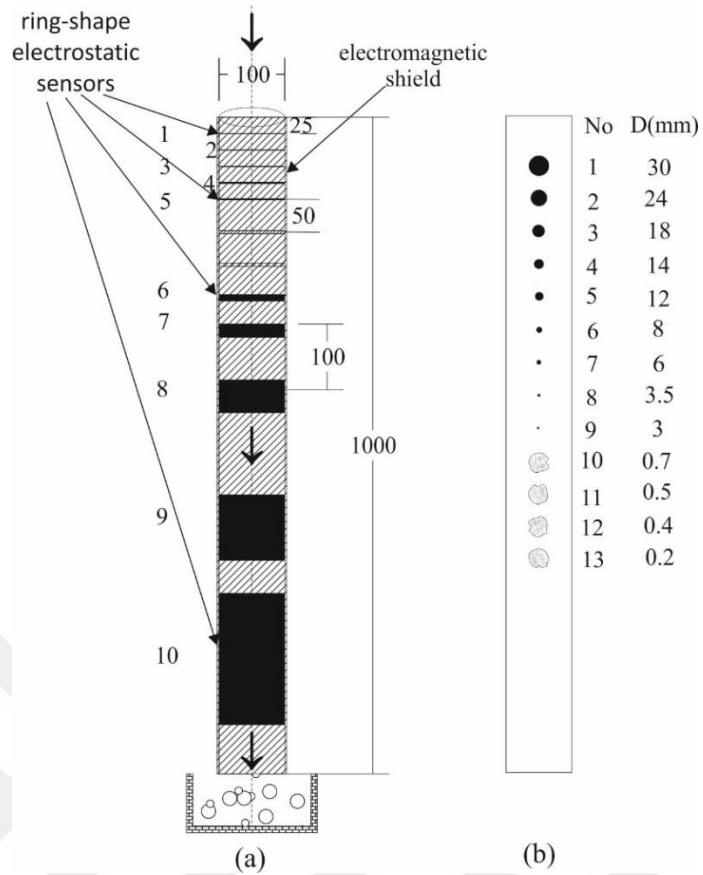


Figure 7.3 The cross-section of test rig and test materials

All the velocities of materials rely on gravitation, namely freely falling object principle. As shown in Table 7.2, the velocities and elapsed times at the midpoints of the electrodes between the first electrode and the last electrode range approximately from 0.7 to 4 m/s and from 71 to 410 milliseconds, respectively. The velocity at any point is can be calculated by this equation.

$$v = \sqrt{2gh} \quad (7.1)$$

where g is free-fall acceleration or the acceleration due to gravity and h is height of test material.

The elapsed time at any point is given by:

$$t = \sqrt{\frac{2h}{g}} \quad (7.2)$$

where t is elapsed time.

The elapsed time values in Table 7.2 are consistent with the time values measured by the data storage oscilloscope in Figure 7.6.

The voltage output is expressed as following,

$$U_{out}(t) = R_f I_{13}(t) = R_f Q'(t) = R_f \frac{dQ}{dt} = \frac{-2R_f C A v^2 t}{[h^2 + (vt)^2]^2} \quad (7.3)$$

The comprehensive model is shown in Figure 7.4. Because of little effect of some circuit component, the circuit model in Figure 7.5 can be employed and the components R_{12} , C_{12} , R_{23} and C_{23} can be neglected due to high input impedance of charge amplifier. For =10G ohm, Even R_{13} , C_{13} can be neglected.

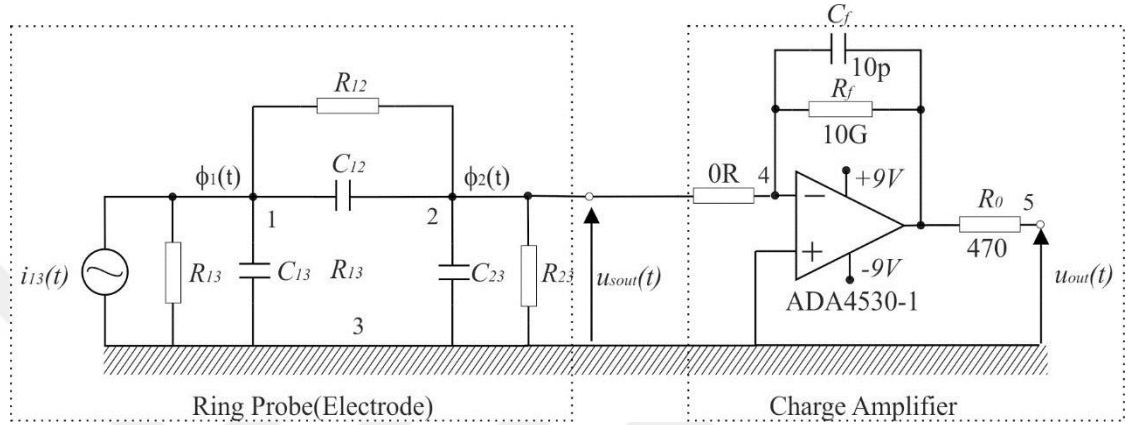


Figure 7.4 The measuring head of test rig with compherensive model.

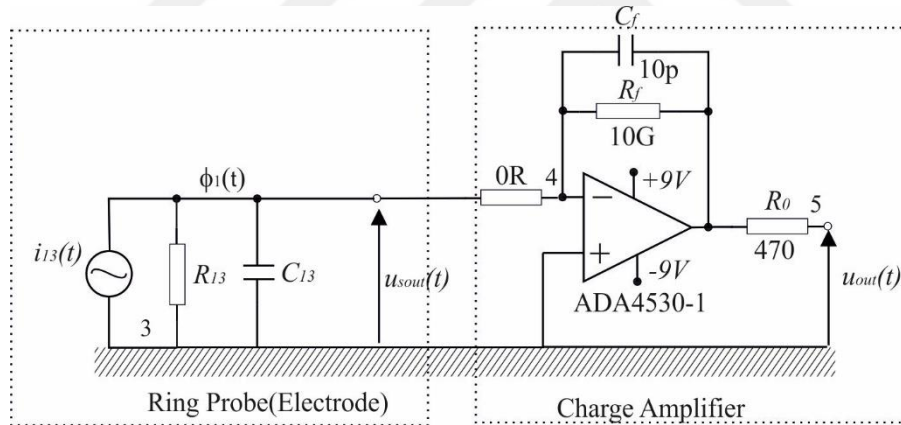


Figure 7.5 The measuring head of test rig with simplified model

The lack of faraday cage applications, the accuracies of data of measurement remain limited. Namely, some data in the input of the amplifier may not be determined; it is measured only in output of amplifier because of input noise.

Some material properties and measured peak-to-peak voltages are presented in Table 7.1 and their photographs are shown in Figure 7.6.

Table 7.1 The list of test materials used in test rig

No	Type of Material	Single or multiple	Diameter of sphere (mm)	Unit /Total Weight (g)	V _{pp} _{min} (mVolt)	V _{pp} _{max} (Volt)	Min Current (pA)	Max Current (pA)
1	Acrylic	Single	30	14	9.4	14.23	0.94	1423
2	Acrylic		24	7	7.7	9.71	0.77	970
3	Acrylic		18	2.8	6.4	7.33	0.64	733
4	Acrylic		14	1.4	4.5	6.82	0.45	682
5	Acrylic		12	0.9	3.2	6.19	0.32	619
6	Acrylic		8	0.25	2.8	4.23	0.28	423
7	Acrylic		6	0.1	2.1	3.11	0.21	311
8	Acrylic		3	0.05	1.3	2.04	0.13	204
9	Acrylic		2.5	0.01	0.6	1.67	0.06	167



(a)



(b)

Figure 7.6 The views of test materials used in test rig

Table 7.2 The calculated velocities and elapsed times for all electrodes

No of electrode	Width	Type	W/D	Velocity at center of electrode (m/s)	Elapsed time at center of electrode (ms)
1	0.18	Narrow	0.0018	0.7016	71.52
2	0.56		0.0056	0.9932	101.25
3	1		0.01	1.2171	124.07
4	2		0.02	1.4042	143.14
5	5		0.05	1.8662	190.23
6	10		0.1	2.1243	216.54
7	20		0.2	2.5637	261.34
8	50		0.5	2.9714	302.89
9	100	Wide	1	3.3588	342.38
10	200		2	4.0232	410.12

In Table 7.3, the measured peak to peak voltages of selected electrodes and charge amplifier outputs according to test materials are presented.

Table 7.3 *The peak to peak voltages*

		The Type of Circular Probe										Input Probe(V)	Charge Amp Output(V)	Charge Amp Input (pA)
		1	2	3	4	5	6	7	8	9	10			
The Type of Material	1	0.450	0.660	0.730	0.790	0.820	0.918	1.51	2.11	3.84	4.93	1	7.70	770
		0.620	0.970	1.16	1.40	1.21	1.36	1.96	2.52	5.75	7.32	1	9.50	950
	2	0.230	0.340	0.340	0.356	0.411	0.452	0.629	0.980	1.88	2.41	1	3.40	340
		0.218	0.330	0.360	0.385	0.397	0.435	0.603	0.960	1.94	3.58	1	3.60	360
	3	0.245	0.350	0.369	0.420	0.461	0.486	0.615	0.943	1.88	2.48	1	3.13	313
		0.774	1.08	1.19	1.36	1.46	1.61	2.41	2.68	2.19	2.79	1	5.20	520
	4	0.305	0.469	0.494	0.533	0.621	0.790	1.170	1.43	2.38	3.11	1	4.31	431
		0.253	0.394	0.450	0.482	0.513	0.652	0.935	1.38	2.53	3.26	1	3.94	394
	5	0.104	0.156	0.163	0.176	0.197	0.237	0.353	0.423	0.560	0.723	1	1.06	106
		0.403	0.631	0.694	0.733	0.813	0.873	1.09	1.09	3.00	3.81	1	5.19	519
	6	0.109	0.119	0.138	0.158	1.63	1.739	1.61	1.97	0.630	0.806	1	1.06	106
		0.206	0.319	0.256	0.420	0.420	0.609	0.805	1.21	1.97	2.54	1	3.56	356
	7	0.210	0.313	0.350	0.383	0.512	0.503	0.736	0.7953	1.56	1.97	1	2.69	269
		0.052	0.288	0.300	0.422	0.417	0.473	0.702	0.945	1.47	1.85	1	2.56	256
	8	0.043	0.066	0.081	0.097	0.108	0.124	0.185	0.192	0.213	0.270	1	0.310	31
		0.053	0.055	0.103	0.126	0.147	0.173	0.196	0.213	0.275	0.352	1	0.400	40
	9	0.037	0.042	0.069	0.084	0.103	0.138	0.121	0.156	0.169	0.214	1	0.200	20
		0.054	0.066	0.081	0.101	0.124	0.151	0.164	0.182	0.213	0.268	1	0.310	31

As shown in Figure 7.7, the signal shapes of selected electrodes of various charge levels according to test material-1. Where Ch 1 (yellow), Ch2 (green), Ch3 (purple), Ch4 (red) are connected Electrode1, Electrode 2, Electrode 9 and amplifier output of Electrode1

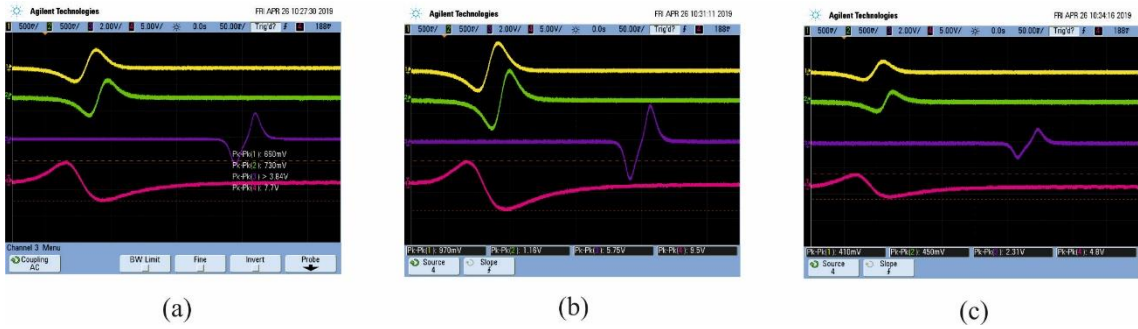


Figure 7.7 The peak to peak voltages of selected electrodes according to test material-1

As shown in Figure 7.8, the signal shapes of selected electrodes of various charge levels according to test material-2. Connection the same as in Figure 7.7

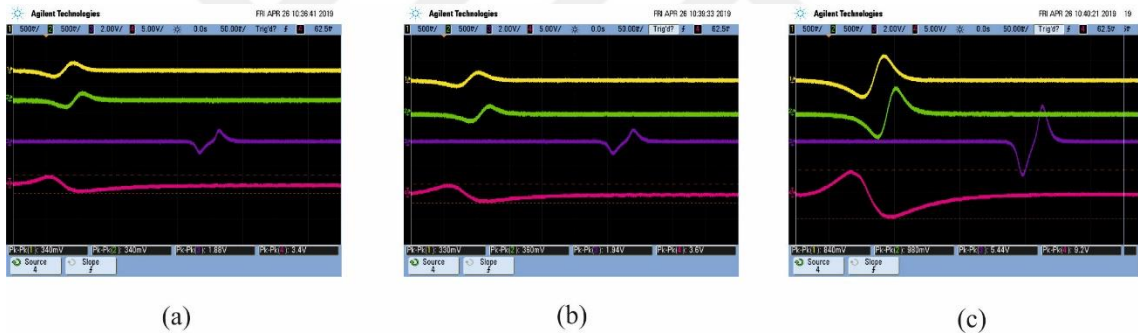


Figure 7.8 The peak to peak voltages of selected electrodes according to test material-2

In Figure 7.9, and Figure 7.10 represented the signals of related electrodes for material-8 and 9 respectively

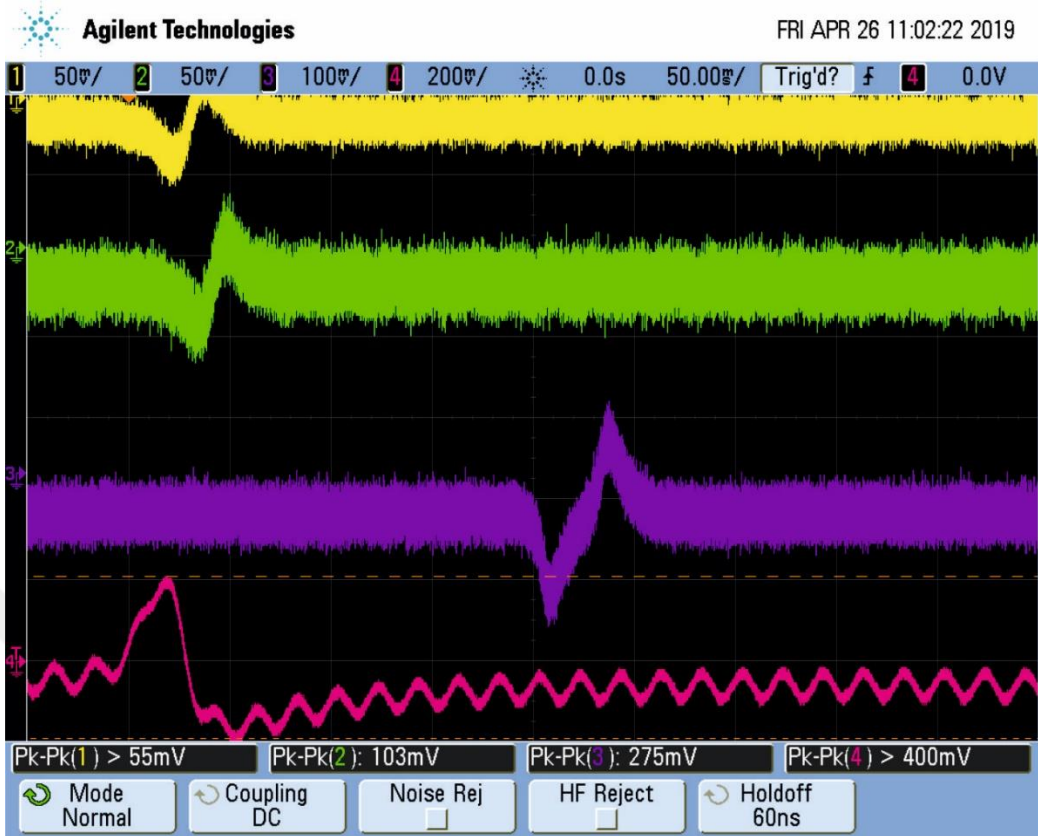


Figure 7.9 The peak to peak voltages of selected electrodes according to test material-8

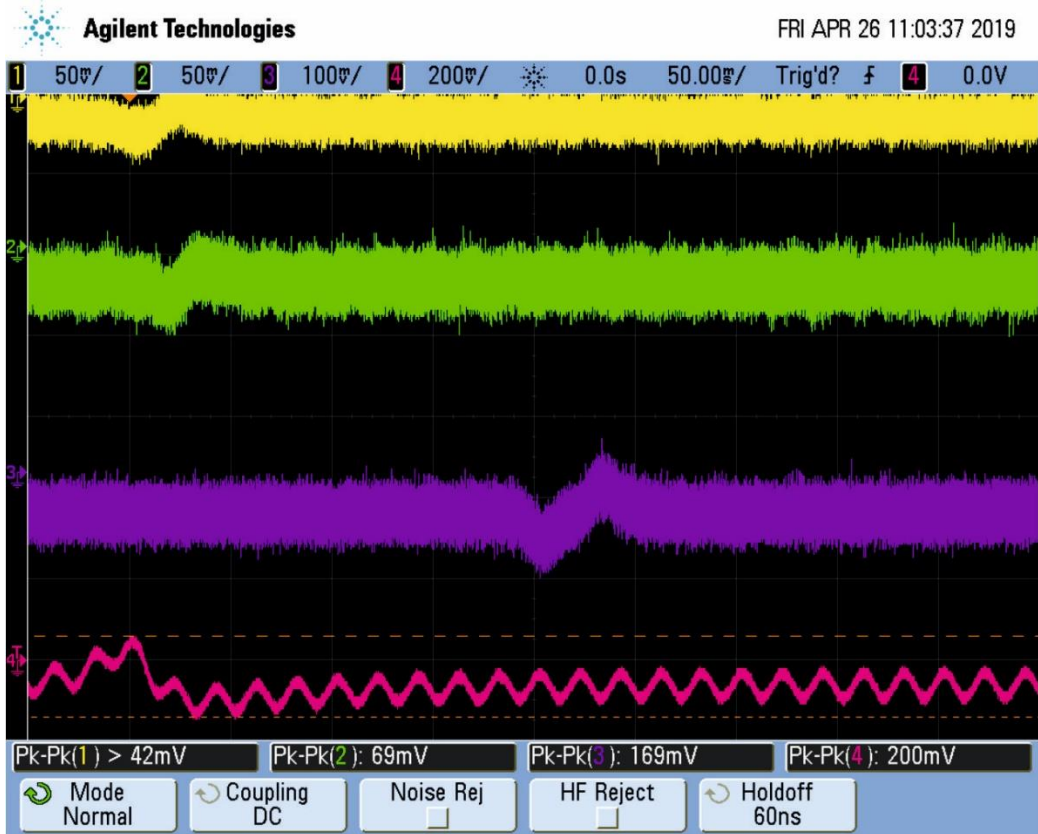


Figure 7.10 The peak to peak voltages of selected electrodes according to test material-8

It is preferred to state the signal waveforms mathematically in order to proceed a more comprehensive analysis of the sensor characteristic. But some equations can only be solved numerically. Modelling of the charge induced on an insulated circular electrode due to a single charged particle has been developed by Gajewski [48], Yan [24] and Cheng [27]. Gajewski did not consider the variation of induced charge proportional to the geometry in the sensor (spatial sensitivity), whereas Yan did not consider the charge distribution in the sensor owing to a single particle. Cheng has developed a FEM model considering both aspects. In the experiments of single studies are based on Cheng's study [27] and its further study by Zhang [22]. From observing the some groups of curves shown it was apparent that the data resulting from finite-element analysis can be fitted to curves defined by the following equations (5.34), (5.35) and (5.36), it can be expressed following:

$$\begin{aligned}
\frac{I_1(x_1)}{I_1(x_2)} &= \frac{\frac{dQ_1}{dt}}{\frac{dQ_2}{dt}} & (7.4) \\
&= \frac{\frac{d A_1 e^{-k_1 x_1^2}}{dt}}{\frac{d A_2 e^{-k_2 x_2^2}}{dt}} \\
&= \frac{-2k_1 A_1 x_1 e^{-k_1 x_1^2}}{-2k_2 A_2 x_2 e^{-k_2 x_2^2}} \\
&= \frac{k_1 v_1^2 e^{-(k_1 v_1^2 t_1^2)}}{k_2 v_2^2 e^{-(k_2 v_2^2 t_2^2)}}
\end{aligned}$$

we can extract from aforementioned equations (5.59) and (5.60) the following proportional equation:

$$\begin{aligned}
\frac{Q_1(r_1, W_1, x_1)}{Q_2(r_2, W_2, x_2)} &= \frac{A_1(r_1, W_1) e^{-k_1(r, W) x_1^2}}{A_2(r_2, W_2) e^{-k_2(r, W) x_2^2}} & (7.5) \\
&= \frac{\beta_1 \pi D_1^2 A_1(r, W) N(r, x) e^{-k_1(r, W) x_1^2}}{\beta_2 \pi D_2^2 A_2(r, W) N(r, x) e^{-k_2(r, W) x_2^2}} \\
&= \frac{\beta_1 \pi D_1^2 A_1(r, W) N(r, x) e^{-k_1(r, W) x_1^2}}{\beta_2 \pi D_2^2 A_2(r, W) N(r, x) e^{-k_2(r, W) x_2^2}}
\end{aligned}$$

In accordance with the analysis Cheng [27] and Zhang [22], when the width of the circular electrode is less than $\frac{1}{2}$ radius of the pipe, the relationship between $A(r, W)$, $k(r, W)$ and r, W can be obtained by Gauss curve fitting as follows;

$$A(r, W) = a_0 \left(\frac{W}{R}\right) \left[1 + a_1 \left(\frac{r}{R}\right)^2\right] \quad \text{for } 0 \leq \frac{W}{R} < \frac{1}{2}, 0 \leq \frac{r}{R} < \frac{6}{10} \quad (7.6)$$

$$k(r, W) = k_0 \left[1 - k_1 \left(\frac{W}{R}\right)\right] \left[1 + k_2 \left(\frac{r}{R}\right)^2\right] \quad \text{for } 0 \leq \frac{W}{R} < \frac{1}{2}, 0 \leq \frac{r}{R} < \frac{6}{10} \quad (7.7)$$

$$A(r, W) = a_2 \left(\frac{W}{R}\right) \left[a_3 \left(\frac{r}{R}\right)^2 - 1\right] \quad \text{for } 0 \leq \frac{W}{R} < \frac{1}{2}, \frac{6}{10} \leq \frac{r}{R} < 1 \quad (7.8)$$

$$k(r, W) = k_3 \left[1 - k_1 \left(\frac{W}{R}\right)\right] \left[k_4 \left(\frac{r}{R}\right)^2 - 1\right] \quad \text{for } 0 \leq \frac{W}{R} < \frac{1}{2}, \frac{6}{10} \leq \frac{r}{R} < 1 \quad (7.9)$$

where coefficients $a_0, a_1, a_2, a_3, k_0, k_1, k_2, k_3, k_4$ are positive constants. R and W are the radius and the width of the electrode.

7.2 Results

The measurements are consistent with the first model of single-particle model reported by Law [45] with Equations (5.7), (5.8) and (5.9) and Gajewski's study [46-48] with related Equation (5.12) and the research by Cheng [27] related with Equations (5.34), (5.35) and (5.36) and Figure 5.11, and Zhang's study [22] related with Figure 5.16 and equation (5.59). Measurement accuracies are the same as that of the oscilloscope used.

According to Figure 4.16 for the same charged particle, the peak value of the charge signal increases as the W/D value increases, thus increasing the peak values of the signal V and I , the derivative of the charge sensitivity of signal. The studies mentioned previously are validated the data given by the Figure 7.7, Figure 7.8 and Table 7.3.

In accordance with Equation (5.60) for the same material, as the diameter, accordingly the material surface area, increases, the electrode peak value of induction voltage increases. In other words, the higher the particle size, the higher the charge capacity and the induction voltage.

For the same electrode and test material, as the velocity increases, the response time decreases but the signal frequency increases. As it can be seen in Figures 7.7, 7.8 and Table 7.3. It can be stated following,

(1) The peak value of the signal increases as the sensor width W increases for the same single particle material, provided that the sensor passes through the center. This is consistent with by the FEM equation (7.1).

(2) For the particle material having different surface area due to different diameters passing through the center of the same sensor, the peak value of the signal increases as the particle gets bigger. This is consistent with the proportional equation (7.2).

8. DISCUSSION, CONCLUSIONS AND FUTURE WORK

Practical studies in this thesis are based on a single particle model by Gajewski [48], Yan[24] and Cheng [27] which forms the starting point for defining and calculating fluid noise and some single particle models have been examined, but especially the Gaussian curve fitting is emphasized by Cheng [27].

Copper, aluminum, brass and iron materials of various thicknesses have been tested in the selection of electrode materials. Copper is chosen as the most suitable material due to its high conductivity and easy shaping.

Acrylic, glass, PVC, polyamide, natural stone, metal cladding stone, metal materials have been used as test materials. Since the highest voltage value for our measurement system is obtained in acrylic material tests comparative studies have been carried out with acrylic test materials.

Electromagnetic shielding is important for these experiments. Therefore, all sensors, cables, and measuring circuitry are enclosed in electromagnetic shield. However, some electric supply system and high frequency noise signals originating from the location have been detected cannot be prevented. Even if the effects have been reduced to some extent, the real solution would be the room that is formed from the Faraday cage.

In addition, various sensitive op-amp circuits have been tested. Texas Instruments, Analog Devices (AD), Intersil (Renesas), National Instruments. However, as determined from both the data sheets and the experiments, the AD4530-1 produced by AD is preferred due to both new technology and very low input current.

The computer programs was written by Yan [24], Cheng [27] and Zhang [22] which gave a numerical solution to equations is in accordance with the experiments in the thesis. As visually shown in Figure 5.11, Figure 5.13, Figure 5.14 and Figure 5.16 the spatial sensitivity of the electrostatic sensor for variable W/D ratios. Several consequences can be drawn out from the results

- (1) The electrostatic sensor is more sensitive to the particles adjacent to the pipe wall.
- (2) The W/D ratio is a crucial factor influencing the uniformity of the spatial sensitivity, with higher W/D ratio resulting in a more uniform sensitivity.
- (3) The W/D ratio also significantly affects the sensitivity at a particular position. The sensor with a very small W/D ratio yields an extremely low sensitivity to the particles over most of the pipe cross sectional area.

Since the beginning of the triboelectric study conducted by Shaw, a number of studies have been carried out on a two-phase solid-gas flow ranging from a single particle model to a complex flow. Studies are being carried out separately in the fields of physics, chemistry, electrostatic and electrical engineering, but much more work is needed in the field of particle flow rate, solid concentration and process tomography. The multidisciplinary studies in the mentioned areas may lead to more important results.

For further study, FEM, advanced probability, statistical DSP, artificial intelligence, electrochemistry fields should be examined to obtain deeper knowledge

Predictive maintenance, agriculture and pollination, airborne particles that affect health, atmospheric phenomena, occupational health and safety can be chosen a future research field.

Modified geometrical sensor array, composite sensor array which composed of some different electrodes such as capacitive and electrodynamic ones can be developed in the further research phase.

REFERENCES

- [1] Shaw, P. E., (1917). Experiments on Tribo- Electricity. I. The Tribo-Electric Series. *University College, Nottingham*.
- [2] Mazumder, M. K., (1999) Electrostatic Processes. in *Wiley Encyclopedia of Electrical and Electronics Engineering*.
- [3] Zhong Lin Wang, L. L., Jun Chen, Simiao Niu, Yunlong Zi (2016). *Triboelectric Nanogenerators*.
- [4] Forward, K. M., (2009) "Triboelectrification of Granular Materials," Doctor of Philosophy, Department of Chemical Engineering, Case Western Reserve University
- [5] Cheng, D. K. (2006). *Field and Wave Electromagnetics* Second Edition
- [6] Woodhead, S., (1992) "The measurement of particle velocity and suspension density in pneumatic coal injection systems," Thesis (Ph. D.), University of Greenwich.
- [7] Lawrence B. Schein, G. S. P. C., Daniel J. Lacks, (2014) Triboelectrification. in *Wiley Encyclopedia of Electrical and Electronics Engineering*.
- [8] J. Lowell, A. C. R.-I., (1980). Contact electrification. *Advances in Physics*, vol. 29, no. 6, pp. 947-1023.
- [9] Raymond A. Serway, J. W. J. (2014). *Physics for Scientists and Engineers with Modern Physics* Ninth Edition
- [10] Shuji Matsusaka, H. M., (2003). Electrostatics of particles. *Advanced Powder Technology*, vol. 14, no. 2, pp. 143-166.
- [11] Harper, W. R., (1951). The Volta effect as a cause of static electrification. *Proceedings of the Royal Society of London. Series A. Mathematical and Physical Sciences*, vol. 205, no. 1080, pp. 83-103.
- [12] Davies, D. K., (1969). Charge generation on dielectric surfaces. *Journal of Physics D: Applied Physics*, vol. 2, no. 11, p. 1533.
- [13] Schein, L. B. (1992). *Electrophotography and Development Physics*.
- [14] A. Mukherjee, D. G., D. Wasan, "Surface charge of Illinois coal and pyrites for dry electrostatic cleaning," 1987, vol. 32.
- [15] Zhenhua Wen, J. H., Jason Atkin, (2017). A review of electrostatic monitoring technology: The state of the art and future research directions. vol. 94.
- [16] Shuji Matsusaka, M. G., Hiroaki Masuda, (2000). Electrification of an elastic sphere by repeated impacts on a metal plate. *Journal of Physics D: Applied*

Physics, vol. 33, no. 18, p. 2311.

- [17] Stephen P. Timoshenko, J. N. G. (1951). *Theory of Elasticity*.
- [18] Bailey, A. G., (1993). Charging of Solids and Powders. *Journal of Electrostatics*, vol. 30, pp. 167-180.
- [19] G.E. Klinzing, F. R., R. Marcus, L.S. Leung (2010). *Pneumatic Conveying of Solids A Theoretical and Practical Approach*.
- [20] Mills, D. (2016). *Pneumatic Conveying Design Guide*. Third Edition: Butterworth-Heinemann
- [21] Zhang, J., (2012) Air solids flow measurement using electrostatic techniques. in *Electrostatic*, Canbolat, H., Ed.: InTech, p.^pp.
- [22] Zhang, J., (2002) "A Study of An Electrostatic Flowmeter," Ph. D, University of Teesside.
- [23] N. Huber, M. S., (1994). Characterization of the cross-sectional particle concentration distribution in pneumatic conveying systems. *Powder Technology*, vol. 79, no. 3, pp. 191-210.
- [24] Yan, Y., (1992) "Mass flow measurement of pneumatically conveyed solids.," University of Teesside.
- [25] *Electrostatics - Code of practice for the avoidance of hazards due to static electricity*, 2003.
- [26] Yan, Y., (1996). Mass flow measurement of bulk solids in pneumatic pipelines. *Measurement Science and Technology*, vol. 7, no. 12, p. 1687.
- [27] Cheng, R., (1996) "A study of electrostatic pulverised fuel meters.," University of Teesside.
- [28] Yingna Zheng, Q. L., (2011). Review of techniques for the mass flow rate measurement of pneumatically conveyed solids. *Measurement*, vol. 44, no. 4, pp. 589-604.
- [29] R. S. Medlock, R. A. F., (1990). Mass Flow Measurement A State of the Art Review. *Measurement and Control*, vol. 23, no. 4, pp. 100-112.
- [30] M. Machida, M. K., (2008). Sensor design for development of tribo-electric tomography system with increased number of sensors. *Journal of Visualization*, vol. 11, no. 4, pp. 375-385.
- [31] RAHMAT, M. F., (1996) "Instrumentation of particle conveying using electrical charge tomography.."
- [32] Mohd F. RAHMAT, H. A. S., (2004). Flow Regime Identification Using Neural Networkbased Electrodynamic Tomography System.

- [33] R. G. Green, M. F. R., K. Evans, A. Goude, M. Henry, J. A. R. Stone, (1997). Concentration profiles of dry powders in a gravity conveyor using an electrodynamic tomography system. *Measurement Science and Technology*, vol. 8, no. 2, p. 192.
- [34] R. M. Carter, Y. Y., (2005). An instrumentation system using combined sensing strategies for online mass flow rate measurement and particle sizing. *IEEE Transactions on Instrumentation and Measurement*, vol. 54, no. 4, pp. 1433-1437.
- [35] Y. Yant, B. B., S. Woodhead, J. Coulthard, (1995). Velocity measurement of pneumatically conveyed solids using electrodynamic sensors.
- [36] C. L. Xu, G. T., B. Zhou, D. Yang, J. Zhang, S. Wang,, (2007). Electrostatic introduction theory based spatial filtering method for solid particle velocity measurement. (in en),*Multiple flow: the ultimate measurement challenge*.
- [37] Jian Qiu, Z., Ya Jun, Guo, Yi Shen, (2004). A wavelet-based method for measuring particulate velocity by an active electrostatic sensor. *IEEE Transactions on Instrumentation and Measurement*, vol. 53, no. 4, pp. 1345-1351.
- [38] Anton Fuchs, H. Z., (2007). Measurement of Slug Length and Slug Velocity in Pneumatic Conveying Using Capacitive Sensing. *Particle & Particle Systems Characterization*, vol. 24, no. 3, pp. 201-209.
- [39] Yong Yan, L. W., Tao Wang, Xue Wang, Yonghui Hu, Quansheng Duan, (2018). Application of soft computing techniques to multiphase flow measurement: A review. *Flow Measurement and Instrumentation*, vol. 60, pp. 30-43.
- [40] Gajewski, J. B., (2008). Electrostatic Nonintrusive Method for Measuring the Electric Charge, Mass Flow Rate, and Velocity of Particulates in the Two-Phase Gas–Solid Pipe Flows—Its Only or as Many as 50 Years of Historical Evolution. *IEEE Transactions on Industry Applications*, vol. 44, no. 5, pp. 1418-1430.
- [41] Cooper, W. F., (1953). The electrification of fluids in motion. *British Journal of Applied Physics*.
- [42] Hignett, E. T., (1967). Particle-charge magnitudes in electrostatic precipitation. *Electrical Engineers, Proceedings of the Institution of*, vol. 114, no. 9, pp. 1325-1328.
- [43] E. T. Hignett, J. C. G., (1968). Electrostatic streaming current developed in the turbulent flow through a pipe. *Journal of Electroanalytical Chemistry and Interfacial Electrochemistry*, vol. 16, no. 2, pp. 239-249.
- [44] W.D. Curtis, J. D. L., W.A. Parker, (1982). Dimensional Analysis and the Pi Theorem.
- [45] Law, S. E., (1975). Electrostatic induction instrumentation for tracking and charge measurement of airborne agricultural particulates. *Trans. of ASAE 18(1):40-45.*, vol. vol. 18, no. 1, p. 40,.

- [46] J. B. Gajewski, A. S., (1981). Charge measurement of dust particles in motion part I. *Journal of Electrostatics*, vol. 10, pp. 229-234.
- [47] Gajewski, J. B., (1984). Charge measurement of dust particles in motion - part II. *Journal of Electrostatics*, vol. 15, no. 1, pp. 67-79.
- [48] Gajewski, J. B., (1984). Mathematical model of non-contact measurements of charges while moving. *Journal of Electrostatics*, vol. 15, no. 1, pp. 81-92.
- [49] Gajewski, J. B., "Continuous non-contact measurement of electric charges of solid particles in pipes of pneumatic transport. I. Physical and mathematical models of a method," 1989, pp. 1958-1963 vol.2.
- [50] Gajewski, J. B., "Continuous non-contact measurement of electric charges of solid particles in pipes of pneumatic transport. II. Physical and mathematical models of a method," in *Conference Record of the IEEE Industry Applications Society Annual Meeting*, 1989, pp. 1958-1963 vol.2.
- [51] J. B. Gajewski, B. J. G., W. S. Kala, (1993). Electrostatic method for measuring the two-phase pipe flow parameters. *IEEE Transactions on Industry Applications*, vol. 29, no. 3, pp. 650-655.
- [52] Gajewski, J. B., (1997). Dynamic effect of charged particles on the measuring probe potential. *Journal of Electrostatics*, vol. 40-41, pp. 437-442.
- [53] Gajewski, J. B., (1996). Electrostatic, inductive ring probe bandwidth. *Measurement Science and Technology*, vol. 7, no. 12, p. 1766.
- [54] D. I. Armour-Chélu, S. R. W., R. N. Barnes, (1998). The electrostatic charging trends and signal frequency analysis of a particulate material during pneumatic conveying. *Powder Technology*, vol. 96, no. 3, pp. 181-189.
- [55] S. N. Murnane, R. N. B., S. R. Woodhead, J. E. Amadi-Echendu, (1996). Electrostatic modelling and measurement of airborne particles concentration. *IEEE TRANSACTIONS ON INSTRUMENTATION AND MEASUREMENT*, , vol. VOL. 45,, no. NO. 2, APRIL 1996, pp. 485-492.
- [56] Gajewski, J. B., (1999). Electrostatic flow probe and measuring system calibration for solids mass flow rate measurement. *Journal of Electrostatics*, vol. 45, no. 4, pp. 255-264.
- [57] Gajewski, J. B., (1999). Static characteristics of an electrostatic flow probe. *Journal of Electrostatics*, vol. 48, no. 1, pp. 49-64.
- [58] Gajewski, J. B., (2000). Frequency response and bandwidth of an electrostatic flow probe. *Journal of Electrostatics*, vol. 48, no. 3, pp. 279-294.
- [59] Gajewski, J. B., (2006). Non-contact electrostatic flow probes for measuring the flow rate and charge in the two phase gas–solid flows. vol. 61, pp. 2262-2270.
- [60] Jianyong Zhang, B. Z., Chuanlong Xu, Shimin Wang, "Modelling and calibration

of a ring-shaped electrostatic meter," 2009, vol. 147, p. 012001.

- [61] Jianyong Zhang, C. X., Donglai Xu, John Coulthard, Shimin Wang, (2009). Analyses of Characteristics of Ring-shaped Electrostatic Meter.
- [62] Jun Lin, Z.-S. C., Zheng Hu, Yong-Min Yang, Xin Tang,, (2014). Analytical and Numerical Investigations into Hemisphere-Shaped Electrostatic Sensors. *Sensors (Basel, Switzerland)*, vol. 14, no. 8, pp. 14021-14037.
- [63] Li, J., Kong, M., Xu, C., Wang, S. and Fan, Y., (2015). An Integrated Instrumentation System for Velocity, Concentration and Mass Flow Rate Measurement of Solid Particles Based on Electrostatic and Capacitance Sensors. *Sensors (Basel, Switzerland)*, vol. 15, no. 12, pp. 31023-31035.
- [64] Gajewski, J. B., (1999). Non-intrusive solids charge and mass flow measurements with an electrostatic flow probe. *Journal of Electrostatics*, vol. 46, no. 4, pp. 271-284.

CURRICULUM VITAE

Name and Surname: Özcan KAMIŞLI

Language: English

Date and Place of Birth: 01/09/1969, Çorum

E-Mail: ozcan.kamisli@gmail.com

Education and Work Experience

- 1993, Anatolia University, Faculty of Engineering and Architecture, Department of Electrical and Electronics
- 2012, General Coordinator, IDEA TECHNOLOGY CONSULTANCY INCORPORATED COMPANY Ankara,
- 1998, Co-Founder, EKON CONTROL SYSTEMS LIMITED, Ankara, METU, Technopolis,
- 2003, Co-Founder, EKON IT SYSTEMS LIMITED, Ankara, INDUSTRIAL ZONE OF OSTİM, 2003
- Expert of Occupational Health and Security, A Class (Include Dangerous Works at All Levels)

Memberships

- TOSYOY, Member of The Trustee Committee
- The Chamber of Electrical Engineers (EMO)
- Cluster for Defence for Industry (OSSA) of OSTİM
- Cluster for Clean Energy of OSTİM
- Clean Energy Foundation (TEMEV)